UNIVERSITY OF CALIFORNIA
RIVERSIDE

Network Dynamics of 4-Aminopyridine-Induced Ictogenesis

A Dissertation submitted in partial satisfaction
of the requirements for the degree of

Doctor of Philosophy

in

Neuroscience

by

Timothy L Myers

March 2021

Dissertation Committee:

Dr. Maxim Bazhenov, Co-Chairperson
Dr. Margarita Curras-Collazo, Co-Chairperson
Dr. Hyle Park
Dr. Emma Wilson

The Dissertation of Timothy L Myers is approved:

_____

_____

_____

Committee Co-Chairperson

_____

Committee Co-Chairperson

University of California, Riverside

ACKNOWLEDGEMENTS

Foremost, I express my deepest gratitude to Dr. Maxim Bazhenov and Dr. Oscar González. Dr. Bazhenov recruited me to conduct experimental research to reinforce his computational publications. Yet, upon request of a graduate student with zero programming experience, he forged a collaboration with a leader in the field of neuropathology who sought an *in silico* model of his experimental data. The resultant publication was one of the most profound accomplishments of my life with far reaching significance into the pathogenesis of epilepsy syndromes. Dr. González was tasked with teaching me to code while meeting progress milestones for the project. Aside from being a friend, best man, and contemporary, he was a phenomenal and patient mentor with respect to my developing proficiencies in programming and data analysis. Additionally, I must thank the many postdoctoral researchers who discussed, and often debated, the ideal analysis approach to my wet lab data. It was an honor to observe and participate in conversations with such brilliant mathematicians and biophysicists. I will always reflect upon your tutelage and advice as I continue to develop mastery over these skillsets. Thank you.

I would like to thank my committee for their commitment and the last-minute nature of my defense. I must single out my co-chair Dr. Margarita Curras-Collazo whom I first worked under as an undergraduate researcher in 2002. Her empathy and commitment to under-represented groups reinforces her commitment to education and instruction in its purest form. Her passion and enthusiasm for teaching infects students

with an enduring curiosity for neuroscience. My teaching style is heavily borrowed from experiences in her classroom as both a student and teaching assistant.

To my wife, Dr. Kimberly Stephens, you epitomize the persistence, indomitable spirit, focused intellect, and insatiable curiosity exhibited by the greatest scientific minds. I strive daily to be a partner worthy of the unconditional love, support and trust you bestow upon me. Without a shadow of a doubt, completion of this degree would not have transpired without your support.

Here, I wish to acknowledge individuals who directly influenced the successful completion of this degree. These individuals are acquired family and as such are listed in no significant order: Iliana Becerra, Dr. Curt Erikson, Dawn Livaudais, Justin Everett Nichol, Dr. Deanna Nielson, Dr. Rod Oka (RIP), Debbie Sampson, Hailey Sampson, Rebecca Sampson, Dorothy Inez Skates, Kelsey Rose Slater, Dr. Kerri Stephens, Caroline Flynne Templeton, and Mechelle Timmons.

I acknowledge the educational and career opportunities born from the financial sacrifices shouldered by my parents Linda and Orville Myers. I offer thanks to the rest of my family and in-laws for their unwavering support. I cannot in good conscience forget the contributions of my scaled and furry exotic companions over the years—Komodo (RIP), Isis (RIP), Mizu (RIP) and Hiryu.

I acknowledge the venerable and significant contributions of the NoStigmas organization to the mental health community. Their message of encouragement and open discussion of shared experience empowered me to recognize and confront mental health discrimination in my life. Their outreach and collective efforts are greatly appreciated.

The text of this dissertation, Chapter 2 in full, is a reprint of the material as it appears in *Neurobiology of Disease*, 2018. Dr. Maxim Bazhenov and Dr. Massimo Avoli listed in that publication directed and supervised the research which forms the basis for this dissertation.

The text of this dissertation, Chapter 3 in full, is a reprint of the material as it appears in *Epilepsy Journal*, 2018. Dr. Maxim Bazhenov listed in that publication directed and supervised the research which forms the basis for this dissertation.

I, Timothy Myers, attest that I significantly contributed to the conception, experimental design, data collection, data analysis, data interpretation, coding, article drafting and critical article revisions for the content within the chapters of this dissertation. The optogenetic experiments in Chapter 2 were designed and conducted by our collaborator Dr. Zahra Shiri. The optical density data and error correction methods in Chapter 3 were designed, coded and analyzed by our collaborator Dr. Mohmmad Hasan.

DEDICATION

I dedicate this dissertation to my grandmother June E Fordham (1928-2017). She provided the guidance and compassion which established the foundation of my adult identity despite a tumultuous adolescence. She passed on June 26, 2017. I have not confronted the significance of her loss nor was I able to be at her side in the end. With the closing of this chapter, I will visit your resting place to pay my respects, celebrate your life, and grant us both a degree of peace. Ma, I miss you!

Moreover, I dedicate this dissertation to those individuals who coexist with a bipolar disorder diagnosis. I can relate to the years of childhood misdiagnoses. I experienced the numerous and often debilitating side effects of pharmacological intervention. I too felt the lack of empathy and discrimination from colleagues, friends, family, and the lay public. The disorder grants access to bouts of transformative creativity and infinite energy, yet that that ruse often incites behaviors that flag us as social outcasts. You can succeed, but your path will likely not follow a normative trajectory. Therefore, it is imperative to value and relish your achievements without comparison to others in your program, social circles, job and/or family. You are not alone! Good luck.

ABSTRACT OF THE DISSERTATION

Network Dynamics of 4-Aminopyridine-Induced Ictogenesis

by

Timothy L Myers

Doctor of Philosophy, Graduate Program in Neuroscience
University of California, Riverside, March 2021
Dr. Maxim Bazhenov, Co-Chairperson
Dr. Margarita Curras-Collazo, Co-Chairperson

It is well established that one-third of epilepsy patients receive an intractable prognosis, yet 13% of those referred with a pharmacoresistant diagnosis are determined not to have refractory epilepsy. The literature attributes this discrepancy to the misdiagnosis and/or mistreatment of epilepsy syndromes. There is a significant gap in knowledge with respect to the pathogenesis of seizure disorders. Therefore, further insight into the mechanisms of ictogenesis is critical.

Here, I present a multimodal series of studies exploring the 4-aminopyridine (4AP) chronic model of epilepsy. The research incorporates computational, experimental, and translational experiments with methods drawing upon the fields of neuropharmacology, electrophysiology, optophysiology and biorealistic modeling. The aims of the research are three-fold: **(1)** propose a novel mechanism for ictogenesis, **(2)** elucidate the spatiotemporal dynamics and role of KCC2 in 4AP-induced ictogenesis, and

(3) demonstrate proof of concept for the practical application of spectral-domain optical coherence tomography (SD-OCT) in bedside treatment of seizure disorders.

Our computational modeling predicts that highly synchronized inhibition, in response to reduction of I_A, can drive seizure generation. This mechanism involves the recruitment of the KCC2 cotransporter to compensate for the large increase of intracellular chloride. Upon recruitment of the KCC2 cotransporter, substantial potassium efflux increases extracellular potassium resulting in the net depolarization of excitatory neurons and seizure generation. Furthermore, I demonstrate that spatiotemporal patterns of 4AP epileptiform activity reveal a dose-dependent response with increased waveform complexity at higher concentrations. I show that pharmacological inhibition of KCC2 further reinforced the computational simulations and implicated KCC2 in potassium channelopathy-induced seizure disorders. Lastly, we determine that SD-OCT sensitivity is sufficient to detect a decrease in backscattered light intensity in 4AP perfused hippocampal slices. We developed a protocol to correlate SD-OCT and simultaneous electrophysiological recordings using a 60-channel multielectrode array (MEA). These findings encourage future consideration of SD-OCT in the clinical setting for seizure diagnosis and treatment. Together, these studies address a critical research need in the study of epilepsy and raise additional questions for future research.

TABLE OF CONTENTS

LIST OF FIGURES & TABLES

Chapter 2: Computational Study

Chapter 3: Experimental Study

Chapter 4: Translational Study

Chapter 5: Conclusion

Appendix

CHAPTER 1: LITERATURE REVIEW

Epilepsy in Research: A Comprehensive Review

Epilepsy

Fifty million people worldwide have active epilepsy which accounts for 0.5% of the global burden of disease (World Health Organization, 2019). Epilepsy is a neurological disorder wherein a patient suffers two or more unprovoked spontaneous seizures. Provoked seizures that result from acute insults to the central nervous system (CNS) such as a bacterial infection or dysregulation of glucose homeostasis are not classified as epilepsy but rather acute symptomatic seizures irrespective of the frequency of occurrence. Diagnosis between provoked acute symptomatic seizures and epileptic seizures is often a challenging task that may lead to misdiagnosis. Epilepsy syndromes are complex pathologies that may initially present as acute seizures and later develop into chronic epilepsy. In addition, patients may present epileptiform and seizure-like activity without presenting true seizures. Epileptiform (EF) activity is a distinct pattern of paroxysmal activity resembling those recorded in a proportion of patients suffering from epileptic disorders. In experimental studies, the spontaneous unprovoked electrical events that epitomize epilepsy are classified as seizures and epileptic activity when observed *in vivo*. Whereas analogous events recorded *ex vivo* or *in vitro* are generally referred to as seizure-like discharges (SLDs) and/or epileptiform activity. Note, that medical science often applies the term seizure-like activity to indicate large abnormal electrical events in patients who present symptoms that resemble epilepsy without the characteristic electroencephalogram (EEG) activity. The proper nomenclature for pathologies that fall under this category are non-epileptic seizure. Here, for clarity, any reference to SLDs

and/or epileptiform activity will reference recorded electrical events in *ex vivo* or *in vitro* tissue samples.

The epidemiology of epilepsy is not wholly understood due to methodology problems and the heterogeneous nature of epileptic disorders, for these reasons it remains one of the most common and serious neurological pathologies (Bell & Sander, 2002; Sander & Shorvon, 1996). In epidemiology, prevalence and incidence are used to measure the frequency of a disease. Incidence, commonly expressed as a rate, is useful for describing how rapidly a disease occurs in a population but assumes that the risk of disease is the same for one person over 5 years as 5 people over one year which is generally inaccurate. Prevalence, however, is a snapshot that describes the number of people in a population currently suffering from the disease of interest. This measure is useful in the coordination of preventive, proactive healthcare but is limited in that the value is highly dynamic, fluxing with patient survival rates. The prevalence of epilepsy is between 4 to 10/1,000 people in a given population with the variation attributed to the methodological methods used in the studies (MacDonald et al., 2000; Olafsson & Hauser, 1999; Placencia et al., 1992; Rocca et al., 2001). The incidence rate of epilepsy, on the other hand, is 50 per 100,000 people/year in industrialized countries and ranges from 100 to 190 per 100,000 people/year in resource poor countries with socioeconomically disadvantaged populations being at higher risk (Gaitatzis et al., 2002; Heaney et al., 2002; Kotsopoulos et al., 2002; Lindsten et al., 2002; MacDonald et al., 2000; Zarrelli et al., 1999).

There are several etiologies and risk factors that result in the development of excessive and abnormal population spiking characteristic of epileptic disorders; these vary with age and geographic location (Bell & Sander, 2002; Sander & Shorvon, 1996). In childhood, adolescence, and early adulthood the most common causes for these disorders stem from congenital, developmental and genetic disorders. Throughout the literature, epilepsies stemming from genetic disorders are referred to as idiopathic while those without a determined etiology are termed cryptogenic epilepsies (J. W. Sander, 2003). As an individual ages, the most prevalent cause of epilepsy shifts to traumatic brain/head injuries (TBIs), CNS infection, and intracranial tumors (J. W. Sander, 2003). The cause of age-related increases in susceptibility for developing epilepsy following TBI or CNS infection remains to be fully understood.

Seizures

Seizures are characterized by dysregulation in electrophysiological homeostasis which elicit a sudden and excessive discharge of electrical activity. The spread of this pathophysiological synchrony may be defined by a single locus or spread in a more generalized manner throughout the cerebral hemispheres. These excessive neuronal discharges have been documented over the past 144 years since the discovery of electrical activity in the CNS. The etiology of these pathological, sustained, and synchronous activations of neural networks is multivariate. Seizure initiation has been associated with dysregulation of electrical activity, metabolism, blood flow, receptor trafficking, receptor functionality, gene activation, network connectivity or combinatorial

permutations of these physiological processes. The characteristic uncontrolled rhythmic convulsions often associated with seizure arise from the involuntary recruitment of the primary motor and association motor cortices. These aberrant muscle spasms are most prevalent in tonic-clonic seizures, but it should be noted that many seizure variants exhibit little to no involvement with motor functionality and therefore patients do not present any motor abnormalities. Epilepsy and seizure disorders are far from being fully understood.

While the literature contains a wealth of information on epilepsy and seizures, additional research needs to be conducted into seizure ictogenesis to aid in the development of novel therapeutics, computational and experimental models, and pathogenesis detection techniques. A more thorough understanding of the cellular and molecular mechanisms of seizure will indubitably result in better engineered systems for seizure detection and ultimately prevention. EEG systems are cumbersome to read. The inherent complexity of electrical activity in the brain and the subtle changes in physiology induced during seizure facilitate misinterpretation of data.

An EEG device measures population activity through strategically placed macroelectrodes on the scalp. The data produced by an EEG is a summation of excitatory and inhibitory postsynaptic potentials derived from neurons adjacent to the cortical surface whose signal is fed through one or more amplifiers. The electrical oscillations recorded have associations with specific brain functionality. Ictal activity is defined by rhythmic burst activity characterized by spike and wave waveforms or sharp waves of varying frequencies. Ictogenesis refers to the initiation of seizure and the resultant ictal

activity as visualized from an eletrophysiological recording. Conversely, periods of relative quiescence between ictal bursts is termed interictal activity yet high frequency interictal activity is correlated to ictal onset (Brázdil et al., 2010; Zijlmans et al., 2009). Electrical activity recorded just prior to seizure onset is referred to as preictal activity while the period immediately following seizure is referred to as postictal activity (Mula & Monaco, 2011). The duration of seizure captured on an EEG recording correlates to ictal activity and often abnormal spiking behavior is captured during the interictal phase, period between ictal discharges (Mula & Monaco, 2011). Long-term video EEG is standard of care for presurgical evaluation of pharmacoresistant focal epilepsies during which interical epileptiform and ictal activity are recorded (Rosenow & Lüders, 2001). Generally, EEG data permits epileptologists and other specialists to determine seizure propagation, severity and spread. These EEG and other electrophysiological recordings define the two main subtypes of seizure, generalized and focal. Generalized seizures propagate throughout the entire brain, whereas focal seizures occur in a localized brain region.

The two main subtypes of generalized seizure are absence and tonic-clonic. Absence seizures involve impaired awareness, staring into space and are often accompanied by automatisms, stereotyped and repetitive behaviors which manifest as rapid blinking, lip smacking, picking etc. Atypical absence seizures present a longer duration and involve a slower recovery.

Unlike absence seizures, tonic-clonic seizures may induce loss consciousness, an increase in muscle tonicity, incontinence, and muscle jerks or spasms. The increase in

muscle tonicity often creates a falling risk for patients with this seizure subtype. The nomenclature tonic-clonic references the two characteristic stages and the order in which they generally progress in patients and *in vivo* studies. The tonic stage exhibits muscle stiffness while the clonic phase induces the characteristic rhythmic convulsions (Conradsen et al., 2011; ILAE, 1981) that are often incorrectly generalized to all seizure disorders. Disruption in serotonin release by neurons in the midbrain raphe nuclei may provide insight into the postictal loss of consciousness and impaired cardiopulmonary function (Zhan et al., 2016). Serotonergic projections from the raphe nuclei stimulate breathing and arousal (Richerson & Buchanan, 2011; Zhan et al., 2016) and therefore may contribute to postictal cyanosis documented in tonic-clonic patients. Additionally, the postictal period of a tonic-clonic seizure often involves severe fatigue (Hamelin et al., 2010) and may include the aforementioned loss of consciousness and compromised respiration.

Focal seizures can be divided into multiple subtypes: partial complex seizures, partial simple seizures, and secondary generalized seizures (ILAE, 1981). The designation of partial refers to epileptogenesis occurring in a single locus and is contained within a single cerebral hemisphere, whereas generalized seizure spreads throughout the ipsilateral hemisphere and then propagates into the contralateral hemisphere. The partial versus generalized designation does not, however, reflect differences in the focal initiation of single seizure events. Partial complex seizures induce a state of confusion and/or disorientation which may precede auditory hallucinations, visual auras and/or a generalized fear response (Elallenger et al., 1983; Huff & Fountain,

2011). Patients presenting a partial complex seizure are unresponsive to external stimuli for the duration of the episode which ranges from seconds to minutes and often have no recollection of the event (Hermann et al., 1987). While recurrent collaterals in the temporal and frontal cortices make these areas prone to partial complex seizures, all brain regions are susceptible (Bains et al., 1999). The duration and symptoms of this seizure disorder are dependent upon the site of seizure generation and the affected cortical regions. Partial simple seizures evoke twitching or changes in somatosensation but do not terminate in loss of consciousness as with the generalized tonic-clonic seizures (O. Devinsky et al., 1989; Orrin Devinsky et al., 1988). Patients experiencing a partial simple seizure are awake, alert and retain the ability to recall events that occurred during the seizure. The patient may or may not be able to respond to external stimuli and, if present, the unresponsiveness will pass in less than two minutes. Postictal symptoms are usually non-existent.

Increased excitation in neural networks is a characteristic of epileptic seizures (Lytton, 2008). The pioneering work of Wilder Penfield and Herbert Jasper (Jasper & Penfield, 1949) documented this heightened excitatory behavior in cortical populations which ultimately spurred an enduring hypothesis of ictogenesis. This hypothesis suggests that pathologic hyperexcitation (Hall & Kuhlmann, 2013; Ursino & La Cara, 2006) is induced through a decrease in inhibition (Karnup & Stelzer, 1999; Sivakumaran et al., 2015). This traditional paradigm stoked great debate in the field of neuroelectrophysiology. This dogma cultured a myopic perspective into seizure initiation by researchers and clinicians for decades. While it is well documented that an increase in

inhibitory activity prior to seizure onset and a general increase in firing frequency of inhibitory interneurons persists throughout the duration of seizure (Lillis et al., 2012; Ziburkus et al., 2006), the epileptogenic mechanisms behind ictogenesis remain elusive. These paradigms often discount the modulatory mechanisms that microcircuit motifs, synaptic properties, intrinsic properties, and cell signaling contribute to excitation-inhibition balance (Bui et al., 2018; Paz & Huguenard, 2015; Shao et al., 2019). A paradigm shift in the field recontextualized the debate following advancements in research technologies and techniques. The current direction of the field is heavily biased towards mechanisms of seizure initiation, preventative therapies and treatment of epilepsy syndromes examined in a subtype specific manner. Indeed, novel research suggests a mechanism for inhibition-induced epileptiform activity (Avoli & de Curtis, 2011; González et al., 2018; Hamidi & Avoli, 2015; Lévesque et al., 2016). It is worth consideration that while the therapeutic value of antiepileptic drugs (AEDs) lay in their ability to reduce network hyperexcitation, the mechanisms of action are highly varied (Cook & Bensalem-Owen, 2011; Kwan et al., 2001).

A seizure state reflects an imbalance in ion dynamics. This imbalance in electrochemical homeostasis highlights the gamut of factors involved in ictogenesis. These factors include, but are not limited to, gene regulation, neural plasticity, microcircuitry, signaling cascades, cellular diversity, spatiotemporal dynamics, and synaptic reorganization (Engel, 1996; Noebels et al., 2010; Paz & Huguenard, 2015). A critical component in the reduction of network excitability in the CNS are gamma-aminobutyric acid (GABA) inputs. GABAergic interneurons release the neurotransmitter

GABA at the postsynaptic terminal which diffuses across the synaptic cleft to interact with ionotropic and metabotropic receptors on the presynaptic neuron. $GABA_A$ receptors require docking of two GABA molecules to induce a conformational change that permits the flux of both chloride and bicarbonate (Staley et al., 1995). In adulthood under physiological conditions, these channels influx chloride ions and efflux bicarbonate ions when activated (Rivera et al., 2005; M. Watanabe & Fukuda, 2015; Yamada et al., 2004). The hyperpolarization caused by the influx of chloride is counterbalanced by the depolarization from bicarbonate efflux. The significance of this interaction is that the depolarizing bicarbonate current maintains the hyperpolarizing reversal potential of chloride, thereby maintaining its inhibitory action (Tang, 2020). Epileptogenic mechanisms exploit the diversity, connectivity, distribution, trafficking, and density of GABAergic interneurons (Liu et al., 2014; Zhu et al., 2018). Dysfunction in feed-forward inhibition, feedback inhibition, counter inhibition in tandem to disruption in recurrent excitation has been implicated in epilepsy syndromes (Paz & Huguenard, 2015). In addition, GABAergic inputs contribute to oscillatory activity and network synchronization where enhanced GABAergic transmission promotes the spread of epileptiform activity to neighboring networks (Uhlhaas & Singer, 2006). Indeed, research into absence seizure induction suggests a role for GABAergic signaling via synchronized low frequency oscillations propagated through low-threshold calcium channels (Huguenard & Prince, 1994; McCormick & Williamson, 1989; Ulrich & Huguenard, 1996). The complexity of ictogenesis mirrors the diversity of seizure subtypes which reflect the underlying neuroanatomy. Advancement in epilepsy syndrome therapies and

pharmaceutical interventions must rely on a more targeted approach to account for the inherent complexity of both phenotype and mechanisms of seizure disorders.

Antiepileptic drugs are anticonvulsant medications administered to prevent epileptic seizures. These drugs enhance inhibition or reduce excitation by affecting the electrical properties of the neuron. This is accomplished through modification of sodium, potassium, chloride or calcium ion flux through ionotropic membrane channels. AEDs are successful in suppressing seizures in most patients, but it is recognized that several types of epilepsy have excellent outcomes independent of AED treatment. Twenty to thirty percent of patients with epilepsy will develop pharmacoresistant seizures (J. W. A. S. Sander, 1993). Misdiagnosis and mismanagement of care likely inflate the case incidence of refractory epilepsy. A study following newly diagnosed epilepsy patients reported that 20% received substandard care for their symptoms (Lhatoo et al., 2001). Proper care and prompt accurate diagnosis for epilepsy syndromes are critical as patients presenting uncontrolled epilepsy are at greater risk to perish from trauma, sudden unexpected death in epilepsy (SUDEP), and status epilepticus (Logroscino et al., 2002; Nilsson et al., 2002; Y. W. Wu et al., 2002).

4-aminopyridine (4AP) Model of Epilepsy & Potassium Channelopathies

There are many experimental models of epilepsy. These experimental models attempt to replicate the characteristics of human epilepsies and seizure disorders. These models provide critical data on the general and subtype specific mechanisms involved in epileptogenesis and ictogenesis. This research often guides future studies into novel

therapeutic targets. Chemoconvulsants utilize a pharmacological agent to induce either chronic or acute seizure. Agents that induce permanent, long-term seizure such as kanic acid, pilocarpine, and 4-aminopyridine produce a chronic seizure model. Agents that generate acute, transient, seizure include pentylenetetrazol (PTZ), strychnine, and N-methyl-D-aspartic acid (NMDA). These drug models often permit a high degree of cell-type specificity and exhibit a dose-dependent response. Electrical models of seizure are induced by direct electrical stimulation or electroshock—whole brain stimulation protocols. These models are low mortality with high reproducibility but exhibit no cell-type specificity. The kindling model induces seizure through repeated chemical or electrical insult. This phenomenon reflects a summation in priming events that culminate in a plateau of enhanced seizure activity. The posttraumatic seizure model measures mixed diffuse and focal brain insults. A fluid pressure pulse is induced via a fluid percussion device onto the dura mater mimicking a posttraumatic brain insult. This model is highly specific to research of posttraumatic epilepsy. The audiogenic seizure model usually involves a pure tone delivered at 100-120 dB until a seizure is evoked. The utility of this model ranges from studies exploring fragile X syndrome (S. E. Rotschafer & Razak, 2014; S. Rotschafer & Razak, 2013) to synaptic plasticity (Feng & Faingold, 2002). Hyperthermic or febrile seizures occur in about 5% of children. *In vivo*, *in vitro* and *ex vitro* hyperthermic models of seizure involve a transient increase in temperature within an immature organism or tissue. All these experimental seizure models are often employed to elucidate human epilepsy syndromes and therefore, it is of critical importance to understand their respective mechanisms of ictogenesis. The

chemoconvulsant models of epilepsy produce stereotypic epileptiform events *in vitro* and faithfully provoke status epilepticus proceeded by chronic recurrent seizures *in vivo*. These drugs are easy to acquire and not cost prohibitive for large research projects. 4-aminopyradine is one such proconvulsant and ideal for exploring the pathophysiology of hyperexcitable networks.

The organic molecule 4-aminopyridine, $C_5H_4N—NH_2$, is a versatile agent able to antagonize voltage-gated potassium (Kv) channels, and potentiate synaptic and neuromuscular transmission by targeting high voltage-activated calcium channels (HVACCs) (Basavappa et al., 1994; Z. Z. Wu et al., 2009). This potentiation is independent of the 4AP block of Kv channels. Indeed, this presynaptic potentiation is HVACC-subunit dependent (Li et al., 2014). Furthermore, it has been reported that millimolar 4AP concentrations indirectly stimulate HVACCs in Kv channel studies. 4AP is clinically administered as fampridine or dalfampridine to reduce motor deficits in multiple sclerosis, spinal cord injury, myasthenia gravis, and alleviate gait dysfunction in Parkinsonian patients (Li et al., 2014; Luca & Singer, 2013). Additionally, there is evidence for the administration of 4AP in the treatment of nerve crush injury (Clark et al., 2020). 4AP is significant to biomedical research as a commonly used chronic epilepsy model in animal studies (Avoli et al., 1996; D'Adamo et al., 2013; González et al., 2018; Hamidi & Avoli, 2015; Lévesque et al., 2013; Lopantsev & Avoli, 1998; Myers et al., 2018; Uva et al., 2015). 4AP is ubiquitous in epilepsy research. Therefore, characterization of evoked waveforms, impacts on ion dynamics and determination of mechanism are of critical importance.

The Kv family of voltage-gated potassium channels are pore-forming alpha subunits that have associations with various beta subunits that include Kv1, Kv2, Kv3, and Kv4 (Birnbaum et al., 2004; Carrasquillo et al., 2012). The subunits are classified based on sequence and function. In mammals, the Kv channel contains six transmembrane segments named S1-S6 with a pore-forming loop that contains K^+ ion selectivity between segments S5 and S6 (Bright & Sansom, 2004; Soler-Llavina et al., 2006). The predominant voltage-sensing domain is located on segment S4 (Sansom, 2000; Soler-Llavina et al., 2006). When the membrane potential changes, the voltage sensor located at S4 causes a conformational change that opens the pore (Sansom, 2000). The A-current (I_A) is generated by a transient A-type potassium channel, which constitutes the dominant potassium current in mature neurons (Keros & McBain, 1997). A combination of Kv4 subunits: Kv4.1, Kv4.2, and Kv4.3 allow the transient A-type potassium channels to function (Serôdio & Rudy, 1998). These Kv4 subunits are responsible for fast, transient A-type currents which demonstrate moderate sensitivity to 4AP (Shibata et al., 2000; Yuan et al., 2005). Epileptiform activity induced by 4AP consists of both A and D-currents (Hyun et al., 2013; Metz et al., 2007; Storm, 1987). However, I_A is more prevalent in the CNS than the slow inactivating dendrotoxin-sensitive transient currents (I_D).

Conditions that arise from dysfunction in potassium channels are well documented in humans (D'Adamo et al., 2013). These genetic or acquired defects are referred to as potassium channelopathies. The efflux of potassium through transient A-type potassium channels in neurons is hyperpolarizing and, in part, responsible for

maintaining the interspike interval and determining spike frequency (Mitterdorfer & Bean, 2002; Serôdio & Rudy, 1998). A defect in mechanisms that directly or indirectly affect I_A compromise the interspike interval. A reduction in I_A reduces hyperpolarizing currents leading to more depolarized membrane potentials which are more likely to surpass a threshold potential triggering more action potentials and higher firing rates (González et al., 2018; Myers et al., 2018; Segal et al., 1984). This effectively lowers spiking threshold and thus increases excitability in the neuron.

Kv4a subunit mutations, specifically truncation mutations in the Kv4.2a subunit, have been reported in some intractable TLE patients (D'Adamo et al., 2013; Singh et al., 2006). These mutations mimic the reduction of I_A by 4AP thereby priming the network towards a more hyperexcitable state. Biophysically realistic simulations suggest that I_A reduction alone is insufficient to induce epileptiform activity in an *in silico* model of 4AP-induced epilepsy (González et al., 2018). Furthermore, recent studies have explored 4AP-primed dynamics involving the neuronal KCC2 cotransporter in ictogenesis (Myers et al., 2018).

Ion Flux & Potassium-Chloride Cotransporter Isoform 2 (KCC2)

At the resting membrane potential (RMP), the intracellular potassium concentration is greater than the extracellular potassium concentration. After the rising phase of the action potential due to sodium influx, voltage-gated potassium channels efflux potassium ions decreasing the membrane potential (Hodgkin & Huxley, 1952). The influx of positively (or efflux of negatively) charged particles depolarizes the cell.

Conversely, the efflux of a positively (or influx of a negatively) charged particle repolarizes the cell. At the tripartite synapse, any transient increase in the extracellular potassium concentration affects the rate of the electrogenic Na/K ATPase and potassium buffering through the astrocytic syncytium. Indeed, disruption in potassium clearance through astrocytic inwardly rectifying Kir4.1 channels is involved in the pathogenesis of epilepsy syndromes (Haj-Yasein et al., 2011). The extracellular potassium concentration is maintained around 3.0 mM under physiologic conditions but pathological concentrations from 7.5-8.5 mM are sufficient to induce seizure (Korn et al., 1987; Traynelis & Dingledine, 1988).

Chloride ion dynamics also contribute to action potential and cell volume regulation (Okada, 1997). Chloride fluxes in response to its electrochemical gradients through channels thereby modulating the membrane potential. Chloride influx is gated predominantly by $GABA_A$ and glycine ionotropic receptors although many other mechanisms for chloride flux and transport are localized in the neuronal membrane (Roberts & Frankel, 1950). NKCC1 is a symporter that is highly expressed in neurons during development which maintains electroneutrality through influx of one sodium, one potassium and two chloride ions. In fact, pharmacological antagonism of NKCC1 receptors show no effect on ictal activity in adult rats yet abolishes ictal activity in P6-P7 mice (Hamidi & Avoli, 2015) suggesting a role for NKCC1 in ictogenesis throughout early development. However, the potassium-chloride cotransporter isoform 2 (KCC2) is highly expressed in adulthood and is functions to efflux one potassium and one chloride ion. Indeed, the reversal in expression levels of these membrane proteins during

development and adulthood is responsible for the depolarizing effect of GABA and glycine during development and their hyperpolarizing effect in adulthood (Achilles et al., 2007; M. Watanabe & Fukuda, 2015; Yamada et al., 2004). Additionally, volume regulated anion channels (VRACs) play a supportive roll in chloride and osmolyte transport into the extracellular space. The reversal potential for chloride (E_{Cl}) is near the RMP and leak conductance reversal potential therefore there is no electromotive force and no net flux of chloride ions at rest. The pathophysiology of dysfunctional chloride channels is highly debated in the literature. While intracellular concentrations of chloride increase by 7mM during seizure (Raimondo et al., 2015), experimental evidence refutes the prediction that an increase in chloride concentration alone is sufficient for ictogenesis (González et al., 2018).

KCC2 is a symporter that effluxes potassium and chloride in a one-to-one ratio into the extracellular space. KCC2 is one of a vast cation-chloride superfamily of proteins which is highly expressed around synapses and colocalized with $GABA_A$ receptors (Williams et al., 1999). As chloride floods the neuron following GABA release, KCC2 will efflux both potassium and chloride thereby increasing the extracellular potassium concentration. Therefore, KCC2 is dependent upon the influx of chloride through $GABA_A$ receptors and physiological fluctuations in extracellular potassium will affect the intracellular chloride concentration (Viitanen et al., 2010).

KCC2 is encoded by *SLC12A5* and associated with epilepsy syndromes. Missense mutations in *SLC12A5* manifest as idiopathic generalized epilepsy (Kahle et al., 2014) while *SLC12A5* loss-of-function studies exhibit epilepsy of infancy with migrating focal

seizures (EIMFS) (Stödberg et al., 2015). Recently, many studies advocate for the development of novel epilepsy therapeutics that target phosphorylation sites to modulate KCC2 activity (Kahle et al., 2013; Moore et al., 2019). It is imperative that mechanisms involved in KCC2 epileptogenesis be further teased apart prior to development of pharmaceutical intervention. Indeed, computational data suggest that an enhancement of KCC2 activity increases the duration of seizure and decreases seizure onset delay (González et al., 2018).

The role of KCC2 in epilepsy is well documented in humans yet the mechanism is highly debated in the literature. Indeed, pharmacological block of KCC2 abolishes ictal discharges and increases the average event number and frequency (Hamidi & Avoli, 2015; Myers et al., 2018). Moreover, KCC2 downregulation is observed following idiopathic epileptogenesis (Huberfeld et al., 2007). One argument for impaired inhibition during seizure onset suggests that dysfunction in KCC2 results in a rise in intracellular chloride during network hyperexcitability. This increase in intracellular chloride reduces the electromotive force on chloride influx thereby disrupting inhibition through depolarizing $GABA_A$ currents. This hypothesis proposes that these diminished hyperpolarizing currents result in ictogenesis. Conversely, recent studies show that optogenetic stimulation of PV and SOM-positive interneurons perfused in 4AP induce ictal discharges (González et al., 2018; Yekhlef et al., 2015). Furthermore, pharmacological enhancement of KCC2 increases the duration of ictal discharges (Hamidi & Avoli, 2015). Recent studies suggest that a sustained increase in extracellular potassium through KCC2 efflux induces ictogenesis (González et al., 2018). The

observed postictal reduction of KCC2 is likely a homeostatic mechanism to compensate for the increase in $GABA_A$ and KCC2 activity.

Optical Coherence Tomography (OCT)

OCT is a high-resolution imaging technique, like ultrasound, that is increasingly used in clinical practice and emergency diagnosis of disease (Böhringer et al., 2009; Giese et al., 2006; Tsai & Yi Chiou, 2019; H. Watanabe et al., 2011). Over the last decade, OCT has been instrumental in the study of neurodegenerative diseases and continues to advance translational medicine (Bernardes et al., 2020; Frohman et al., 2009; Morgia et al., 2017). There are numerous reports using OCT to measure the degeneration of tissue within the retina, colon, and integument, yet physiological studies remain elusive despite the high temporal and depth resolutions of the technique (Bouma et al., 2000; Ferrante di Ruffano et al., 2018; Kim et al., 2019; Sivak et al., 2000). OCT has an inversely proportional relationship between the transmittance of near-infrared light and optical attenuation. Optical attenuation coefficients can distinguish between physiological and edematous tissues (de Bruin et al., 2016; Van der Meer et al., 2010). These differences in reflectance are presumably due to changes in cell volume. Computational and experimental studies suggest that neurons swell under both physiological and pathological circumstances including seizure (Hübel & Ullah, 2016; Rungta et al., 2015). Spectral domain OCT (SD-OCT) can detect reflectance changes characteristic of seizure propagation in generalized seizures (Eberle et al., 2012, 2015). It is evident that intractable epilepsies require precise localization of epileptic foci and accurate placement

of surgical instrumentation. Novel targeted and minimally invasive strategies are necessary for prevention and treatment of refractory seizure disorders.

Ninety-seven years after epileptiform spikes were first characterized during clinical seizure, epileptologists continue to rely primarily on surface electrodes recording population activity to diagnosis seizure disorders despite technological advancements in translational medicine. OCT probes are currently employed in clinical settings to detect histopathological conditions in patients (Sivak et al., 2000). Portable OCT devices bring micron-level diagnostic capabilities to the bedside, yet barriers include complexity of data interpretation and cost. The development of machine learning algorithms capable of real-time analysis and interpretation of OCT output suggest the technology may be pivotal in next generation bedside seizure detection and prevention.

References

Achilles, K., Okabe, A., Ikeda, M., Shimizu-Okabe, C., Yamada, J., Fukuda, A., Luhmann, H. J., & Kilb, W. (2007). Kinetic properties of Cl- uptake mediated by Na +-dependent K+-2Cl- cotransport in immature rat neocortical neurons. *Journal of Neuroscience*. https://doi.org/10.1523/JNEUROSCI.5041-06.2007

Avoli, M., Barbarosle, M., Lücke, A., Nagao, T., Lopantsev, V., & Köhling, R. (1996). Synchronous GABA-mediated potentials and epileptiform discharges in the rat limbic system in vitro. *Journal of Neuroscience*. https://doi.org/10.1523/jneurosci.16-12-03912.1996

Avoli, M., & de Curtis, M. (2011). GABAergic synchronization in the limbic system and its role in the generation of epileptiform activity. In *Progress in Neurobiology*. https://doi.org/10.1016/j.pneurobio.2011.07.003

Bains, J. S., Longacher, J. M., & Staley, K. J. (1999). Reciprocal interactions between CA3 network activity and strength of recurrent collateral synapses. *Nature Neuroscience*. https://doi.org/10.1038/11184

Basavappa, S., Romano-Silva, M. A., Mangel, A. W., Laro, D., Campbell, L., & Brammer, M. (1994). Inhibition of K+ channel activity by 4-AP stimulates N-type Ca2+ channels in CHP-100 cells. *NeuroReport*. https://doi.org/10.1097/00001756-199406020-00025

Bell, G. S., & Sander, J. W. (2002). The epidemiology of epilepsy: The size of the problem. *Seizure*, *11*(SUPPL. A).

Bernardes, R., Jorge, L., Nunes, A., & Castelo-Branco, M. (2020). Machine learning approaches in OCT: Application to neurodegenerative disorders. In *OCT and Imaging in Central Nervous System Diseases: The Eye as a Window to the Brain: Second Edition*. https://doi.org/10.1007/978-3-030-26269-3_23

Birnbaum, S. G., Varga, A. W., Yuan, L. L., Anderson, A. E., Sweatt, J. D., & Schrader, L. A. (2004). Structure and function of Kv4-family transient potassium channels. In *Physiological Reviews*. https://doi.org/10.1152/physrev.00039.2003

Böhringer, H. J., Lankenau, E., Stellmacher, F., Reusche, E., Hüttmann, G., & Giese, A. (2009). Imaging of human brain tumor tissue by near-infrared laser coherence tomography. *Acta Neurochirurgica*. https://doi.org/10.1007/s00701-009-0248-y

Bouma, B. E., Tearney, G. J., Compton, C. C., & Nishioka, N. S. (2000). High-resolution imaging of the human esophagus and stomach in vivo using optical coherence tomography. *Gastrointestinal Endoscopy*. https://doi.org/10.1016/S0016-5107(00)70449-4

Brázdil, M., Halámek, J., Jurák, P., Daniel, P., Kuba, R., Chrastina, J., Novák, Z., & Rektor, I. (2010). Interictal high-frequency oscillations indicate seizure onset zone in patients with focal cortical dysplasia. *Epilepsy Research*, *90*(1–2). https://doi.org/10.1016/j.eplepsyres.2010.03.003

Bright, J. N., & Sansom, M. S. P. (2004). Kv channel S6 helix as a molecular switch: Simulation studies. *IEE Proceedings Nanobiotechnology*. https://doi.org/10.1049/ip-nbt:20040101

Bui, A. D., Nguyen, T. M., Limouse, C., Kim, H. K., Szabo, G. G., Felong, S., Maroso, M., & Soltesz, I. (2018). Dentate gyrus mossy cells control spontaneous convulsive seizures and spatial memory. *Science*, *359*(6377). https://doi.org/10.1126/science.aan4074

Carrasquillo, Y., Burkhalter, A., & Nerbonne, J. M. (2012). A-type K+ channels encoded by Kv4.2, Kv4.3 and Kv1.4 differentially regulate intrinsic excitability of cortical pyramidal neurons. *Journal of Physiology*. https://doi.org/10.1113/jphysiol.2012.229013

Clark, A., Hsu, C., Hassan Talukder, M., Noble, M., & Elfar, J. (2020). Transdermal delivery of 4-aminopyridine accelerates motor functional recovery and improves nerve morphology following sciatic nerve crush injury in mice. *Neural Regeneration Research*. https://doi.org/10.4103/1673-5374.264471

Conradsen, I., Wolf, P., Sams, T., Sorensen, H. B. D., & Beniczky, S. (2011). Patterns of muscle activation during generalized tonic and tonic-clonic epileptic seizures. *Epilepsia*. https://doi.org/10.1111/j.1528-1167.2011.03286.x

Cook, A. M., & Bensalem-Owen, M. K. (2011). Mechanisms of action of antiepileptic drugs. In *Therapy*. https://doi.org/10.2217/thy.11.19

D'Adamo, M. C., Catacuzzeno, L., di Giovanni, G., Franciolini, F., & Pessia, M. (2013). K+ channelepsy: Progress in the neurobiology of potassium channels and epilepsy. In *Frontiers in Cellular Neuroscience*. https://doi.org/10.3389/fncel.2013.00134

de Bruin, D. M., Broekgaarden, M., van Gemert, M. J. C., Heger, M., de la Rosette, J. J., Van Leeuwen, T. G., & Faber, D. J. (2016). Assesment of apoptosis induced changes in scattering using optical coherence tomography. *Journal of Biophotonics*. https://doi.org/10.1002/jbio.201500198

Devinsky, O., Sato, S., Kufta, C. V., Ito, B., Rose, D. F., Theodore, W. H., & Porter, R. J. (1989). Electroencephalographic studies of simple partial seizures with subdural electrode recordings. *Neurology*. https://doi.org/10.1212/wnl.39.4.527

Devinsky, Orrin, Kelley, K., Porter, R. J., & Theodore, W. H. (1988). Clinical and electroencephalographic features of simple partial seizures. *Neurology*. https://doi.org/10.1212/wnl.38.9.1347

Eberle, M. M., Hsu, M. S., Rodriguez, C. L., Szu, J. I., Oliveira, M. C., Binder, D. K., & Park, B. H. (2015). Localization of cortical tissue optical changes during seizure activity in vivo with optical coherence tomography. *Biomedical Optics Express*. https://doi.org/10.1364/boe.6.001812

Eberle, M. M., Reynolds, C. L., Szu, J. I., Wang, Y., Hansen, A. M., Hsu, M. S., Islam, M. S., Binder, D. K., & Park, B. H. (2012). In vivo detection of cortical optical changes associated with seizure activity with optical coherence tomography. *Biomedical Optics Express*. https://doi.org/10.1364/boe.3.002700

Elallenger, C. E., King, D. W., & Gallagher, B. B. (1983). Partial complex status epilepticus. *Neurology*. https://doi.org/10.1212/wnl.33.12.1545

Engel, J. (1996). Excitation and inhibition in epilepsy. In *Canadian Journal of Neurological Sciences* (Vol. 23, Issue 3). https://doi.org/10.1017/S0317167100038464

Feng, H. J., & Faingold, C. L. (2002). Synaptic plasticity in the pathway from the medial geniculate body to the lateral amygdala is induced by seizure repetition. *Brain Research*.

https://doi.org/10.1016/S0006-8993(02)02884-6
Ferrante di Ruffano, L., Dinnes, J., Deeks, J. J., Chuchu, N., Bayliss, S. E., Davenport, C., Takwoingi, Y., Godfrey, K., O'sullivan, C., Matin, R. N., Tehrani, H., & Williams, H. C. (2018). Optical coherence tomography for diagnosing skin cancer in adults. In *Cochrane Database of Systematic Reviews*. https://doi.org/10.1002/14651858.CD013189
Frohman, E. M., Fujimoto, J. G., Frohman, T. C., Calabresi, P. A., Cutter, G., & Balcer, L. J. (2009). Optical Coherence Tomography : A Window Into the Mechanisms of Multiple Sclerosis Optical Coherence Tomography : A Window Into MS The Eye as a Model of Neurodegeneration. *Nature Clinical Practice. Neurology*.
Gaitatzis, A., Purcell, B., Carroll, K., Sander, J. W. A. S., & Majeed, A. (2002). Differences in the use of health services among people with and without epilepsy in the United Kingdom: Socio-economic and disease-specific determinants. *Epilepsy Research*, *50*(3). https://doi.org/10.1016/S0920-1211(02)00031-1
Giese, A., Böhringer, H. J., Leppert, J., Kantelhardt, S. R., Lankenau, E., Koch, P., Birngruber, R., & Hüttmann, G. (2006). Non-invasive intraoperative optical coherence tomography of the resection cavity during surgery of intrinsic brain tumors. *Photonic Therapeutics and Diagnostics II*. https://doi.org/10.1117/12.674436
González, O. C., Shiri, Z., Krishnan, G. P., Myers, T. L., Williams, S., Avoli, M., & Bazhenov, M. (2018). Role of KCC2-dependent potassium efflux in 4-Aminopyridine-induced Epileptiform synchronization. *Neurobiology of Disease*. https://doi.org/10.1016/j.nbd.2017.10.011
Haj-Yasein, N. N., Jensen, V., Vindedal, G. F., Gundersen, G. A., Klungland, A., Ottersen, O. P., Hvalby, Ø., & Nagelhus, E. A. (2011). Evidence that compromised K + spatial buffering contributes to the epileptogenic effect of mutations in the human kir4.1 gene (KCNJ10). *GLIA*. https://doi.org/10.1002/glia.21205
Hall, D., & Kuhlmann, L. (2013). Mechanisms of Seizure Propagation in 2-Dimensional Centre-Surround Recurrent Networks. *PLoS ONE*, *8*(8). https://doi.org/10.1371/journal.pone.0071369
Hamelin, S., Kahane, P., & Vercueil, L. (2010). Fatigue in epilepsy: A prospective inter-ictal and post-ictal survey. *Epilepsy Research*. https://doi.org/10.1016/j.eplepsyres.2010.07.006
Hamidi, S., & Avoli, M. (2015). KCC2 function modulates in vitro ictogenesis. *Neurobiology of Disease*. https://doi.org/10.1016/j.nbd.2015.04.006
Heaney, D. C., MacDonald, B. K., Everitt, A., Stevenson, S., Leonardi, G. S., Wilkinson, P., & Sander, J. W. (2002). Socioeconomic variation in incidence of epilepsy: Prospective community based study in south east England. *British Medical Journal*, *325*(7371). https://doi.org/10.1136/bmj.325.7371.1013
Hermann, B. P., Wyler, A. R., Richey, E. T., & Rea, J. M. (1987). Memory Function and Verbal Learning Ability in Patients with Complex Partial Seizures of Temporal Lobe Origin. *Epilepsia*. https://doi.org/10.1111/j.1528-1157.1987.tb03687.x
Hodgkin, A. L., & Huxley, A. F. (1952). Currents carried by sodium and potassium ions through the membrane of the giant axon of Loligo. *The Journal of Physiology*. https://doi.org/10.1113/jphysiol.1952.sp004717
Hübel, N., & Ullah, G. (2016). Anions govern cell volume: A case study of relative astrocytic and neuronal swelling in spreading depolarization. *PLoS ONE*. https://doi.org/10.1371/journal.pone.0147060
Huberfeld, G., Wittner, L., Clemenceau, S., Baulac, M., Kaila, K., Miles, R., & Rivera, C. (2007). Perturbed chloride homeostasis and GABAergic signaling in human temporal lobe epilepsy. *Journal of Neuroscience*. https://doi.org/10.1523/JNEUROSCI.2761-07.2007
Huff, J. S., & Fountain, N. B. (2011). Pathophysiology and Definitions of Seizures and Status Epilepticus. In *Emergency Medicine Clinics of North America*. https://doi.org/10.1016/j.emc.2010.08.001
Huguenard, J. R., & Prince, D. A. (1994). Intrathalamic rhythmicity studied in vitro: Nominal T-current modulation causes robust antioscillatory effects. *Journal of Neuroscience*, *14*(9). https://doi.org/10.1523/jneurosci.14-09-05485.1994
Hyun, J. H., Eom, K., Lee, K. H., Ho, W. K., & Lee, S. H. (2013). Activity-dependent downregulation of D-type K+ channel subunit Kv1.2 in rat hippocampal CA3 pyramidal neurons. *Journal of Physiology*. https://doi.org/10.1113/jphysiol.2013.259002
ILAE. (1981). Proposal for Revised Clinical and Electroencephalographic Classification of Epileptic

Seizures. *Epilepsia*. https://doi.org/10.1111/j.1528-1157.1981.tb06159.x
Jasper, H., & Penfield, W. (1949). Electrocorticograms in man: Effect of voluntary movement upon the electrical activity of the precentral gyrus. *Archiv Für Psychiatrie Und Nervenkrankheiten*. https://doi.org/10.1007/BF01062488
Kahle, K. T., Deeb, T. Z., Puskarjov, M., Silayeva, L., Liang, B., Kaila, K., & Moss, S. J. (2013). Modulation of neuronal activity by phosphorylation of the K-Cl cotransporter KCC2. In *Trends in Neurosciences*. https://doi.org/10.1016/j.tins.2013.08.006
Kahle, K. T., Merner, N. D., Friedel, P., Silayeva, L., Liang, B., Khanna, A., Shang, Y., Lachance-Touchette, P., Bourassa, C., Levert, A., Dion, P. A., Walcott, B., Spiegelman, D., Dionne-Laporte, A., Hodgkinson, A., Awadalla, P., Nikbakht, H., Majewski, J., Cossette, P., … Rouleau, G. A. (2014). Genetically encoded impairment of neuronal KCC 2 cotransporter function in human idiopathic generalized epilepsy . *EMBO Reports*. https://doi.org/10.15252/embr.201438840
Karnup, S., & Stelzer, A. (1999). Temporal overlap of excitatory and inhibitory afferent input in guinea-pig CA1 pyramidal cells. *Journal of Physiology*, *516*(2). https://doi.org/10.1111/j.1469-7793.1999.0485v.x
Keros, S., & McBain, C. J. (1997). Arachidonic acid inhibits transient potassium currents and broadens action potentials during electrographic seizures in hippocampal pyramidal and inhibitory interneurons. *Journal of Neuroscience*. https://doi.org/10.1523/jneurosci.17-10-03476.1997
Kim, K., Kim, E. S., Kim, D. G., & Yu, S. Y. (2019). Progressive retinal neurodegeneration and microvascular change in diabetic retinopathy: longitudinal study using OCT angiography. *Acta Diabetologica*. https://doi.org/10.1007/s00592-019-01395-6
Korn, S. J., Giacchino, J. L., Chamberlin, N. L., & Dingledine, R. (1987). Epileptiform burst activity induced by potassium in the hippocampus and its regulation by GABA-mediated inhibition. *Journal of Neurophysiology*. https://doi.org/10.1152/jn.1987.57.1.325
Kotsopoulos, I. A. W., Van Merode, T., Kessels, F. G. H., De Krom, M. C. T. F. M., & Knottnerus, J. A. (2002). Systematic review and meta-analysis of incidence studies of epilepsy and unprovoked seizures. *Epilepsia*, *43*(11). https://doi.org/10.1046/j.1528-1157.2002.t01-1-26901.x
Kwan, P., Sills, G. J., & Brodie, M. J. (2001). The mechanisms of action of commonly used antiepileptic drugs. In *Pharmacology and Therapeutics*. https://doi.org/10.1016/S0163-7258(01)00122-X
Lévesque, M., Herrington, R., Hamidi, S., & Avoli, M. (2016). Interneurons spark seizure-like activity in the entorhinal cortex. *Neurobiology of Disease*. https://doi.org/10.1016/j.nbd.2015.12.011
Lévesque, M., Salami, P., Behr, C., & Avoli, M. (2013). Temporal lobe epileptiform activity following systemic administration of 4-aminopyridine in rats. *Epilepsia*. https://doi.org/10.1111/epi.12041
Lhatoo, S. D., Sander, J. W. A. S., & Shorvon, S. D. (2001). The dynamics of drug treatment in epilepsy: An observational study in an unselected population based cohort with newly diagnosed epilepsy followed up prospectively over 11-14 years. *Journal of Neurology Neurosurgery and Psychiatry*, *71*(5). https://doi.org/10.1136/jnnp.71.5.632
Li, L., Li, D. P., Chen, S. R., Chen, J., Hu, H., & Pan, H. L. (2014). Potentiation of high voltage-activated calcium channels by 4-Aminopyridine depends on subunit composition. *Molecular Pharmacology*. https://doi.org/10.1124/mol.114.095505
Lillis, K. P., Kramer, M. A., Mertz, J., Staley, K. J., & White, J. A. (2012). Pyramidal cells accumulate chloride at seizure onset. *Neurobiology of Disease*, *47*(3). https://doi.org/10.1016/j.nbd.2012.05.016
Lindsten, H., Stenlund, H., Edlund, C., & Forsgren, L. (2002). Socioeconomic prognosis after a newly diagnosed unprovoked epileptic seizure in adults: A population-based case-control study. *Epilepsia*, *43*(10). https://doi.org/10.1046/j.1528-1157.2002.51101.x
Liu, Y. Q., Yu, F., Liu, W. H., He, X. H., & Peng, B. W. (2014). Dysfunction of hippocampal interneurons in epilepsy. In *Neuroscience Bulletin* (Vol. 30, Issue 6). https://doi.org/10.1007/s12264-014-1478-4
Logroscino, G., Hesdorffer, D. C., Cascino, G. D., Annegers, J. F., Bagiella, E., & Hauser, W. A. (2002). Long-term mortality after a first episode of status epilepticus. *Neurology*, *58*(4). https://doi.org/10.1212/WNL.58.4.537
Lopantsev, V., & Avoli, M. (1998). Participation of GABA(A)-mediated inhibition in ictallike discharges in the rat entorhinal cortex. *Journal of Neurophysiology*. https://doi.org/10.1152/jn.1998.79.1.352
Luca, C. C., & Singer, C. (2013). 4-Aminopyridine improves freezing of gait in Parkinson's disease. In

Journal of Neurology. https://doi.org/10.1007/s00415-013-7090-0
Lytton, W. W. (2008). Computer modelling of epilepsy. In *Nature Reviews Neuroscience* (Vol. 9, Issue 8). https://doi.org/10.1038/nrn2416
MacDonald, B. K., Cockerell, O. C., Sander, J. W. A. S., & Shorvon, S. D. (2000). The incidence and lifetime prevalence of neurological disorders in a prospective community-based study in the UK. *Brain*, *123*(4). https://doi.org/10.1093/brain/123.4.665
McCormick, D. A., & Williamson, A. (1989). Convergence and divergence of neurotransmitter action in human cerebral cortex. *Proceedings of the National Academy of Sciences of the United States of America*, *86*(20). https://doi.org/10.1073/pnas.86.20.8098
Metz, A. E., Spruston, N., & Martina, M. (2007). Dendritic D-type potassium currents inhibit the spike afterdepolarization in rat hippocampal CA1 pyramidal neurons. *Journal of Physiology*. https://doi.org/10.1113/jphysiol.2006.127068
Mitterdorfer, J., & Bean, B. P. (2002). Potassium currents during the action potential of hippocampal CA3 neurons. *Journal of Neuroscience*. https://doi.org/10.1523/jneurosci.22-23-10106.2002
Moore, Y. E., Conway, L. C., Wobst, H. J., Brandon, N. J., Deeb, T. Z., & Moss, S. J. (2019). Developmental Regulation of KCC2 Phosphorylation Has Long-Term Impacts on Cognitive Function. *Frontiers in Molecular Neuroscience*. https://doi.org/10.3389/fnmol.2019.00173
Morgia, C. La, di Vito, L., Carelli, V., & Carbonelli, M. (2017). Patterns of retinal ganglion cell damage in neurodegenerative disorders: Parvocellular vs magnocellular degeneration in optical coherence tomography studies. In *Frontiers in Neurology*. https://doi.org/10.3389/fneur.2017.00710
Mula, M., & Monaco, F. (2011). Ictal and peri-ictal psychopathology. *Behavioural Neurology*, *24*(1). https://doi.org/10.3233/BEN-2011-0314
Myers, T., C Gonzalez, O., B Stein, J., & Bazhenov, M. (2018). Characterizing Concentration-Dependent Neural Dynamics of 4-Aminopyridine-Induced Epileptiform Activity. *Epilepsy Journal*. https://doi.org/10.4172/2472-0895.1000128
Nilsson, L., Ahlbom, A., Farahmand, B. Y., Åsberg, M., & Tomson, T. (2002). Risk factors for suicide in epilepsy: A case control study. *Epilepsia*, *43*(6). https://doi.org/10.1046/j.1528-1157.2002.40001.x
Noebels, J. L., Avoli, M., Rogawski, M., Olsen, R., & Delgado-Escueta, A. V. (2010). "Jasper's basic mechanisms of the epilepsies" workshop. *Epilepsia*, *51*(SUPPL. 5). https://doi.org/10.1111/j.1528-1167.2010.02792.x
Okada, Y. (1997). Volume expansion-sensing outward-rectifier Cl- channel: Fresh start to the molecular identity and volume sensor. In *American Journal of Physiology - Cell Physiology*. https://doi.org/10.1152/ajpcell.1997.273.3.c755
Olafsson, E., & Hauser, W. A. (1999). Prevalence of epilepsy in rural Iceland: A population-based study. *Epilepsia*, *40*(11). https://doi.org/10.1111/j.1528-1157.1999.tb02036.x
Paz, J. T., & Huguenard, J. R. (2015). Microcircuits and their interactions in epilepsy: Is the focus out of focus? *Nature Neuroscience*, *18*(3). https://doi.org/10.1038/nn.3950
Placencia, M., Shorvon, S. D., Paredes, V., Bimos, C., Sander, J. W. A. S., Suarez, J., & Cascante, S. M. (1992). Epileptic seizures in an andean region of ecuador: Incidence and prevalence and regional variation. *Brain*, *115*(3). https://doi.org/10.1093/brain/115.3.771
Raimondo, J. V., Burman, R. J., Katz, A. A., & Akerman, C. J. (2015). Ion dynamics during seizures. In *Frontiers in Cellular Neuroscience*. https://doi.org/10.3389/fncel.2015.00419
Richerson, G. B., & Buchanan, G. F. (2011). The serotonin axis: Shared mechanisms in seizures, depression, and SUDEP. *Epilepsia*. https://doi.org/10.1111/j.1528-1167.2010.02908.x
Rivera, C., Voipio, J., & Kaila, K. (2005). Two developmental switches in GABAergic signalling: The K+-Cl- cotransporter KCC2 and carbonic anhydrase CAVII. *Journal of Physiology*. https://doi.org/10.1113/jphysiol.2004.077495
Roberts, E., & Frankel, S. (1950). gamma-Aminobutyric acid in brain: its formation from glutamic acid. *The Journal of Biological Chemistry*. https://doi.org/10.1016/S0021-9258(19)50929-2
Rocca, W. A., Savettieri, G., Anderson, D. W., Meneghini, F., Grigoletto, F., Morgante, L., Reggio, A., Salemi, G., Patti, F., & Di Perri, R. (2001). Door-to-door prevalence survey of epilepsy in three sicilian municipalities. *Neuroepidemiology*, *20*(4). https://doi.org/10.1159/000054796
Rosenow, F., & Lüders, H. (2001). Presurgical evaluation of epilepsy. In *Brain* (Vol. 124, Issue 9).

https://doi.org/10.1093/brain/124.9.1683
Rotschafer, S. E., & Razak, K. A. (2014). Auditory processing in fragile X syndrome. In *Frontiers in Cellular Neuroscience*. https://doi.org/10.3389/fncel.2014.00019
Rotschafer, S., & Razak, K. (2013). Altered auditory processing in a mouse model of fragile X syndrome. *Brain Research*. https://doi.org/10.1016/j.brainres.2013.02.038
Rungta, R. L., Choi, H. B., Tyson, J. R., Malik, A., Dissing-Olesen, L., Lin, P. J. C., Cain, S. M., Cullis, P. R., Snutch, T. P., & Macvicar, B. A. (2015). The cellular mechanisms of neuronal swelling underlying cytotoxic edema. *Cell*. https://doi.org/10.1016/j.cell.2015.03.029
Sander, J. W. (2003). The epidemiology of epilepsy revisited. In *Current Opinion in Neurology* (Vol. 16, Issue 2). https://doi.org/10.1097/00019052-200304000-00008
Sander, J. W. A. S. (1993). Some Aspects of Prognosis in the Epilepsies: A Review. *Epilepsia*. https://doi.org/10.1111/j.1528-1157.1993.tb02126.x
Sander, & Shorvon, S. D. (1996). Epidemiology of the epilepsies. In *Journal of Neurology Neurosurgery and Psychiatry* (Vol. 61, Issue 5). https://doi.org/10.1136/jnnp.61.5.433
Sansom, M. S. P. (2000). Potassium channels: Watching a voltage-sensor tilt and twist. In *Current Biology*. https://doi.org/10.1016/S0960-9822(00)00354-7
Segal, M., Rogawski, M. A., & Barker, J. L. (1984). A transient potassium conductance regulates the excitability of cultured hippocampal and spinal neurons. *Journal of Neuroscience*. https://doi.org/10.1523/jneurosci.04-02-00604.1984
Serôdio, P., & Rudy, B. (1998). Differential expression of Kv4 K+ channel subunits mediating subthreshold transient K+ (A-type) currents in rat brain. *Journal of Neurophysiology*. https://doi.org/10.1152/jn.1998.79.2.1081
Shao, L.-R., Habela, C. W., & Stafstrom, C. E. (2019). Pediatric Epilepsy Mechanisms: Expanding the Paradigm of Excitation/Inhibition Imbalance. *Children*, *6*(2). https://doi.org/10.3390/children6020023
Shibata, R., Nakahira, K., Shibasaki, K., Wakazono, Y., Imoto, K., & Ikenaka, K. (2000). A-type K+ current mediated by the Kv4 channel regulates the generation of action potential in developing cerebellar granule cells. *Journal of Neuroscience*. https://doi.org/10.1523/jneurosci.20-11-04145.2000
Singh, B., Ogiwara, I., Kaneda, M., Tokonami, N., Mazaki, E., Baba, K., Matsuda, K., Inoue, Y., & Yamakawa, K. (2006). A Kv4.2 truncation mutation in a patient with temporal lobe epilepsy. *Neurobiology of Disease*. https://doi.org/10.1016/j.nbd.2006.07.001
Sivak, M. V., Kobayashi, K., Izatt, J. A., Rollins, A. M., Ung-runyawee, R., Chak, A., Wong, R. C. K., Isenberg, G. A., & Willis, J. (2000). High-resolution endoscopic imaging of the GI tract using optical coherence tomography. *Gastrointestinal Endoscopy*. https://doi.org/10.1016/S0016-5107(00)70450-0
Sivakumaran, S., Cardarelli, R. A., Maguire, J., Kelley, M. R., Silayeva, L., Morrow, D. H., Mukherjee, J., Moore, Y. E., Mather, R. J., Duggan, M. E., Brandon, N. J., Dunlop, J., Zicha, S., Moss, S. J., & Deeb, T. Z. (2015). Selective inhibition of KCC2 leads to hyperexcitability and epileptiform discharges in hippocampal slices and in vivo. *Journal of Neuroscience*, *35*(21). https://doi.org/10.1523/JNEUROSCI.5205-14.2015
Soler-Llavina, G. J., Chang, T. H., & Swartz, K. J. (2006). Functional Interactions at the Interface between Voltage-Sensing and Pore Domains in the Shaker Kv Channel. *Neuron*. https://doi.org/10.1016/j.neuron.2006.10.005
Staley, K. J., Soldo, B. L., & Proctor, W. R. (1995). Ionic mechanisms of neuronal excitation by inhibitory GABAA receptors. *Science*. https://doi.org/10.1126/science.7638623
Stödberg, T., McTague, A., Ruiz, A. J., Hirata, H., Zhen, J., Long, P., Farabella, I., Meyer, E., Kawahara, A., Vassallo, G., Stivaros, S. M., Bjursell, M. K., Stranneheim, H., Tigerschiöld, S., Persson, B., Bangash, I., Das, K., Hughes, D., Lesko, N., … Kurian, M. A. (2015). Mutations in SLC12A5 in epilepsy of infancy with migrating focal seizures. *Nature Communications*. https://doi.org/10.1038/ncomms9038
Storm, J. F. (1987). Action potential repolarization and a fast after-hyperpolarization in rat hippocampal pyramidal cells. *The Journal of Physiology*. https://doi.org/10.1113/jphysiol.1987.sp016517
Tang, X. (2020). Neuronal Chloride Transporters in Health and Disease. In *Neuronal Chloride*

Transporters in Health and Disease. https://doi.org/10.1016/c2017-0-02771-4
Traynelis, S. F., & Dingledine, R. (1988). Potassium-induced spontaneous electrographic seizures in the rat hippocampal slice. *Journal of Neurophysiology*. https://doi.org/10.1152/jn.1988.59.1.259
Tsai, T. Y., & Yi Chiou, D. (2019). An OCT-enable Minimally-invasive Neurosurgical Guide for in-situ Brain Monitoring. *ICIIBMS 2019 - 4th International Conference on Intelligent Informatics and Biomedical Sciences*. https://doi.org/10.1109/ICIIBMS46890.2019.8991485
Uhlhaas, P. J., & Singer, W. (2006). Neural Synchrony in Brain Disorders: Relevance for Cognitive Dysfunctions and Pathophysiology. In *Neuron* (Vol. 52, Issue 1). https://doi.org/10.1016/j.neuron.2006.09.020
Ulrich, D., & Huguenard, J. R. (1996). γ-Aminobutyric acid type B receptor-dependent burst-firing in thalamic neurons: A dynamic clamp study. *Proceedings of the National Academy of Sciences of the United States of America*, *93*(23). https://doi.org/10.1073/pnas.93.23.13245
Ursino, M., & La Cara, G. E. (2006). Travelling waves and EEG patterns during epileptic seizure: Analysis with an integrate-and-fire neural network. *Journal of Theoretical Biology*, *242*(1). https://doi.org/10.1016/j.jtbi.2006.02.012
Uva, L., Breschi, G. L., Gnatkovsky, V., Taverna, S., & de Curtis, M. (2015). Synchronous inhibitory potentials precede seizure-like events in acute models of focal limbic seizures. *Journal of Neuroscience*. https://doi.org/10.1523/JNEUROSCI.3692-14.2015
Van der Meer, F. J., Faber, D. J., Aalders, M. C. G., Poot, A. A., Vermes, I., & Van Leeuwen, T. G. (2010). Apoptosis- and necrosis-induced changes in light attenuation measured by optical coherence tomography. *Lasers in Medical Science*. https://doi.org/10.1007/s10103-009-0723-y
Viitanen, T., Ruusuvuori, E., Kaila, K., & Voipio, J. (2010). The K+-Cl- cotransporter KCC2 promotes GABAergic excitation in the mature rat hippocampus. *Journal of Physiology*. https://doi.org/10.1113/jphysiol.2009.181826
Watanabe, H., Rajagopalan, U. M., Nakamichi, Y., Igarashi, K. M., Kadono, H., & Tanifuji, M. (2011). Swept source optical coherence tomography as a tool for real time visualization and localization of electrodes used in electrophysiological studies of brain in vivo. *Biomedical Optics Express*. https://doi.org/10.1364/boe.2.003129
Watanabe, M., & Fukuda, A. (2015). Development and regulation of chloride homeostasis in the central nervous system. In *Frontiers in Cellular Neuroscience*. https://doi.org/10.3389/fncel.2015.00371
Williams, J. R., Sharp, J. W., Kumari, V. G., Wilson, M., & Payne, J. A. (1999). The neuron-specific K-Cl cotransporter, KCC2: Antibody development and initial characterization of the protein. *Journal of Biological Chemistry*. https://doi.org/10.1074/jbc.274.18.12656
World Health Organization. (2019). WHO | Epilepsy: a public health imperative. In *Who*.
Wu, Y. W., Shek, D. W., Garcia, P. A., Zhao, S., & Johnston, S. C. (2002). Incidence and mortality of generalized convulsive status epilepticus in California. *Neurology*, *58*(7). https://doi.org/10.1212/WNL.58.7.1070
Wu, Z. Z., Li, D. P., Chen, S. R., & Pan, H. L. (2009). Aminopyridines potentiate synaptic and neuromuscular transmission by targeting the voltage-activated calcium channel β subunit. *Journal of Biological Chemistry*. https://doi.org/10.1074/jbc.M109.075523
Yamada, J., Okabe, A., Toyoda, H., Kilb, W., Luhmann, H. J., & Fukuda, A. (2004). Cl- uptake promoting depolarizing GABA actions in immature rat neocortical neurones is mediated by NKCC1. *Journal of Physiology*. https://doi.org/10.1113/jphysiol.2004.062471
Yekhlef, L., Breschi, G. L., Lagostena, L., Russo, G., & Taverna, S. (2015). Selective activation of parvalbumin- or somatostatin-expressing interneurons triggers epileptic seizurelike activity in mouse medial entorhinal cortex. *Journal of Neurophysiology*. https://doi.org/10.1152/jn.00841.2014
Yuan, W., Burkhalter, A., & Nerbonne, J. M. (2005). Functional role of the fast transient outward K+ current I A in pyramidal neurons in (rat) primary visual cortex. *Journal of Neuroscience*. https://doi.org/10.1523/JNEUROSCI.2858-05.2005
Zarrelli, M. M., Beghi, E., Rocca, W. A., & Hauser, W. A. (1999). Incidence of epileptic syndromes in Rochester, Minnesota: 1980-1984. *Epilepsia*, *40*(12). https://doi.org/10.1111/j.1528-1157.1999.tb01587.x
Zhan, Q., Buchanan, G. F., Motelow, J. E., Andrews, J., Vitkovskiy, P., Chen, W. C., Serout, F.,

Gummadavelli, A., Kundishora, A., Furman, M., Li, W., Bo, X., Richerson, G. B., & Blumenfeld, H. (2016). Impaired serotonergic brainstem function during and after seizures. *Journal of Neuroscience*, *36*(9). https://doi.org/10.1523/JNEUROSCI.4331-15.2016

Zhu, Q., Ke, W., He, Q., Wang, X., Zheng, R., Li, T., Luan, G., Long, Y. S., Liao, W. P., & Shu, Y. (2018). Laminar Distribution of Neurochemically-Identified Interneurons and Cellular Co-expression of Molecular Markers in Epileptic Human Cortex. *Neuroscience Bulletin*, *34*(6). https://doi.org/10.1007/s12264-018-0275-x

Ziburkus, J., Cressman, J. R., Barreto, E., & Schiff, S. J. (2006). Interneuron and pyramidal cell interplay during in vitro seizure-like events. *Journal of Neurophysiology*, *95*(6). https://doi.org/10.1152/jn.01378.2005

Zijlmans, M., Jacobs, J., Zelmann, R., Dubeau, F., & Gotman, J. (2009). High-frequency oscillations mirror disease activity in patients with epilepsy. *Neurology*, *72*(11). https://doi.org/10.1212/01.wnl.0000344402.20334.81

CHAPTER 2: COMPUTATIONAL STUDY

Role of KCC2-Dependent Potassium Efflux in 4-Aminopyridine-Induced Epileptiform Synchronization

Abstract

A balance between excitation and inhibition is necessary to maintain stable brain network dynamics. Traditionally, seizure activity is believed to arise from the breakdown of this delicate balance in favor of excitation with loss of inhibition. Surprisingly, recent experimental evidence suggests that this conventional view may be limited, and that inhibition plays a prominent role in the development of epileptiform synchronization. Here, we explored the role of the KCC2 co-transporter in the onset of inhibitory network-induced seizures. Our experiments in acute mouse brain slices, of either sex, revealed that optogenetic stimulation of either parvalbumin- or somatostatin-expressing interneurons induced ictal discharges in rodent entorhinal cortex during 4-aminopyridine application. These data point to a proconvulsive role of $GABA_A$ receptor signaling that is independent of the inhibitory input location (i.e., dendritic *vs.* somatic). We developed a biophysically realistic network model implementing dynamics of ion concentrations to explore the mechanisms leading to inhibitory network-induced seizures. In agreement with experimental results, we found that stimulation of the inhibitory interneurons induced seizure-like activity in a network with reduced potassium A-current. Our model predicts that interneuron stimulation triggered an increase of interneuron firing, which was accompanied by an increase in the intracellular chloride concentration and a subsequent KCC2-dependent gradual accumulation of the extracellular potassium promoting epileptiform ictal activity. When the KCC2 activity was reduced, stimulation of the interneurons was no longer able to induce ictal events. Overall, our study provides

evidence for a proconvulsive role of $GABA_A$ receptor signaling that depends on the involvement of the KCC2 co-transporter.

Introduction

Under specific conditions, activation of the inhibitory $GABA_A$ receptor signaling may play a prominent role in the generation of seizures (Hamidi & Avoli, 2015; Lillis et al., 2012; Sessolo et al., 2015; Shiri et al., 2016; Uva et al., 2015; Yekhlef et al., 2015). This evidence is in conflict with the established notion that epileptiform discharges result from excessive glutamatergic signaling due to reduced inhibition (Y. Ben-Ari et al., 1979; Dingledine & Gjerstad, 1980; Schwartzkroin & Prince, 1980). Indeed, it has been shown that inhibitory interneurons discharge action potentials at the onset of seizure-like events both *in vitro* (Lévesque et al., 2016; Lillis et al., 2012; Uva et al., 2015) and *in vivo* (Grasse et al., 2013; Toyoda et al., 2015). Moreover, seizure-like discharges *in vitro* disappear after pharmacological interventions that interfere with $GABA_A$ receptor signaling (Avoli et al., 1996; Lopantsev & Avoli, 1998; Uva et al., 2015). In line with this evidence, direct optogenetic activation of inhibitory interneurons during bath application of 4-aminopyridine (4AP) elicits seizure-like discharges *in vitro* (Shiri et al., 2016; Yekhlef et al., 2015). Together, these data suggest that an increase in the inhibitory interneuron synchrony may lead to development of paroxysmal seizure-like activity under conditions of impaired potassium (K^+) channel conductances. However, the mechanisms of this action remain to be fully understood.

Intracellular chloride concentration ($[Cl^-]_i$) increases in principal neurons at the onset of seizure-like activity in 4AP treated conditions (Lillis et al., 2012). Such intracellular accumulation of $[Cl^-]_i$, which is presumably due to an increase in GABAergic signaling prior to seizure onset, can be accompanied by a large increase in the extracellular potassium concentration ($[K^+]_o$) (Krishnan & Bazhenov, 2011). *In vitro* optogenetic stimulation of inhibitory interneurons can increase $[K^+]_o$ to the level capable of inducing seizure-like discharges (Yekhlef et al., 2015). An elevated level of $[K^+]_o$ may function as a positive feedback loop, increasing overall network excitability and leading to seizure onset (Fröhlich et al., 2008; Fröhlich & Bazhenov, 2006; González et al., 2015; Krishnan & Bazhenov, 2011; Pedley et al., 1974; Somjen, 2002; Traynelis & Dingledine, 1988). Indeed, fast-rising $[K^+]_o$ increases associated with interneuronal network activity preceded the initiation of seizure-like events *in vitro* in the 4AP seizure model (Librizzi et al., 2017). Previous computational studies found that oscillations of $[K^+]_o$ mediate periodic transitions between fast runs and spike-and-wave complexes during seizures (Fröhlich et al., 2008; Fröhlich & Bazhenov, 2006; Krishnan & Bazhenov, 2011), and that increase in baseline $[K^+]_o$ fluctuations may occur following cortical trauma (González et al., 2015). K^+ dynamics have been implicated in the transition to seizure and spreading depression (Wei et al., 2014), two network states previously thought to be mechanistically distinct.

The potassium-chloride co-transporter isoform 2 (KCC2) has been proposed as the critical link between the increase in $[Cl^-]_i$ and subsequent increase in $[K^+]_o$ (Hamidi & Avoli, 2015; Rivera et al., 2005; Shiri et al., 2016). Indeed, reduction of KCC2 activity

prevents generation of seizure-like events induced by 4AP (Hamidi & Avoli, 2015), as well as the increases in $[K^+]_o$ that occur in response to high-frequency stimulation (Viitanen et al., 2010). Therefore, it was postulated that synchronized GABAergic activity may cause a gradual accumulation of $[Cl^-]_i$, leading to the activation of KCC2. This results in the extrusion of both Cl^- and K^+, allowing K^+ to reach the level necessary to elicit seizure (Avoli et al., 2016).

In our new study, we tested this hypothesis by employing biophysically realistic network model with dynamic ion concentrations, Na^+/K^+ ATPase activity, and KCC2 activity. We found that reduction of the outward K^+ (type A) current (I_A), mimicking the effects of 4AP application, changed the network dynamics so interneuron stimulation could initiate seizure-like activity. Importantly, reduction of KCC2 activity (*cf*.,(Hamidi & Avoli, 2015)) prevented seizure generation, thus supporting our hypothesis about the role of KCC2 in ictogenesis.

Materials & Methods

Animals

All procedures were performed according to protocols and guidelines of the Canadian Council on Animal Care and were approved by the McGill University Animal Care Committee. PV-Cre (Jackson Laboratory, B6;129P2-*Pvalb*$^{tm1(cre)Arbr}$/J, stock number 008069) and SOM-Cre (Jackson Laboratory, *Ssttm2.1(cre)Zjh*/J, stock number 013044) homozygote mouse colonies were bred and maintained in house in order to generate pups that were used in this study.

Stereotaxic virus injections

Four PV-Cre (2 male and 2 female) and five SOM-Cre (3 male and 2 female) pups were anesthetized at P15 using isoflurane and positioned in a stereotaxic frame (Stoelting). AAVdj-ChETA-eYFP virus (UNC Vector Core) was delivered in the entorhinal cortex (EC) (0.6 µL at a rate of 0.06 µL/min). Injection coordinates were: anteroposterior -4.00 mm from bregma, lateral +/- 3.60 mm, dorsoventral -4.00 mm. The transverse sinus was used as a point of reference, and the injection needle was inserted with a 2º anteroposterior angle. After completion of the surgery, pups were returned to their home cage.

Brain slice preparation

Mice were deeply anesthetized with inhaled isoflurane and decapitated at P30-40. Brains were quickly removed and immersed in ice-cold slicing solution containing (in mM): 25.2 sucrose, 10 glucose, 26 $NaHCO_3$, 2.5 KCl, 1.25 KH_2PO_4, 4 $MgCl_2$, and 0.1 $CaCl_2$ (pH 7.3, oxygenated with 95% O_2/5% CO_2). Horizontal brain sections (thickness = 400 µm) containing the EC were cut using a vibratome (VT1000S, Leica) and incubated for one hour or more in a slice saver filled with artificial cerebrospinal fluid (ACSF) of the following composition (in mM): 125 NaCl, 25 glucose, 26 $NaHCO_3$, 2 KCl, 1.25 NaH_2PO_4, 2 $MgCl_2$, and 1.2 $CaCl_2$.

Electrophysiological recordings, photostimulation, and analysis

Slices were transferred to a submerged chamber where they were continuously perfused with oxygenated ACSF (KCl and $CaCl_2$ adjusted to 4.5 and 2 mM, respectively)

(30 ºC, 10-15 mL/min). Field potentials were recorded using ACSF-filled microelectrodes (1-2 MΩ) positioned in the EC in the presence of 4AP (150 μM). Signals were recorded with a differential AC amplifier (AM systems), filtered online (0.1-500 Hz), digitized with a Digidata 1440a (Molecular Devices) and sampled at 5 kHz using the pClamp software (Molecular Devices).

For ChR2 excitation, blue light (473 nm, intensity 35 mW) was delivered through a custom-made LED system, where the LED (Luxeon) was coupled to a 3 mm wide fiber-optic (Edmund Optics) and was placed above the recording region. For optogenetic stimulation of interneurons, light pulses (1 s duration) were delivered at 0.2 Hz for 30 s with a 150 s interval between trains. All reagents were obtained from Sigma-Aldrich and were bath applied. Ictal duration and interval are expressed as mean ± SEM. Data were compared using the Student's t-test. Results were considered significant if the p-value was less than 0.05.

Principal neuron and interneuron models

Principal or excitatory neurons (PNs) and inhibitory interneurons (INs) were both modeled as two compartment models as described previously in (M. Bazhenov et al., 2004; Maxim Bazhenov et al., 2002; Fröhlich et al., 2008; González et al., 2015; Houweling et al., 2005; Krishnan et al., 2015; Krishnan & Bazhenov, 2011; Volman, Bazhenov, et al., 2011; Volman, Sejnowski, et al., 2011). The membrane potential dynamics for each compartment were modeled by the following equations:

$$C_m \frac{dV_D}{dt} = -g_D^c (V_D - V_S) - I_D^{leak} - I_D^{pump} - I_D^{Int}$$
$$g_S^c (V_D - V_S) = -I_S^{leak} - I_S^{pump} - I_S^{Int} \quad \textbf{(1)}$$

where $V_{D,S}$ are the dendritic and axosomatic membrane potentials, $g_{D,S}^c$ are the dendritic and axosomatic compartment coupling current conductance, I_D^{pump} and I_S^{pump} are the sum total Na^+/K^+ ATPase currents, I_D^{leak} and I_S^{leak} are the sum of the ionic leak currents, and I_D^{Int} and I_S^{Int} are the intrinsic currents for the dendritic and axosomatic compartments respectively. The intrinsic currents for the dendritic and axosomatic compartments have been previously described in (González et al., 2015; Krishnan et al., 2015; Krishnan & Bazhenov, 2011).

Dynamic ion concentrations

Ionic concentrations dynamics for $[K^+]_o$, $[K^+]_i$, $[Na^+]_o$, $[Na^+]_i$, $[Ca^{2+}]_i$, and $[Cl^-]_i$ were modeled similar to our previous work (González et al., 2015; Krishnan et al., 2015; Krishnan & Bazhenov, 2011). In order to model the KCC2 co-transporter, we made some modifications to the $[K^+]_o$ and $[Cl^-]_i$ equations. Briefly, our previous models included KCC2 regulation of $[Cl^-]_i$ in a $[K^+]_o$ dependent manner. However, the $[K^+]_o$ was not affected by KCC2 activity. In this new study the $[K^+]_o$ and $[Cl^-]_i$ were modeled as follows:

$$\frac{d[K^+]_o}{dt} = \left(\frac{k}{Fd}\right)(I_K^{pump} + I_{\sum K}^{Int} + I_{KCC2}) + \delta_o([K^+]_{oc} - [K^+]_o) + G$$
$$+\delta_o\left(\left(\frac{([K^+]_{o-1} + [K^+]_{o+1})}{2} + \gamma([K^+]_{ox})\right)/(1+\gamma) - [K^+]_o\right) \quad \textbf{(2)}$$
$$\frac{d[Cl^-]_i}{dt} = -\left(\frac{k}{F}\right)(I_{\sum Cl}^{Int} + I_{KCC2})$$

where F = 96489 C/mol is the Faraday constant, the ratio of the extracellular volume to surface area is given by d = 0.15, and the conversion factor k = 10. Additionally, I_K^{pump} is the K^+ current through the Na^+/K^+ ATPase, $[K^+]_{oc}$ is the K^+ concentration in the adjacent compartment, $[K^+]_{o-1}$ and $[K^+]_{o+1}$ are the concentrations of K^+ neighboring cells. $\gamma = 0.06$ is the ion coupling coefficient between PNs and INs, $[K^+]_{ox}$ is the K^+ concentration of the neighboring IN when computing the $[K^+]_o$ for PNs and vice versa. δ_o is the scaled diffusion coefficient ($\delta_o = D/\Delta x$), where $D = 6\text{x}10^{-6}\ cm^2/s$ is the diffusion constant, $\Delta x = 100\mu m$ is distance, and G represents the glial buffering of K^+ as described in detail previously (González et al., 2015; Krishnan et al., 2015; Krishnan & Bazhenov, 2011). $I_{\sum K}^{Int}$ and $I_{\sum Cl}^{Int}$ are the sum total intrinsic K^+ and Cl^- currents respectively. I_{KCC2} defines the efflux of $[K^+]_o$ and $[Cl^-]_i$ generated by the KCC2 co-transporter and is described as follows:

$$I_{KCC2} = \left(\frac{\alpha_{KCC2}}{1+\exp(([Cl^-]_{i\infty} - [Cl^-]_i)/1.0)}\right)\left(\frac{[Cl^-]_{i\infty} - [Cl^-]_i}{\tau_{Cl}}\right)$$
$$\tau_{Cl} = \left(100 + \frac{\tau_{Cl\infty}}{\left(1+\exp\left(\frac{[Cl^-]_{i\infty} - [K^+]_o}{\tau_{KoCl}}\right)\right)}\right) \quad \textbf{(3)}$$

where α_{KCC2} = 80 defines the strength of the co-transporter, $[Cl^-]_{i\infty}$ = 5mM is the steady-state Cl^- concentration, $[Cl^-]_i$ is the intracellular Cl^- concentration, $\tau_{Cl\infty} = 4x10^3$s, and τ_{KoCl} = 0.08s.

Synapse and network properties

We modeled a one-dimensional network consisting of 100 PNs and 20 INs. Every PN formed local excitatory synapses onto ten neighboring PNs with AMPA conductance strength of 3.5 nS and NMDA conductance of 0.9 nS. PNs also formed excitatory synaptic connections onto INs with AMPA and NMDA conductance strengths of 2.4 nS and 0.24 nS respectively. INs synapsed onto five local PNs, with $GABA_A$ connections of 3.5 nS conductance strength. Additionally, PN and IN received individual afferent excitatory input modeled as a Poisson process as described in our previous studies (González et al., 2015; Krishnan et al., 2015; Krishnan & Bazhenov, 2011).

Estimation of seizure threshold

The seizure threshold was determined using a binary search method that employed an iterative procedure as described in (González et al., 2015). Briefly, at each step of the searching algorithm, the strength of the stimulus would be set to the mean of the upper and lower limits, <*P*>. If this stimulus strength was able to elicit seizure, the upper limit would be set to the current value of <*P*>. If <*P*> was unable to elicit a seizure, the lower limit would take the value of <*P*>. The new stimulus strength, <*P*>, would then be computed based on the updated upper and lower limits. This process

continued until the difference between the upper and lower limits was less than 0.1. The threshold was determined to be the average of these final limits.

Results

Spontaneous 4AP-induced ictal discharges were recorded from the entorhinal cortex (EC) of PV-Cre mice that were transcranially injected with the enhanced ChR2 opsin, ChETA (n = 5 slices). These discharges occurred every 158.07 ± 10.30 s with an average duration of 45.97 ± 1.33 s (n = 124 events). Using a 30 s train of 1 s light pulses at 0.2 Hz that optogenetically activated fast-spiking parvalbumin (PV)-positive interneurons, we were able to trigger ictal discharges of similar duration (i.e., 43.91 ± 2.27 s) but more frequently, at an average interval of 139.45 ± 4.79 s (n = 35 events; $p < 0.05$; figure 2.1A).

Next, we established whether the ability of interneuron activation to drive ictal discharges was linked exclusively to fast-spiking PV-positive interneurons, or whether ictal discharges could also be triggered by activating regular-spiking somatostatin (SOM)-positive interneurons. Therefore, we obtained brain slices containing the EC of SOM-Cre mice that had been transcranially injected with the ChETA opsin (n = 8 slices). Spontaneous 4AP-induced ictal discharges in these experiments occurred every 127.35 ± 6.30 s and lasted on average 63.28 ± 1.84 s (n = 126 events). Using the same protocol used to stimulate PV-interneurons (i.e. 1 s light pulses at 0.2 Hz for 30 s), we were able to trigger ictal discharge of similar duration (55.71 ± 1.90 s), but at a shorter interval of 104.56 ± 5.47 s (n = 44 events; $p < 0.05$; figure 2.1B). The ictal discharges elicited by the

optogenetic activation of either PV- or SOM-expressing interneurons showed characteristic properties of low-voltage, fast (LVF) ictal discharges. Previously, we showed that these LVF ictal discharges are different from the hypersynchronous (HYP) ictal discharges induced by optogenetic stimulation of CamKII-positive principal neurons suggesting a different mechanism between principal neuron- and inhibitory interneuron-induced ictal discharges (Shiri et al., 2016).

In order to establish the mechanisms by which PV- and SOM-interneuron stimulation causes ictal discharges in brain slices treated with 4AP, we developed a biophysically realistic network model implementing dynamic ion concentrations, the electrogenic Na^+/K^+ pump, and the KCC2 co-transporter. The network contained synaptically coupled principal (excitatory) neurons (PN) and inhibitory interneurons (IN), where the extracellular compartments of these two neuron types were ionically coupled (see Methods). In order to make comparisons between our model and experimental data, we modeled the application of 4AP as resulting in a 50 percent reduction of the outward K^+ A-current. Additionally, optogenetic stimulation of interneurons was modeled as a series of 1 s pulses at 0.2 Hz for 30 s similar to those used in our *in vitro* experiments; these "activating" pulses were applied to all interneurons.

In a control network, one without reduction of I_A, the stimuli applied to INs resulted in increased firing rate for the duration of the stimulation, followed by a gradual decay back to baseline firing (figure 2.2A). During baseline activity, the mean IN firing rate fluctuated around 1 Hz, but during stimulation it reached ~25 Hz (figure 2.2C, red). The increase in IN firing during stimulus pulses was accompanied by a hyperpolarization

and relative silencing of the postsynaptic PNs (figure 2.2B and C, black trace). Similar to INs, PNs displayed a gradual return to a baseline mean firing rate of about 5 Hz (figure 2.2C, black trace). This control network behaved as expected, i.e., the transient increase in IN firing caused a transient hyperpolarization of the PNs followed by a gradual return to the baseline activity.

We next tested the effects induced by IN stimulation on the network dynamics during conditions mimicking 4AP application, i.e., a reduction of I_A in both PNs and INs that resulted in a slight increase of the mean intrinsic baseline firing rates of both cell types (~ 4 Hz and ~ 12 Hz for INs and PNs respectively; figure 2.3D). In this condition, a single stimulus applied to INs produced an expected hyperpolarization and silencing of PN activity. We then proceeded to apply a sequence of the stimuli to all INs to model the effect of optogenetic stimulation similar to our experiment in the control network (figure 2.2). IN firing peaked at ~ 35 Hz during each stimulus pulse (figure 2.3A and D, red trace), and during the first 2 pulses PNs were hyperpolarized and silenced by the IN-mediated inhibition (figure 2.3B and C). However, during subsequent stimulation pulses, the mean firing rate of PNs began to increase (figure 2.3D, black trace), and the network developed a seizure-like state, which initiated as focal tonic firing (figure 2.3B, cells 60-100) before spreading to the rest of the network, and eventually transitioning to a clonic bursting phase (figure 2.3B and C). Seizure termination was followed by the postictal depression, and then by a return to baseline firing in both neuron types.

Since reduction of I_A shifted the network to a state where synchronous inhibitory activity could induce seizure, we next tested the effect of I_A strength on the seizure

threshold. Reduction of I_A made networks more susceptible to seizure (figure 2.3E; 40-60% range), which can be attributed to increased intrinsic network excitability due to reduced K^+-dependent inhibition. I_A strengths less than 40% of the baseline resulted in spontaneous seizures, while strengths greater than 60% did not allow transitions to seizure-like activity following interneuron stimulation.

Dynamics of the $[K^+]_o$ and $[Cl^-]_i$ under these two network conditions – i.e., control and under reduced I_A (figures 2.2 and 2.3) - revealed stark differences following IN stimulation. As seen in figure 2.4A, mean $[Cl^-]_i$ and $[K^+]_o$ for all PNs behaved similarly prior to and during IN stimulation in both control and reduced I_A networks (red and black traces respectively). During IN stimulation, both networks revealed increases in the mean $[Cl^-]_i$, and initial decreases in $[K^+]_o$ (figure 2.4A). The increase in $[Cl^-]_i$ in PNs was presumably due to activation of postsynaptic $GABA_A$ receptors, while the transient (initial) decrease in $[K^+]_o$ could reflect the resulting reduction of PN firing. Following termination of the IN stimulation, the $[Cl^-]_i$ in the control network gradually returned to baseline along with the IN firing rate (figure 2.2C, red trace and figure 2.4A, red trace in left panel). PN firing became transiently elevated but then also returned to baseline (figure 2.2C, black trace). In contrast, under conditions of I_A reduction, IN firing remained elevated and $[Cl^-]_i$ continued to increase following the end of the stimulation (figure 2.2C, red trace and figure 2.4A, black trace in left panel). Accumulation of $[Cl]_i$ caused activation of the KCC2 co-transporter. As KCC2 uses K^+ gradient to remove Cl^- (Payne et al., 2003), activation of KCC2 led to accumulation of $[K^+]_o$ (figure 2.4A, right panel, black trace). This increased PNs excitability (already elevated under reduced I_A

conditions) and triggered a positive feedback loop (Fröhlich et al., 2008; Fröhlich & Bazhenov, 2006; Krishnan & Bazhenov, 2011) initiating a network transition to seizure-like activity (figure 2.4B and 2.4C). It is important to emphasize, that while the increase of $[Cl^-]_i$ reduced the effect of inhibition, Cl^- reversal potential never raised above the resting membrane potential of PNs and, therefore, the effect of $GABA_A$ remained hyperpolarizing throughout the entire simulation time.

Both $[Cl^-]_i$ in PNs and $[K^+]_o$ in the surrounding extracellular space remained elevated during the seizure-like activity (figure 2.4B and C, respectively). The expanded sample shown in figure 2.4D illustrates how activation of INs resulted in the silencing and hyperpolarization of PNs during stimulation pulses, while the subsequent accumulation of $[K^+]_o$ increased firing rate and eventually triggered the transition to seizure-like activity. These results reveal that in conditions of increased baseline excitability (such as after reducing I_A), the network is able to generate seizure-like activity following interneuron activation. Our model suggests that the mechanism of seizure initiation involves: (a) IN stimulation leading to the release of GABA and postsynaptic activation of $GABA_A$ receptors; (b) $GABA_A$ receptor activation leading to increase of $[Cl^-]_i$ mediating KCC2 activation; (c) KCC2 activation leading to increase of $[K^+]_o$ sufficiently to initiate the positive feedback loop that mediates an "avalanche" increase of excitability.

To directly test our hypothesis that an increase of KCC2 activity, resulting from $[Cl^-]_i$ accumulation, may underlie initiation of seizure-like activity, we reduced KCC2 co-transporter strength by 50 percent (α_{KCC2} = 40, see Methods) in a network with reduced

I_A, while stimulating INs (figure 2.5). IN stimulation was identical to that performed in the previous experiments (figures 2.2 and 2.3). In this new condition, stimulation of INs resulted only in the transient silencing of PN activity (figure 2.5A, top), and $[K^+]_o$ returned to the baseline levels shortly after the termination of IN stimulation (figure 2.5A, bottom). Unlike the results shown in figure 2.3, no transition to seizure-like activity occurred during or following the termination of IN stimulation. Note, however, that the reduction of KCC2 activity resulted in a less excitable network, which was caused by a decrease of $[K^+]_o$ accumulation due to the reduced KCC2 baseline activity.

To further demonstrate that accumulation of $[Cl^-]_i$ was directly responsible for the activation of the KCC2 co-transporter and subsequent accumulation of $[K^+]_o$, in the next experiment we reduced the effect of KCC2 on the ion concentrations, but prevented the reduction of baseline network activity (Fig. 5A). Thus, we kept the strength of KCC2 intact (α_{KCC2} = 80), but we capped the maximal amount of Cl^- that can enter both PNs and INs. In doing so, we limited the peak KCC2 activity without changing the baseline KCC2 activity and, therefore, baseline network firing rate. In this condition, IN stimulation was still unable to initiate a seizure-like response (figure 2.5B). $[Cl^-]_i$ increased during IN stimulation, however, it was unable to induce sufficient activation of the KCC2 co-transporter to trigger high $[K^+]_o$ increase. Thus, following IN stimulation, only a small and brief increase in $[K^+]_o$ was observed (figure 2.5B, bottom). This suggests that limiting KCC2 performance may prevent transition to the seizure-like activity. We need to mention, however, that limiting peak $[Cl^-]_i$ level also affected other network properties (e.g., reversal potential of Cl^- and therefore effect of inhibition).

Since limiting $[Cl^-]_i$ increase could affect several properties of the model, in the next experiment we artificially limited the effect of $[Cl^-]_i$ on the KCC2 co-transporter only. Therefore, in this condition, though the $[Cl^-]_i$ could exhibit a significant increase, the KCC2 co-transporter would only sense a limited increase in $[Cl^-]_i$. That is, the value of the variable in the I_{KCC2} equation representing intracellular Cl^- concentration (see Methods) was kept below the actual amount of $[Cl^-]_i$. Essentially, this rendered the K^+ extrusion mechanism of the KCC2 co-transporter less sensitive to $[Cl^-]_i$. As shown in figure 2.5C, IN stimulation was unable to elicit seizure-like activity in this network. Brief increases in both $[Cl^-]_i$ and $[K^+]_o$ were observed following the stimulation (figure 2.5C, bottom). Though the KCC2 activity increased $[K^+]_o$ following IN stimulation, $[K^+]_o$ never reached concentrations sufficient for generation of seizure-like activity. Importantly $[Cl^-]_i$ could reach its peak level (the same as in control model) in this experiment, suggesting that the shift of the $GABA_A$ reversal potential, associated with increase of $[Cl^-]_i$, alone is not sufficient to induce seizure-like activity.

Finally, we tested whether a direct increase in $[Cl^-]_i$ in PNs could lead to the activation of the KCC2 co-transporter and subsequent elevation of $[K^+]_o$. In this experiment, we used a baseline model where the effect of $[Cl^-]_i$ on KCC2 was intact (similar to network in figure 2.3). We found that a brief and sufficiently strong increase of $[Cl^-]_i$ in PNs was able to activate KCC2 extrusion of K^+ followed by the development of seizure-like activity (figure 2.5D). Together, these data suggest that Cl^- specific activation of KCC2 activity gives rise to the increase in $[K^+]_o$ sufficient for triggering transition to seizure-like activity.

Our model predicts that $GABA_A$ receptor-dependent increase in $[Cl^-]_i$ results in KCC2 mediated increase of $[K^+]_o$ and may lead to the initiation of seizure. Next, we tested how these two specific properties affect seizure onset and duration. By changing contribution of $GABA_A$ to the $[Cl^-]_i$ in the model, we found that limiting $[Cl^-]_i$ increase in PNs increased the seizure threshold (figure 2.6A). Reducing $GABA_A$ receptor-dependent increase of $[Cl^-]_i$ to 94 % of the baseline, prevented IN stimulation from inducing seizure-like activity in the model. The reduced contribution of $GABA_A$ receptor activations to the $[Cl^-]_i$ also resulted in the shorter seizure duration (figure 2.6C). Both these effects arise from the fact that reduced $[Cl^-]_i$ accumulation led to the lower KCC2 activation and reduced K^+ efflux.

This prediction was further validated by directly changing KCC2 strength (α_{KCC2}). As illustrated in figure 2.6B, increasing KCC2 strength decreased seizure threshold, while decreasing KCC2 strength led to the threshold increase. Decreasing KCC2 strength also resulted in a decrease of seizure duration, while increased KCC2 strength had an opposite effect (figure 2.6D and F). Interestingly, reduction of KCC2 strength also delayed the onset time of seizure-like activity (figure 2.6E). Between the network with control (100 %) KCC2 activity and the network with low KCC2 activity (figure 2.6F, blue), there was a difference of about 11 sec for the seizure onset time. In the networks with stronger KCC2 (figure 2.6E, green), seizure onset occurred earlier as compared to that in a control network with 100% KCC2 strength. This effect can be explained by the different rate of $[K^+]_o$ accumulation resulting from KCC2 activity. When KCC2 activity was enhanced, $[K^+]_o$ accumulated faster and reached the critical

threshold that was sufficient for initiation of seizure-like activity after only a few seconds.

Discussion

Application of potassium channel blocker 4AP may lead to epileptiform activity both *in vivo* and *in vitro* (Avoli & de Curtis, 2011). Optogenetic activation of inhibitory interneurons, in acute mouse brain slices exposed to 4AP, triggered seizure-like discharges (Sessolo et al., 2015; Shiri et al., 2016; Yekhlef et al., 2015). Blocking KCC2 activity with either VU024055 or high doses of bumetanide abolished ictal discharges in 4AP-treated rat brain slices (Hamidi & Avoli, 2015), suggesting that this form of inhibition-induced seizure may involve activation of the KCC2 co-transporter. In this new study, we tested the hypothesis that in conditions of elevated cortical excitability (as in the presence of 4AP), Cl^--dependent activation of the KCC2 co-transporter can trigger the progression of a network to a seizure state by an increase of extracellular K^+. Our *in vitro* data and computer simulation results predict that synchronous activation of the inhibitory interneurons can lead to a Cl^- increase sufficient for KCC2 activation and development of paroxysmal activity. This mechanism does not require synaptic $GABA_A$ to inverse polarity as the epileptiform activity is mediated by increase of the extracellular K^+ and not by the depolarizing effect of the $GABA_A$ signaling, which remains inhibitory.

Various channelopathies, including mutated or misregulated K^+ channels, have been suggested to underlie certain forms of genetic epilepsies (D'Adamo et al., 2013; Lascano et al., 2016). Indeed, mutations in K_V4 α-subunits are present in some patients

suffering from pharmacoresistant temporal lobe epilepsy (D'Adamo et al., 2013; Singh et al., 2006). Specifically, a truncation mutation of the $K_V4.2$ α-subunit, responsible for the I_A, was observed in human patients (Singh et al., 2006). This mutation results in an attenuated I_A and subsequent increases in seizure susceptibility. In addition to mutations of specific ion channels, mutations of genes encoding proteins which modulate ion channel activity were found. Patients suffering from autosomal dominant partial epilepsy with auditory features (ADPEAF) have been shown to have point mutations in the leucine-rich glioma-inactivated 1 (LGI1) gene, resulting in reduced neuronal secretion of LGI1 (Dazzo et al., 2015; Nobile et al., 2009; Ottman et al., 2004). Neuronally secreted LGI1 binds to $K_V1.4$ and $K_V\beta1$, two known subunits comprising the A-type channels, preventing rapid inactivation of A-type currents (Schulte et al., 2006). The reduction of LGI1 expression in patients with ADPEAF results in the rapid inactivation of A-type channels and subsequent hyperexcitability.

The I_A antagonist, 4AP, has been shown to cause increased neuronal excitability and seizure-like discharges *in vivo* (Fragoso-Veloz et al., 1990; Lévesque et al., 2013) and *in vitro* (Avoli et al., 1996; Lopantsev & Avoli, 1998). Interestingly, direct knockout of the $K_V4.2$ α-subunit resulted in increased excitability but did not generate spontaneous seizures. This knockout can, however, increase seizure susceptibility in response to additional proconvulsive pharmacological agents (Barnwell et al., 2009). Previous studies proposed that reduction of A-type K^+ current promotes ictogenesis by directly increasing neuronal excitability (Galvan et al., 1982; Gustafsson et al., 1982; Yamaguchi & Rogawski, 1992). In contrast, our study predicts that the reduction of A-type K^+ current

leads to increased excitability of both excitatory and inhibitory neurons, and that the latter is critical for epileptogenesis. We show that acute brain slices treated with 4AP exhibit transitions to seizure when perturbed by photostimulation of inhibitory interneurons. Using computer modeling, we tested the hypothesis that the mechanism by which increased GABAergic signaling may lead to paroxysmal discharges involves Cl^- -dependent activation of KCC2 followed by increases in the extracellular K^+.

Early studies proposed that reduced inhibition underlies seizure generation and perhaps epilepsy (Y. Ben-Ari et al., 1979; Dingledine & Gjerstad, 1980; Schwartzkroin & Prince, 1980). Later, this view was challenged in several studies, (De Curtis & Avoli, 2016), which revealed that synchronous inhibitory interneuron activity occurs prior to seizure onset in slices treated with 4AP (Lévesque et al., 2016; Lillis et al., 2012; Uva et al., 2015). It has been reported that intense GABAergic stimulation results in an increase of $[K^+]_o$ and long-lasting depolarizations (Rivera et al., 2005; Viitanen et al., 2010). Additionally, application of either bicuculline or furosemide inhibits these events (Viitanen et al., 2010). Indeed, these GABAergic excitatory $[K^+]_o$ transients have been shown to elicit prolonged depolarizations in rat CA1 and EC, and may play a prominent role in seizure generation (Lopantsev & Avoli, 1998; Viitanen et al., 2010). The proconvulsive GABAergic excitatory $[K^+]_o$ transients may give rise to the spontaneous seizure onset in patients with K^+ channel abnormalities.

In vitro and *in silico* results presented in this study predict the mechanisms by which GABAergic signaling can trigger seizure onset. We propose that the increased GABAergic signaling, such as triggered by stimulation of inhibitory interneurons,

induces Cl^- build up, followed by Cl^- dependent activation of the KCC2 co-transporter and subsequent increase of $[K^+]_o$. Indeed, high frequency stimulation has been shown to cause increases in $[K^+]_o$ in response to intense $GABA_A$ receptor activation (Rivera et al., 2005; Ruusuvuori et al., 2004; Viitanen et al., 2010). Optogenetic stimulation of either SOM- or PV-expressing interneurons also causes large increases in $[K^+]_o$ (Yekhlef et al., 2015). It has been shown that sufficiently large initial increase of $[K^+]_o$ can give rise to a positive feedback loop due to an increase in the network excitability through $[K^+]_o$ dependent depolarization of neurons, which in turn results in a further increase of $[K^+]_o$ and can lead to epileptiform activity (Fröhlich et al., 2008; Fröhlich & Bazhenov, 2006; González et al., 2015; Krishnan et al., 2015; Krishnan & Bazhenov, 2011; Somjen, 2002; Wei et al., 2014). Our new study predicts that the mechanisms leading to the initial increase in $[K^+]_o$, which kicks the network into a vicious feedback cycle, may involve KCC2-dependent efflux of K^+.

It has been shown that during early stages of development, GABAergic signaling in the rodent brain produces depolarizing potentials (Yehezkel Ben-Ari et al., 2007; Payne et al., 2003). The transition from depolarizing to hyperpolarizing GABAergic signaling has been attributed to the changes in Cl^- homeostasis as the animal develops (Payne et al., 2003; Watanabe & Fukuda, 2015). During early stages of development, the Na^+-K^+-Cl^- co-transporter (NKCC1) responsible for transporting two Cl^- ions and one K^+ and Na^+ ion into the neuron is highly expressed in rat and mouse neurons (Dzhala et al., 2005). As a result $[Cl^-]_i$ can reach baseline concentrations of 30mM (Achilles et al., 2007) resulting in depolarization of the Cl^- reversal potential and making GABAergic signaling

depolarizing. As the brain develops, NKCC1 expression levels decrease, and KCC2 expression increases (Watanabe & Fukuda, 2015). Indeed, KCC2 mRNA is not detected until E18.5 and E15.5 in mouse CA1 and CA3 hippocampal subfields, respectively, while by P15, KCC2 and NKCC1 expression in the mouse brain reaches adult levels (Watanabe & Fukuda, 2015). In our current study, as well as in previous reports (Sessolo et al., 2015; Shiri et al., 2016; Yekhlef et al., 2015), epileptiform activity was induced through optogenetic stimulation of inhibitory interneurons in juvenile and young adult mice ranging from P15 to P40 during 4AP treatment. Furthermore, experiments in adult rats have shown that the KCC2 co-transporter plays a prominent role in the development of 4AP-induced epileptiform activity (Avoli et al., 1996; Hamidi & Avoli, 2015; Lopantsev & Avoli, 1998). Together, these results suggest that the "epileptogenic" effect of interneuron activation in 4AP conditions, as described in our study, does not depend on the reversal of the $GABA_A$ synaptic potential as found early in development, but may rely on the mechanisms that were tested in our computational model. These mechanisms rest on the increase in the extracellular K^+ concentrations that result from KCC2 activation, triggered by an increase of intracellular Cl^- during intense interneuron firing.

Downregulation of KCC2 expression levels have been suggested to underlie the development of epilepsy in patients (Buchin et al., 2016; Huberfeld et al., 2007). However, other studies have shown that increased KCC2 activation may play a prominent role in seizure generation (Hamidi & Avoli, 2015; Viitanen et al., 2010). Activity dependent regulation of KCC2 expression may explain this seemingly conflicting evidence. Indeed, KCC2 expression has been shown to reduce following

increases in activity and epileptiform discharges (Rivera et al., 2002, 2004, 2005). Our computational model revealed that the reduction of KCC2 activity prevents seizures in response to intense GABAergic signaling, suggesting that the observed reduction of KCC2 expression may not be a seizure triggering factor, but rather a protective mechanism to reduce the likelihood of seizures being triggered by other factors. Our study predicts that an increase of $[Cl^-]_i$ in excitatory neurons activates KCC2 co-transporter and promotes initiation of seizure. Consistent with this prediction, recent experimental studies reported large increase in $[Cl^-]_i$ in excitatory neurons prior to paroxysmal discharges (Lillis et al., 2012). Our model also predicts that increases in KCC2 activity can increase seizure susceptibility and duration. This result is consistent with previous computational modelling and experimental work (Hamidi & Avoli, 2015; Krishnan & Bazhenov, 2011). Importantly, our model predicts a complex effect of $GABA_A$ inhibition in seizure development. On one hand, increase of $GABA_A$ signaling would act to suppress the network activity, on the other it would promote increase of $[Cl^-]_i$ in excitatory neurons which drives KCC2 activation and $[K^+]_o$ efflux, thus paradoxically increasing network excitability. The balance of these opposite factors determines the resulting network dynamics (normal vs epileptic) in the physiological settings.

Conclusion

Patients suffering from pharmacoresistant seizures make up approximately 30% of the total number of people living with epilepsy (Nadkarni et al., 2005; Perucca &

Tomson, 2011). Among the commonly prescribed antiepileptic drugs, several of them (such as benzodiazepine and barbiturates) enhance $GABA_A$ receptor function (Nadkarni et al., 2005; Perucca & Tomson, 2011). Our new study suggests that increased GABAergic signaling, through treatment with these antiepileptic drugs, may exacerbate existing seizures in patients with K^+ channelopathies. We predict that modulation of KCC2 activity may prevent seizure generation in patients. Thus, our findings may provide a new avenue for pharmacological interventions in patients suffering from intractable epilepsy due to K^+ channelopathies.

References

Achilles, K., Okabe, A., Ikeda, M., Shimizu-Okabe, C., Yamada, J., Fukuda, A., Luhmann, H. J., & Kilb, W. (2007). Kinetic properties of Cl- uptake mediated by Na +-dependent K+-2Cl- cotransport in immature rat neocortical neurons. *Journal of Neuroscience*. https://doi.org/10.1523/JNEUROSCI.5041-06.2007

Avoli, M., Barbarosle, M., Lücke, A., Nagao, T., Lopantsev, V., & Köhling, R. (1996). Synchronous GABA-mediated potentials and epileptiform discharges in the rat limbic system in vitro. *Journal of Neuroscience*. https://doi.org/10.1523/jneurosci.16-12-03912.1996

Avoli, M., & de Curtis, M. (2011). GABAergic synchronization in the limbic system and its role in the generation of epileptiform activity. In *Progress in Neurobiology*. https://doi.org/10.1016/j.pneurobio.2011.07.003

Avoli, M., De Curtis, M., Gnatkovsky, V., Gotman, J., Köhling, R., Lévesque, M., Manseau, F., Shiri, Z., & Williams, S. (2016). Specific imbalance of excitatory/inhibitory signaling establishes seizure onset pattern in temporal lobe epilepsy. *Journal of Neurophysiology*. https://doi.org/10.1152/jn.01128.2015

Barnwell, L. F. S., Lugo, J. N., Lee, W. L., Willis, S. E., Gertz, S. J., Hrachovy, R. A., & Anderson, A. E. (2009). Kv4.2 knockout mice demonstrate increased susceptibility to convulsant stimulation. *Epilepsia*, *50*(7). https://doi.org/10.1111/j.1528-1167.2009.02086.x

Bazhenov, M., Timofeev, I., Steriade, M., & Sejnowski, T. J. (2004). Potassium model for slow (2-3 Hz) in vivo neocortical paroxysmal oscillations. *Journal of Neurophysiology*. https://doi.org/10.1152/jn.00529.2003

Bazhenov, Maxim, Timofeev, I., Steriade, M., & Sejnowski, T. J. (2002). Model of thalamocortical slow-wave sleep oscillations and transitions to activated states. *Journal of Neuroscience*. https://doi.org/10.1523/jneurosci.22-19-08691.2002

Ben-Ari, Y., Krnjevic, K., & Reinhardt, W. (1979). Hippocampal seizures and failure of inhibition. *Canadian Journal of Physiology and Pharmacology*. https://doi.org/10.1139/y79-218

Ben-Ari, Yehezkel, Gaiarsa, J. L., Tyzio, R., & Khazipov, R. (2007). GABA: A pioneer transmitter that excites immature neurons and generates primitive oscillations. In *Physiological Reviews*. https://doi.org/10.1152/physrev.00017.2006

Buchin, A., Chizhov, A., Huberfeld, G., Miles, R., & Gutkin, B. S. (2016). Reduced efficacy of the KCC2 cotransporter promotes epileptic oscillations in a subiculum network model. *Journal of Neuroscience*.

https://doi.org/10.1523/JNEUROSCI.4228-15.2016
D'Adamo, M. C., Catacuzzeno, L., di Giovanni, G., Franciolini, F., & Pessia, M. (2013). K+ channelepsy: Progress in the neurobiology of potassium channels and epilepsy. In *Frontiers in Cellular Neuroscience*. https://doi.org/10.3389/fncel.2013.00134
Dazzo, E., Santulli, L., Posar, A., Fattouch, J., Conti, S., Lodén-van Straaten, M., Mijalkovic, J., De Bortoli, M., Rosa, M., Millino, C., Pacchioni, B., Di Bonaventura, C., Giallonardo, A. T., Striano, S., Striano, P., Parmeggiani, A., & Nobile, C. (2015). Autosomal dominant lateral temporal epilepsy (ADLTE): Novel structural and single-nucleotide LGI1 mutations in families with predominant visual auras. *Epilepsy Research*. https://doi.org/10.1016/j.eplepsyres.2014.12.004
De Curtis, M., & Avoli, M. (2016). GABAergic networks jump-start focal seizures. In *Epilepsia*. https://doi.org/10.1111/epi.13370
Dingledine, R., & Gjerstad, L. (1980). Reduced inhibition during epileptiform activity in the in vitro hippocampal slice. *The Journal of Physiology*. https://doi.org/10.1113/jphysiol.1980.sp013364
Dzhala, V. I., Talos, D. M., Sdrulla, D. A., Brumback, A. C., Mathews, G. C., Benke, T. A., Delpire, E., Jensen, F. E., & Staley, K. J. (2005). NKCC1 transporter facilitates seizures in the developing brain. *Nature Medicine*. https://doi.org/10.1038/nm1301
Fragoso-Veloz, J., Massieu, L., Alvarado, R., & Tapia, R. (1990). Seizures and wet-dog shakes induced by 4-aminopyridine, and their potentiation by nifedipine. *European Journal of Pharmacology*. https://doi.org/10.1016/0014-2999(90)90106-G
Fröhlich, F., & Bazhenov, M. (2006). Coexistence of tonic firing and bursting in cortical neurons. *Physical Review E - Statistical, Nonlinear, and Soft Matter Physics*. https://doi.org/10.1103/PhysRevE.74.031922
Fröhlich, F., Bazhenov, M., Iragui-Madoz, V., & Sejnowski, T. J. (2008). Reviews: Potassium dynamics in the epileptic cortex: New insights on an old topic. In *Neuroscientist*. https://doi.org/10.1177/1073858408317955
Galvan, M., Grafe, P., & Bruggencate, G. Ten. (1982). Convulsant actions of 4-aminopyridine on the guinea-pig olfactory cortex slice. *Brain Research*. https://doi.org/10.1016/0006-8993(82)91230-6
González, O. C., Krishnan, G. P., Chauvette, S., Timofeev, I., Sejnowski, T., & Bazhenov, M. (2015). Modeling of age-dependent epileptogenesis by differential homeostatic synaptic scaling. *Journal of Neuroscience*, *35*(39). https://doi.org/10.1523/JNEUROSCI.5038-14.2015
Grasse, D. W., Karunakaran, S., & Moxon, K. A. (2013). Neuronal synchrony and the transition to spontaneous seizures. *Experimental Neurology*. https://doi.org/10.1016/j.expneurol.2013.05.004
Gustafsson, B., Galvan, M., Grafe, P., & Wigström, H. (1982). A transient outward current in a mammalian central neurone blocked by 4-aminopyridine. *Nature*. https://doi.org/10.1038/299252a0
Hamidi, S., & Avoli, M. (2015). KCC2 function modulates in vitro ictogenesis. *Neurobiology of Disease*. https://doi.org/10.1016/j.nbd.2015.04.006
Houweling, A. R., Bazhenov, M., Timofeev, I., Steriade, M., & Sejnowski, T. J. (2005). Homeostatic synaptic plasticity can explain post-traumatic epileptogenesis in chronically isolated neocortex. *Cerebral Cortex*. https://doi.org/10.1093/cercor/bhh184
Huberfeld, G., Wittner, L., Clemenceau, S., Baulac, M., Kaila, K., Miles, R., & Rivera, C. (2007). Perturbed chloride homeostasis and GABAergic signaling in human temporal lobe epilepsy. *Journal of Neuroscience*. https://doi.org/10.1523/JNEUROSCI.2761-07.2007
Krishnan, G. P., & Bazhenov, M. (2011). Ionic dynamics mediate spontaneous termination of seizures and postictal depression state. *Journal of Neuroscience*. https://doi.org/10.1523/JNEUROSCI.6200-10.2011
Krishnan, G. P., Filatov, G., Shilnikov, A., & Bazhenov, M. (2015). Electrogenic properties of the Na+/K+ ATPase control transitions between normal and pathological brain states. *Journal of Neurophysiology*. https://doi.org/10.1152/jn.00460.2014
Lascano, A. M., Korff, C. M., & Picard, F. (2016). Seizures and epilepsies due to channelopathies and neurotransmitter receptor dysfunction: A parallel between genetic and immune aspects. In *Molecular Syndromology*. https://doi.org/10.1159/000447707
Lévesque, M., Herrington, R., Hamidi, S., & Avoli, M. (2016). Interneurons spark seizure-like activity in the entorhinal cortex. *Neurobiology of Disease*. https://doi.org/10.1016/j.nbd.2015.12.011

Lévesque, M., Salami, P., Behr, C., & Avoli, M. (2013). Temporal lobe epileptiform activity following systemic administration of 4-aminopyridine in rats. *Epilepsia*. https://doi.org/10.1111/epi.12041

Librizzi, L., Losi, G., Marcon, I., Sessolo, M., Scalmani, P., Carmignoto, G., & De Curtis, M. (2017). Interneuronal network activity at the onset of seizure-like events in entorhinal cortex slices. *Journal of Neuroscience*. https://doi.org/10.1523/JNEUROSCI.3906-16.2017

Lillis, K. P., Kramer, M. A., Mertz, J., Staley, K. J., & White, J. A. (2012). Pyramidal cells accumulate chloride at seizure onset. *Neurobiology of Disease*, *47*(3). https://doi.org/10.1016/j.nbd.2012.05.016

Lopantsev, V., & Avoli, M. (1998). Participation of GABA(A)-mediated inhibition in ictallike discharges in the rat entorhinal cortex. *Journal of Neurophysiology*. https://doi.org/10.1152/jn.1998.79.1.352

Nadkarni, S., LaJoie, J., & Devinsky, O. (2005). Current treatments of epilepsy. In *Neurology*. https://doi.org/10.1212/wnl.64.12_suppl_3.s2

Nobile, C., Michelucci, R., Andreazza, S., Pasini, E., Tosatto, S. C. E., & Striano, P. (2009). LGI1 mutations in autosomal dominant and sporadic lateral temporal epilepsy. In *Human Mutation*. https://doi.org/10.1002/humu.20925

Ottman, R., Winawer, M. R., Kalachikov, S., Barker-Cummings, C., Gilliam, T. C., Pedley, T. A., & Hauser, W. A. (2004). LGI1 mutations in autosomal dominant partial epilepsy with auditory features. *Neurology*. https://doi.org/10.1212/01.WNL.0000120098.39231.6E

Payne, J. A., Rivera, C., Voipio, J., & Kaila, K. (2003). Cation-chloride co-transporters in neuronal communication, development and trauma. In *Trends in Neurosciences*. https://doi.org/10.1016/S0166-2236(03)00068-7

Pedley, T. A., Fisher, R. S., Moody, W. J., Futamachi, K. J., & Prince, D. A. (1974). Extracellular potassium activity during epileptogenesis: a comparison between neocortex and hippocampus. *Transactions of the American Neurological Association*.

Perucca, E., & Tomson, T. (2011). The pharmacological treatment of epilepsy in adults. In *The Lancet Neurology*. https://doi.org/10.1016/S1474-4422(11)70047-3

Rivera, C., Li, H., Thomas-Crusells, J., Lahtinen, H., Viitanen, T., Nanobashvili, A., Kokaia, Z., Airaksinen, M. S., Voipio, J., Kaila, K., & Saarma, M. (2002). BDNF-induced TrkB activation down-regulates the K+-Cl- cotransporter KCC2 and impairs neuronal Cl- extrusion. *Journal of Cell Biology*. https://doi.org/10.1083/jcb.200209011

Rivera, C., Voipio, J., & Kaila, K. (2005). Two developmental switches in GABAergic signalling: The K+-Cl- cotransporter KCC2 and carbonic anhydrase CAVII. *Journal of Physiology*. https://doi.org/10.1113/jphysiol.2004.077495

Rivera, C., Voipio, J., Thomas-Crusells, J., Li, H., Emri, Z., Sipilä, S., Payne, J. A., Minichiello, L., Saarma, M., & Kaila, K. (2004). Mechanism of activity-dependent downregulation of the neuron-specific K-Cl cotransporter KCC2. *Journal of Neuroscience*. https://doi.org/10.1523/JNEUROSCI.5265-03.2004

Ruusuvuori, E., Li, H., Huttu, K., Palva, J. M., Smirnov, S., Rivera, C., Kaila, K., & Voipio, J. (2004). Carbonic Anhydrase Isoform VII Acts As A Molecular Switch in the Development of Synchronous Gamma-Frequency Firing of Hippocampal CA1 Pyramidal Cells. *Journal of Neuroscience*. https://doi.org/10.1523/JNEUROSCI.5176-03.2004

Schulte, U., Thumfart, J. O., Klöcker, N., Sailer, C. A., Bildl, W., Biniossek, M., Dehn, D., Deller, T., Eble, S., Abbass, K., Wangler, T., Knaus, H. G., & Fakler, B. (2006). The epilepsy-linked Lgi1 protein assembles into presynaptic Kv1 channels and inhibits inactivation by Kvβ1. *Neuron*. https://doi.org/10.1016/j.neuron.2006.01.033

Schwartzkroin, P. A., & Prince, D. A. (1980). Changes in excitatory and inhibitory synaptic potentials leading to epileptogenic activity. *Brain Research*. https://doi.org/10.1016/0006-8993(80)90119-5

Sessolo, M., Marcon, I., Bovetti, S., Losi, G., Cammarota, M., Ratto, G. M., Fellin, T., & Carmignoto, G. (2015). Parvalbumin-positive inhibitory interneurons oppose propagation but favor generation of focal epileptiform activity. *Journal of Neuroscience*. https://doi.org/10.1523/JNEUROSCI.5117-14.2015

Shiri, Z., Manseau, F., Lévesque, M., Williams, S., & Avoli, M. (2016). Activation of specific neuronal networks leads to different seizure onset types. *Annals of Neurology*. https://doi.org/10.1002/ana.24570

Singh, B., Ogiwara, I., Kaneda, M., Tokonami, N., Mazaki, E., Baba, K., Matsuda, K., Inoue, Y., & Yamakawa, K. (2006). A Kv4.2 truncation mutation in a patient with temporal lobe epilepsy. *Neurobiology of Disease*. https://doi.org/10.1016/j.nbd.2006.07.001

Somjen, G. G. (2002). Ion regulation in the brain: Implications for pathophysiology. In *Neuroscientist*. https://doi.org/10.1177/1073858402008003011

Toyoda, I., Fujita, S., Thamattoor, A. K., & Buckmaster, P. S. (2015). Unit activity of hippocampal interneurons before spontaneous seizures in an animal model of temporal lobe epilepsy. *Journal of Neuroscience*. https://doi.org/10.1523/JNEUROSCI.4786-14.2015

Traynelis, S. F., & Dingledine, R. (1988). Potassium-induced spontaneous electrographic seizures in the rat hippocampal slice. *Journal of Neurophysiology*. https://doi.org/10.1152/jn.1988.59.1.259

Uva, L., Breschi, G. L., Gnatkovsky, V., Taverna, S., & de Curtis, M. (2015). Synchronous inhibitory potentials precede seizure-like events in acute models of focal limbic seizures. *Journal of Neuroscience*. https://doi.org/10.1523/JNEUROSCI.3692-14.2015

Viitanen, T., Ruusuvuori, E., Kaila, K., & Voipio, J. (2010). The K+-Cl- cotransporter KCC2 promotes GABAergic excitation in the mature rat hippocampus. *Journal of Physiology*. https://doi.org/10.1113/jphysiol.2009.181826

Volman, V., Bazhenov, M., & Sejnowski, T. J. (2011). Pattern of trauma determines the threshold for epileptic activity in a model of cortical deafferentation. *Proceedings of the National Academy of Sciences of the United States of America*. https://doi.org/10.1073/pnas.1112066108

Volman, V., Sejnowski, T. J., & Bazhenov, M. (2011). Topological basis of epileptogenesis in a model of severe cortical trauma. *Journal of Neurophysiology*. https://doi.org/10.1152/jn.00458.2011

Watanabe, M., & Fukuda, A. (2015). Development and regulation of chloride homeostasis in the central nervous system. In *Frontiers in Cellular Neuroscience*. https://doi.org/10.3389/fncel.2015.00371

Wei, Y., Ullah, G., & Schiff, S. J. (2014). Unification of neuronal spikes, seizures, and spreading depression. *Journal of Neuroscience*. https://doi.org/10.1523/JNEUROSCI.0516-14.2014

Yamaguchi, S. ichi, & Rogawski, M. A. (1992). Effects of anticonvulsant drugs on 4-aminopyridine-induced seizures in mice. *Epilepsy Research*. https://doi.org/10.1016/0920-1211(92)90016-M

Yekhlef, L., Breschi, G. L., Lagostena, L., Russo, G., & Taverna, S. (2015). Selective activation of parvalbumin- or somatostatin-expressing interneurons triggers epileptic seizurelike activity in mouse medial entorhinal cortex. *Journal of Neurophysiology*. https://doi.org/10.1152/jn.00841.2014

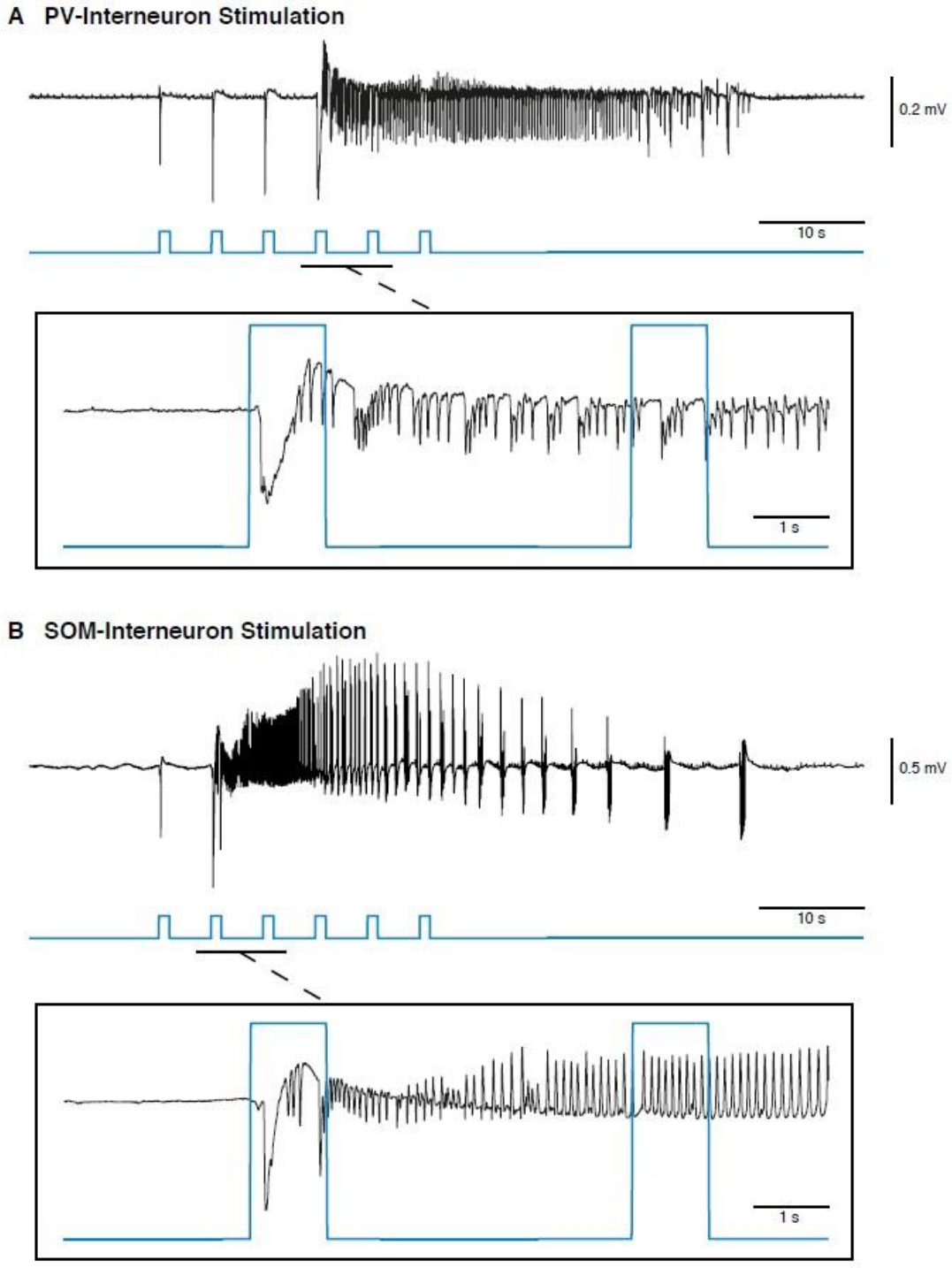

Figure 2.1: Ictal discharges can be triggered by optogenetic stimulation of PV- or SOM-positive interneurons. **(A)** Ictal discharge evoked by 0.2 Hz series of 1 s light pulses stimulating PV-positive interneurons during bath application of 4AP; ictal onset is expanded to show the timing of the light pulse in relation to ictal onset (box). **(B)** The same stimulation parameters applied to SOM-positive interneurons also triggers ictal discharges.

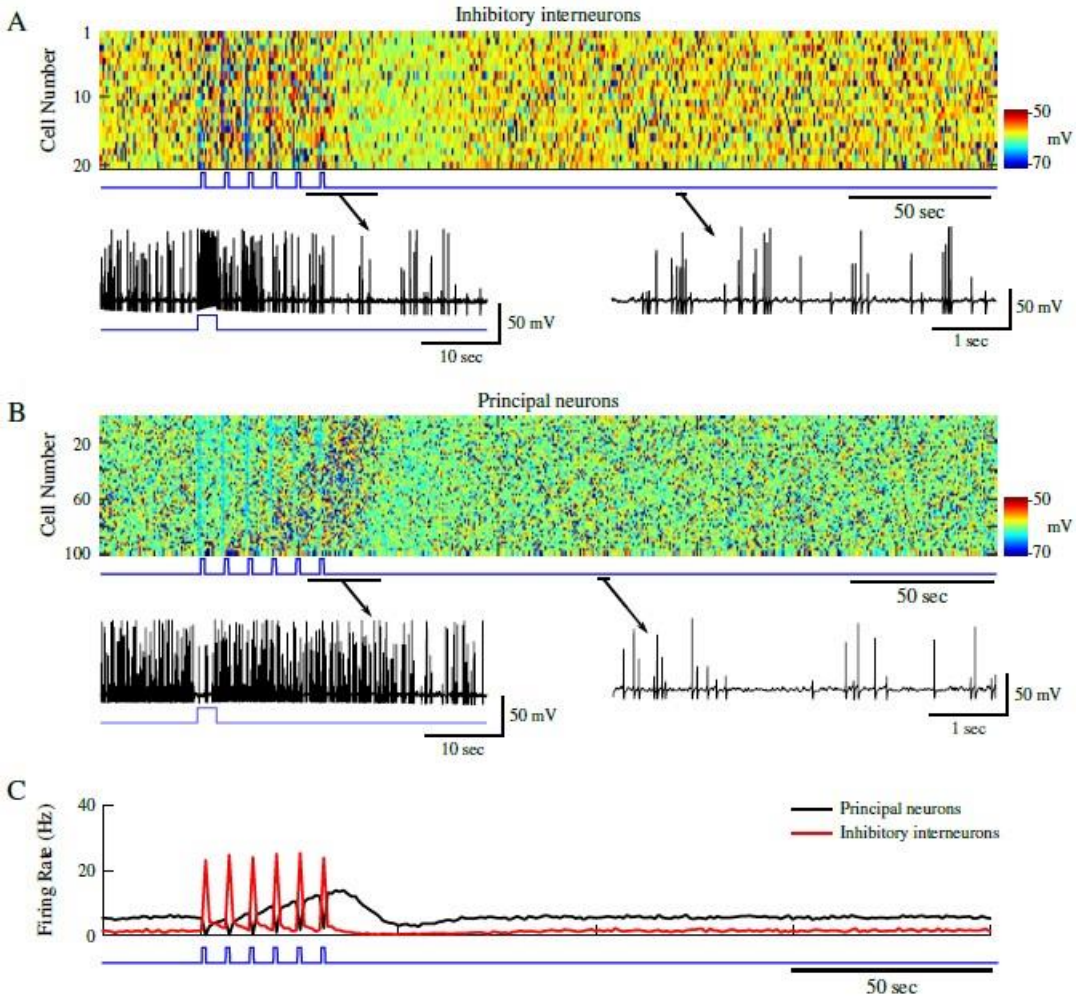

Figure 2.2: Stimulation of inhibitory interneurons in a healthy network results in brief silencing of excitatory neurons. **(A)** Top panel shows raster plot of interneuron activity. Bottom panel shows zoom in of a single representative interneuron spiking from the network in the top panel. Time of interneuron stimulation is indicated by the blue trace. **(B)** Principal neuron network activity with zoom in the spiking pattern of a single principal neuron. The blue trace indicates the time of interneuron stimulation. **(C)** Mean firing rates for the interneurons (red) and the principal neurons (black).

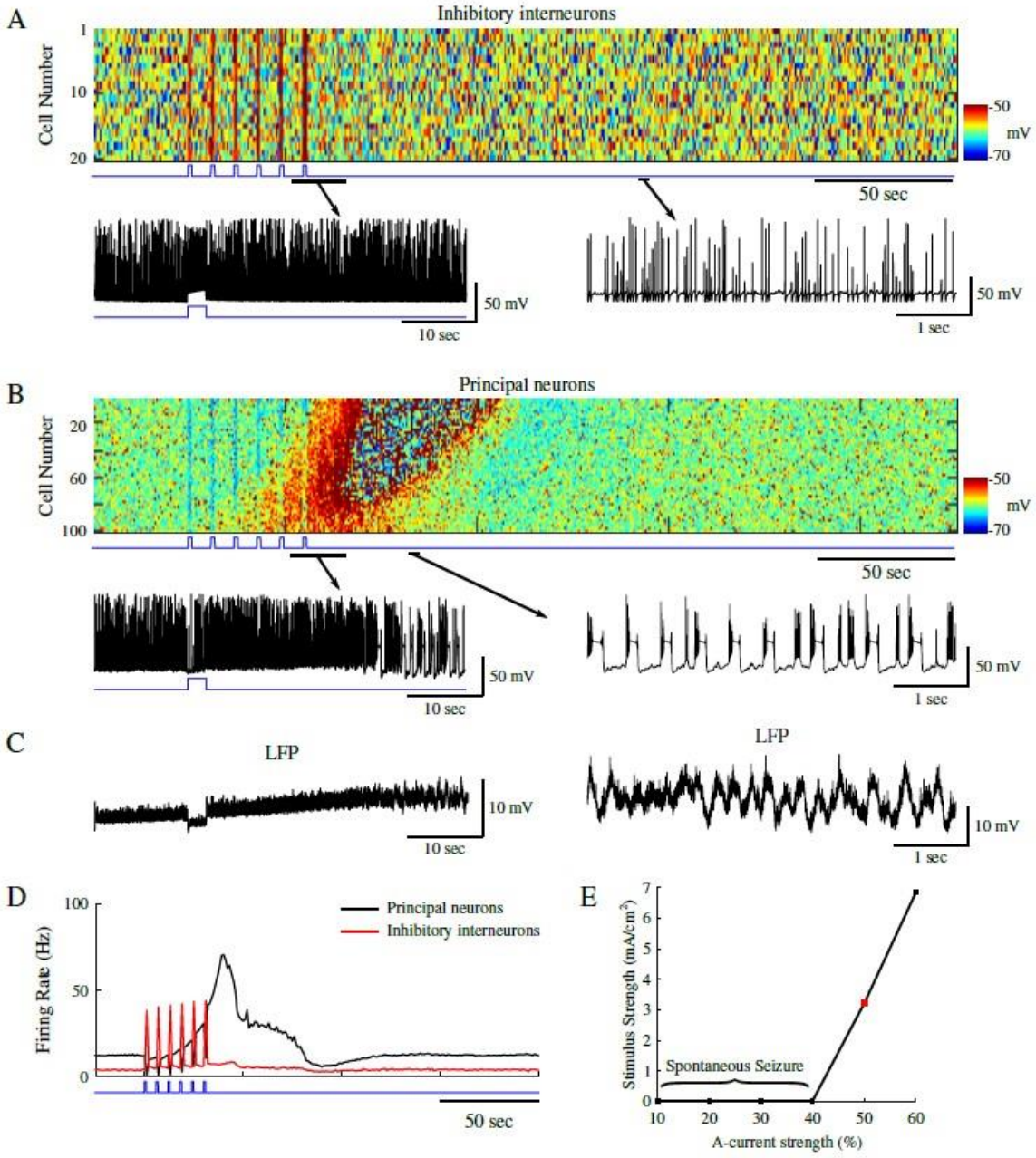

Figure 2.3: Reduction of A-current increases network excitability allowing for ictogenesis upon interneuron stimulation. **(A)** Top panel shows raster plot of interneuron activity. Bottom panel shows zoom in of a single interneuron spiking from the network in the top panel. Time of interneuron stimulation is indicated by the blue trace. **(B)** Principal neuron network activity with zoom in the spiking pattern of a single principal neuron. The blue trace indicates the time of interneuron stimulation. **(C)** Corresponding local field potentials (LFP) for the zoom-ins in B. **(D)** Mean firing rates for the interneurons (red) and principal neurons (black). **(E)** Stimulus strength necessary for seizure generation as a function of A-current strength. Red square indicates the A-current strength used for the network presented in panels A-D.

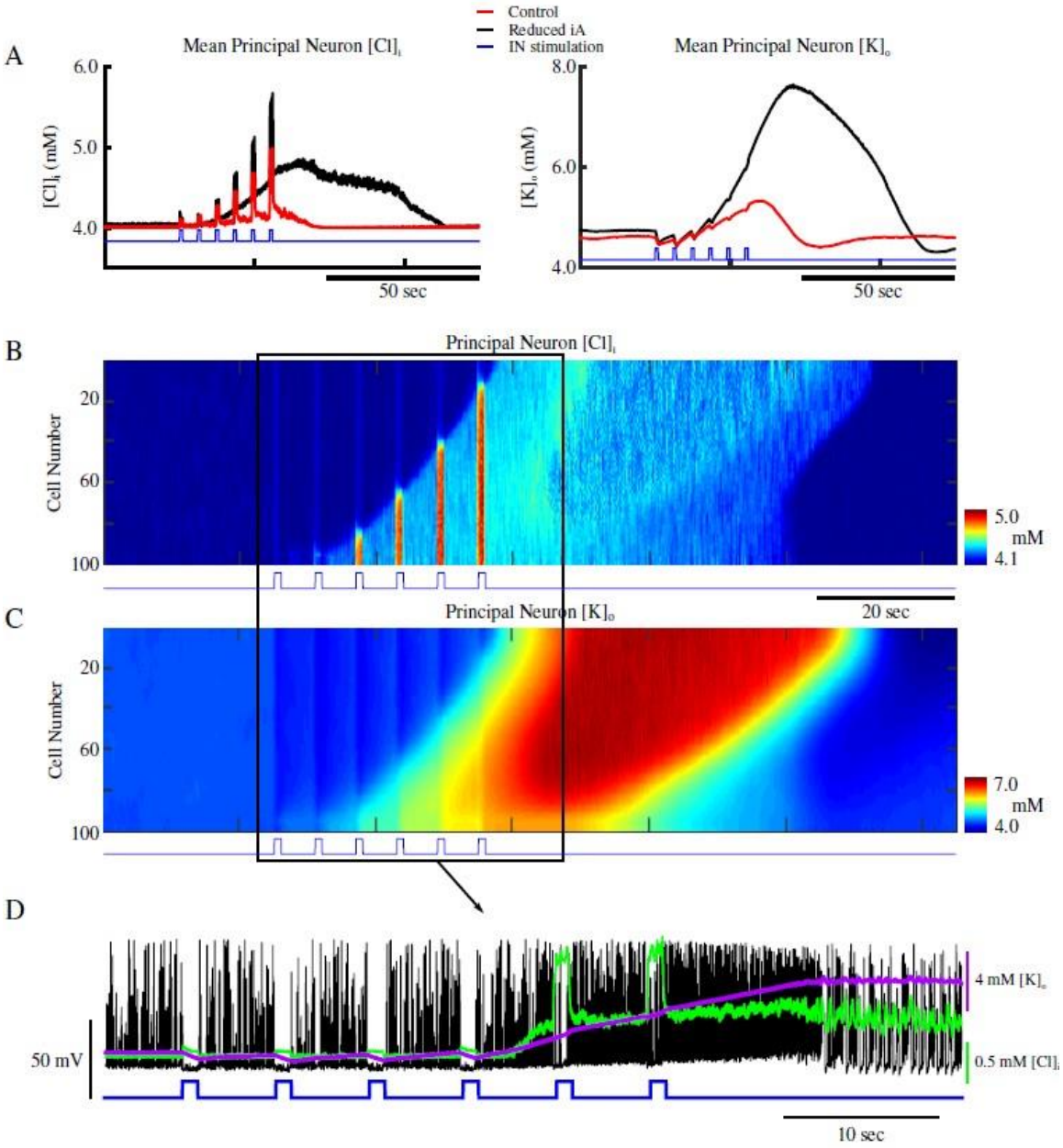

Figure 2.4: Increase of $[Cl^-]_i$ leads to gradual accumulation of $[K^+]_o$ and ictogenesis. **(A)** Mean $[Cl^-]_i$ (left) and $[K^+]_o$ (right) for principal neurons in the control network from figure 2.2, and the reduced A-current network in 2.3 (red and black respectively). The blue trace indicates the pattern of interneuron stimulation. **(B & C)** Network-wide $[Cl^-]_i$ and $[K^+]_o$ for principal neurons. The blue trace indicates the pattern of interneuron stimulation. **(D)** Overlay of the spiking of a single principal neuron (black) from figure 2.3, and the corresponding $[Cl^-]_i$ (green), $[K^+]_o$ (purple) and IN stimulation (blue).

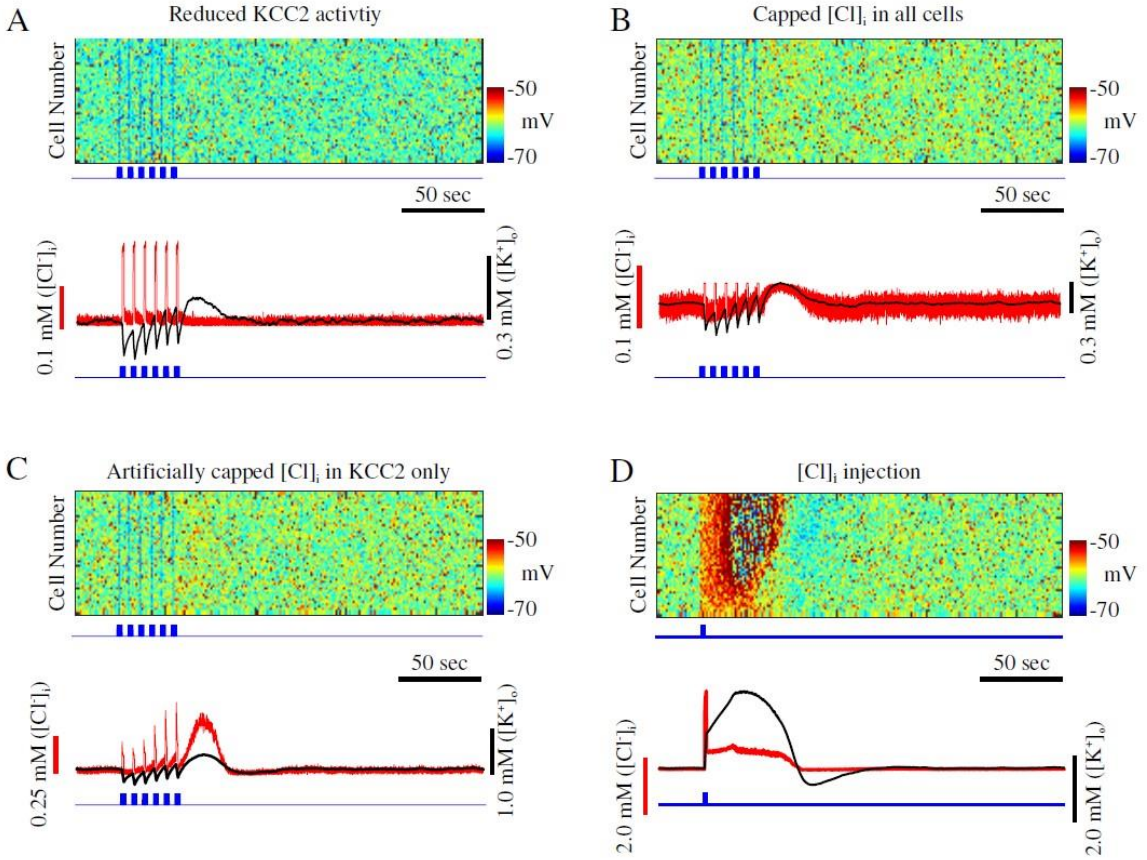

Figure 2.5: Seizure onset is dependent on KCC2 activation. **(A)** Reduction of KCC2 activity prevents seizure. Top, raster plot of principal neurons in a network with reduced A-current and KCC2 activity. Blue trace indicates pattern of interneurons stimulation. Bottom, corresponding mean $[Cl^-]_i$ (red) and mean $[K^+]_o$ (black) for principal neurons in top panel. **(B)** Network with limited $[Cl^-]_i$ accumulation. Top, raster plot showing activity of principal neurons. Bottom, corresponding mean $[Cl^-]_i$ (red) and mean $[K^+]_o$ (black) for principal neurons rom the top panel. **(C)** Network with artificially impaired $[Cl^-]_i$ sensitive K^+ mechanism. Top, raster plot showing activity for principal neurons. Bottom, corresponding mean $[Cl^-]_i$ (red) and mean $[K^+]_o$ (black) for principal neurons in top panel. **(D)** Cl^- injection to principal neurons. Top, raster plot showing activity of principal neurons. Blue trace shows time of Cl^- injection to principal neurons. Bottom, corresponding mean $[Cl^-]_i$ (red) and mean $[K^+]_o$ (black) for principal neurons in top panel.

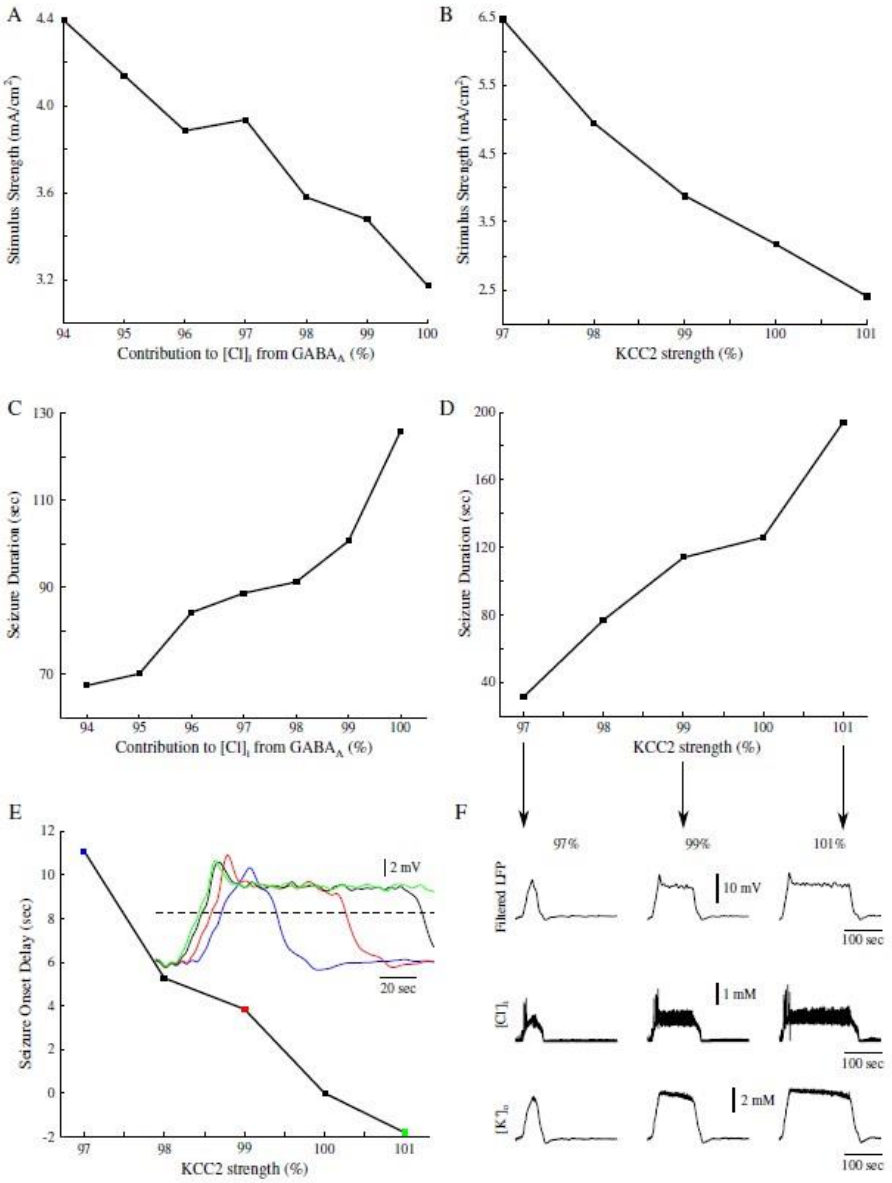

Figure 2.6: Contributions to $[Cl^-]_i$ from $GABA_A$, and KCC2 activity modulate seizure threshold, duration, and onset. **(A)** Seizure threshold as a function of $GABA_A$ contribution to $[Cl^-]_i$. **(B)** Seizure threshold as a function of KCC2 strength. **(C)** Seizure duration as a function of $GABA_A$ contribution to $[Cl^-]_i$. **(D)** Seizure duration as a function of KCC2 activity. **(E)** Seizure onset delay as a function of KCC2 activity. Delay was measured between the onset time of a seizure in the control network with 100% KCC2 strength as compared to the seizure onset time in the networks with varied KCC2 strength. Inset shows examples of the filtered seizure LFPs. Colored data points correspond to the sampled data in the inset. Black trace in the inset represents the control network with 100% KCC2 activity. Dash line shows threshold used to calculate seizure onset times. **(F)** Examples of different seizure durations as a result of varied KCC2 strength. Top, filtered network LFP. Middle and bottom, corresponding mean $[Cl^-]_i$ and $[K^+]_o$ respectively. Arrows point to the corresponding data points in D.

CHAPTER 3: EXPERIMENTAL STUDY

Characterizing Concentration-Dependent Neural Dynamics of 4-Aminopyridine-Induced Epileptiform Activity

Abstract

Epilepsy remains one of the most common neurological disorders. In patients, it is characterized by unprovoked, spontaneous, and recurrent seizures or ictal events. Typically, inter-ictal events or large bouts of population level activity can be measured between seizures and are generally asymptomatic. Decades of research have focused on understanding the mechanisms leading to the development of seizure-like activity using various proconvulsive pharmacological agents, including 4-aimnopyridine (4AP). However, the lack of consistency in the concentrations used for studying 4AP-induced epileptiform activity in animal models may give rise to differences in results and interpretation thereof. Indeed, the range of 4AP concentration in both *in vivo* and *in vitro* studies varies from 3µM to 40mM. Here, we explored the effects of various 4AP concentrations on the development and characteristics of hippocampal epileptiform activity in acute mouse brain slices of either sex. Using multielectrode array recordings, we show that 4AP induces hippocampal epileptiform activity for a broad range of concentrations. The frequency component and the spatiotemporal patterns of the epileptiform activity revealed a dose-dependent response. Finally, in the presence of 4AP, reduction of KCC2 co-transporter activity by KCC2 antagonist VU0240551 prevented the manifestation of the frequency component differences between different concentrations of 4AP. Overall, the study predicts that different concentrations of 4AP can result in the different mechanisms behind hippocampal epileptiform activity, of which some are dependent on the KCC2 co-transporter function.

Introduction

Potassium (K^+) channel activation has been shown to be responsible for the repolarization of the membrane potential following the depolarization phase of an action potential (Bean, 2007; Carrasquillo et al., 2012; Mitterdorfer & Bean, 2002; Pathak et al., 2016; Yuan et al., 2005). Differences in the type of K^+-channels expressed in a given neuron influence the properties of action potentials produced by the neuron (Bean, 2007; Pathak et al., 2016). Outward going K^+ A-type currents (I_A) have been shown to regulate the action potential firing rate by modulating the inter-spike interval in response to subthreshold current injections (Carrasquillo et al., 2012; Mitterdorfer & Bean, 2002; Pathak et al., 2016; Yuan et al., 2005). The I_A is mediated by multimeric channels comprised of mainly K_v4 family α-subunits in combination with modulatory β-subunits (Birnbaum et al., 2004). Functional knock-out, through expression of dominant negative $K_v4.2$ α-subunits ($K_v4.2DN$) in rat cortical pyramidal neurons has been shown to selectively eliminate I_A, resulting in reduced action potential threshold, increased action potential duration, and increased neuronal excitability (Yuan et al., 2005). Additionally, experiments in rat hippocampal neurons have shown that nearly all of the K^+ current underlying the repolarization phase of an action potential can be accounted for by the I_A and the dendrotoxin-sensitive K^+ D-current (I_D) (Mitterdorfer & Bean, 2002). Due to its important role in regulating neuronal excitability, it is not surprising that the I_A has been the subject of intense study in its relation to epileptic seizures.

Certain genetic epilepsies have been linked to misregulated or mutated K^+ channels in humans (Barnwell et al., 2009; D'Adamo et al., 2013; Dazzo et al., 2015;

Lascano et al., 2016; Nobile et al., 2009; Schulte et al., 2006; Singh et al., 2006). Some patients suffering from intractable temporal lobe epilepsy have been shown to express K_v4 α-subunit mutations, specifically truncation mutations in $K_v4.2$ α-subunits (D'Adamo et al., 2013; Singh et al., 2006). In these patients, the mutation manifests as a reduction of the I_A thereby leading to hyperexcitability. Similarly, I_A and I_D antagonist 4-aminopyridine (4AP) has been shown to cause hyperexcitability and the development of seizure-like epileptiform discharges both *in vivo* and *in vitro* (Ahn et al., 2016; Avoli et al., 2016; De Curtis & Avoli, 2016; González et al., 2018; Hamidi & Avoli, 2015; Lévesque et al., 2016; Shiri et al., 2016; Uva et al., 2015; Viitanen et al., 2010; Yekhlef et al., 2015). Recent work suggests that the mechanism by which 4AP induces epileptiform activity is not through its direct reduction of I_A or I_D and increased principle neuron excitation; rather, 4AP increases the excitability of both inhibitory and excitatory neurons, the former of which is pivotal in the development of seizure-like activity (Avoli et al., 2016; González et al., 2018; Hamidi & Avoli, 2015; Lévesque et al., 2016; Shiri et al., 2016; Uva et al., 2015; Yekhlef et al., 2015). Previous studies have shown that the potassium-chloride co-transporter isoform 2 (KCC2) plays an important role in the generation of 4AP-induced seizure (Avoli et al., 2016; González et al., 2018; Hamidi & Avoli, 2015; Lévesque et al., 2016; Viitanen et al., 2010). Indeed, in rat brain slices treated with 4AP, reduction of KCC2 activity prevents seizure-like discharges while inter-ictal activity remained relatively intact (Hamidi & Avoli, 2015). The mechanism and extent to which KCC2 influences the properties of 4AP-induced inter-ictal activity remains to be fully understood.

Previous studies have attempted to fill this gap in our understanding of the precise effects of 4AP on neuronal activity, but lack of consistency in their methodologies and concentrations of 4AP, ranging from 3 µM to 40 mM, used for such studies has prevented the development of a complete picture (Ahn et al., 2016; Galvan et al., 1982; Guo et al., 2016; Hamidi & Avoli, 2015; Lévesque et al., 2013; Shiri et al., 2016; Yekhlef et al., 2015; Yu et al., 2014). In our new study, we explored the concentration-dependent effects of 4AP on the spatiotemporal properties of induced epileptiform activity in acute mouse hippocampal brain slices. We found that bath applied 4AP produced dose-specific epileptiform bursts, the properties of which depended on 4AP concentration. Additionally, the reduction of KCC2 co-transporter activity through bath applied VU0240551 prevented the generation of the higher frequency component of epileptiform bursts at high 4AP concentrations.

Materials & Methods

Animals

All experiments and procedures were performed according to University of California, Riverside Institutional Animal Care and Use Committee-approved protocols. Wild-type (Jackson Laboratory, C57BL/6J, stock number 000664) mice colonies were bred and maintained in house to generate pups for this study. All mice were provided fresh water and mouse chow *ad libitum*, and a consistent circadian cycle was maintained by the vivarium facility. Both male and female mice were used in this study.

Brain slice preparation

Postnatal day (P) 15-20 mice were anesthetized with isoflurane and quickly decapitated. The brain was rapidly removed and submerged in ice-cold, low $[Ca^{2+}]_o$, high sucrose dissecting solution continuously oxygenated with carbogen (95%-5% O_2-CO_2) gas. Horizontal whole brain slices (300 μm) were made with a Leica 1200S vibratome. Slices containing both hippocampus and entorhinal cortex were recovered in oxygenated normal artificial cerebrospinal fluid (ACSF) for 1 h at 32C, and then stored at room temperature until use. The standard dissecting solution contained (mM): 87 NaCl, 2.5 KCl, 25 $NaHCO_3$, 1.25 NaH_2PO_4, 4 $MgCl_2$, 0.5 $CaCl_2$, 10 D-glucose, and 75 sucrose. During recordings, brain slices were continuously perfused with ACSF (3 ml/min flow rate) containing (mM): 125 NaCl, 2.5 KCl, 25 $NaHCO_3$, 1.25 NaH_2PO_4, 1 $MgCl_2$, 2 $CaCl_2$, 25 D-glucose, and 10 sucrose. Both solutions were maintained at pH 7.4 by continuous oxygenation with carbogen gas. All chemicals were obtained though Fisher Scientific unless otherwise specified.

Electrophysiological recordings

Multielectrode array (MEA) recordings were performed on a 60-channel perforated array (60pMEA200/30-Ti) with a low-noise amplifier (MEA1060-BC) from MultiChannel Systems. Hippocampal slices were prepared, as described above, placed on the array, and positioned such that the CA1, CA3, and dentate gyrus (DG) were centered over the recording electrodes. Channels with high noise level were silenced prior to recording. Experiments consisted of an initial 30 min ACSF control followed by eight consecutive 30 min conditions of increasing 4-aminopyridine concentrations (25 – 200

μM in 25 μM step sizes). To test the effect of the KCC2 co-transporter on the characteristics of 4AP-induced epileptiform activity, we followed the same procedure outlined above, but added 10 μM of the KCC2 co-transporter antagonist VU0240551 to the perfusate containing 4AP. All MEA recordings were performed at 32C, which was sufficient to generate stable epileptiform activity. For 4AP only experiments n = 4 slices from 4 different mice, and for 4AP + VU0240551 n = 6 slices from 6 different mice.

Analysis

Data were acquired using MC Rack software (MultiChannel Systems) and exported to MATLAB (MathWorks) for further processing. Data from all 60 MEA channels were collected at 25 kHz and downsampled offline to 5 kHz. Synchronized network activity or epileptiform bursts recorded by the MEA were detected using our previously described percentile-based method (Krishnan et al., 2013). Briefly, a low (1.25 ± 0.75) and high (98.75 ± 0.75) percentile were used on unfiltered data from a single channel recording from each of the hippocampal subfields mentioned above. The low percentile was used for events with negative polarity, while the high percentile was used for events with positive polarity. The amplitude corresponding to the low or high percentile was used as a threshold for detecting the epileptiform bursts. Similar to (Krishnan et al., 2013), burst onset was defined as the moment when the LFP crossed the percentile-defined threshold. The bursts were extracted from all channels with 500 ms before and after burst onset, and a non-overlapping period of 1 s was used. Inter-event intervals were computed as the difference between timing of the peak of a given event and that of the event prior to it. Event frequency was computed as the inverse of the inter-

event interval. Fourier transforms were performed on the unfiltered, downsampled data using Matlab function fft. We used a sliding window of size 60 s with a 30 s overlap to compute the mean power spectrum. The mean was computed across all resulting transform signals across all slices for each condition. Data are presented as mean +/- standard error (SEM).

Results

We induced epileptiform activity throughout the hippocampal cortex by bath application of 4-aminopyridine (4AP). Local field potentials (LFPs) were recorded from the hippocampal subfields CA1, CA3, and DG using a 60-channel MEA (figure 3.1A). Control, ACSF only, recordings showed minimal multiunit activity (data not shown). Spontaneous epileptiform activity was not observed in control conditions. Bath applied 4AP at all concentrations tested in this study (25 – 200 μM) resulted in a transition from quiescence to a seizure-like state characterized by stereotyped continuous epileptiform activity (figure 3.1). Epileptiform activity was robust, and highly synchronized across all MEA electrodes (figure 3.1B). Single channel recordings from CA1, CA3, and DG revealed a bias towards CA3 as the generator of the largest epileptiform activity (figure 3.1C, E). Figure 3.1D shows all the extracted epileptiform bursts (see Methods) from a single channel in CA3 superimposed (black traces) with the average burst superimposed in red. This revealed that the events recorded from the same channel show similar temporal properties throughout the duration of the burst. The temporal similarities in burst progression were not constrained to recordings from CA3. Figure 3.1F shows

heatmaps of all bursts recorded in the same channels from CA1, CA3, and DG revealing stereotyped activity induced throughout the hippocampus by 4AP.

As shown in figure 3.1, 100 µM 4AP resulted in stereotyped epileptiform activity. Since 4AP selectively blocks outward going K^+ A- and D-currents, we hypothesized that varying the concentration of 4AP may lead to differences in the properties of the resulting epileptiform activity. To test this, we varied the concentration of bath applied 4AP, ranging from 25 – 200 µM in 25 µM step sizes. Epileptiform activity was reliably elicited for all 4AP concentrations from that range. We first examined the differences in the spatiotemporal distribution of epileptiform bursts throughout the hippocampus. Figure 3.2 shows the propagation of a single epileptiform burst (such as, e.g., shown in figure 3.1D), resulting from different concentrations of bath applied 4AP, throughout the hippocampus. For all concentrations, the initiation of epileptiform bursts occurred near the CA3 subfield before propagating to the rest of the hippocampus (figure 3.2). These epileptiform bursts initiated with a positive electrical potential (source) within the areas of the proximal and distal dendrites, which was accompanied by a negative potential (sink) within stratum pyramidale. Similar findings have been reported for epileptiform activity induced through elevated extracellular K^+ concentration ($[K^+]_o$) (Krishnan et al., 2013). This was then followed by a reversal of the polarity of the field potentials in their respective locations.

We observed a much wider spatial distribution of epileptiform activity for low concentrations (figure 3.2A). As seen for 25 and 50 µM concentrations, the electrical activity recorded during the 50 – 100 ms frame showed electrical activity propagating

from CA3 to CA1. As mentioned previously, the stratum pyramidale exhibited a negative LFP while the regions containing pyramidal cell dendrites exhibited a positive LFP during early and middle phases of the epileptiform burst, which reversed in time during the later phase of the event. Additionally, in low concentrations (25 – 50 μM) the negative potential recorded from stratum pyramidale remained for 200 ms before reversing polarity. Unlike the prolonged period of negative LFP for low concentrations of 4AP, concentrations ranging from 75 – 100 μM exhibited a slightly prolonged period of positive LFP within CA3 and DG (compare time frames 150-200ms, 200-250ms, and 250-300ms for concentrations 25 – 100 μM of figures 3.2A and 3.2B). For high concentrations of 4AP (125 – 200 μM), the spatial distribution of the epileptiform burst became more focal and short lived (figure 3.2C). Indeed, little activity was observed following 100 ms after the initiation of the epileptiform burst. These data suggest that the extent of the reduction of A- and D-current activity may cause substantial differences in the dynamics of the epileptiform activity.

The differences in the spatiotemporal distributions of the epileptiform activity shown in figure 3.2 could reflect underlying differences in the frequency components of the epileptiform bursts. To explore this, we computed power spectrums of the electrical signals generated by the hippocampal slice under the conditions of bath applied 4AP. We observed that low concentrations of 4AP, 25 – 50 μM, generated epileptiform bursts that were mainly characterized by low frequencies <5 Hz (figure 3.3A). The activity generated with 75 μM 4AP showed a small increase in higher frequencies (around 7 – 15 Hz), a trend also observed in epileptiform bursts generated at 100 μM 4AP (figure 3.3B).

These higher frequencies became more prominent at higher concentrations, 125 – 200 µM (figure 3.3C). Insets show an example of a single corresponding epileptiform burst, for the concentration indicated, showing increased burst complexity with increasing 4AP concentration. Interestingly, the low frequency component of the epileptiform bursts remained largely intact at high concentrations. These data, along with the previously described data (figure 3.2), support our hypothesis that differentially impairing A- and D-current activity results in different epileptiform activity profiles.

Recent evidence has suggested that the potassium-chloride co-transporter isoform 2 (KCC2) may play a key role in the generation of 4AP-induced epileptiform activity (Avoli et al., 2016; González et al., 2018; Hamidi & Avoli, 2015; Lévesque et al., 2016; Viitanen et al., 2010). We hypothesized that the reduction of KCC2 activity by KCC2 antagonist VU0240551 may reduce the complexity of epileptiform activity elicited at higher concentrations of 4AP, resulting in more stereotyped epileptiform activity across various 4AP concentrations. To test this hypothesis, we bath applied the KCC2 specific antagonist VU0240551, and varied the bath applied 4AP concentrations. Similar to our previous experiment (figure 3.1), we observed 4AP-induced epileptiform for all concentrations tested with CA3 exhibiting the largest amplitude epileptiform bursts. Low 4AP concentration conditions (25 – 50 µM), once again, produced epileptiform activity dominated by low frequency activity (figure 3.4A). Interestingly, increasing the 4AP concentrations from 75 – 200 µM did not lead to a power spectrum peak at higher frequencies as seen previously in conditions of normal functioning KCC2 (compare figures 3.3B, C and 3.4B, C). Additionally, the epileptiform activity elicited in the

presence of the KCC2 antagonist became stereotyped across 4AP concentrations (compare figure 3.4 insets). These findings suggest that the high frequency component of the epileptiform activity for high 4AP concentrations may be dependent on the recruitment of KCC2-dependent mechanisms.

Since application of the KCC2 co-transporter antagonist resulted in overall low frequency epileptiform activity for all 4AP concentrations tested, we hypothesized that this trend may be reflected in the inter-arrival times of the epileptiform bursts. To this end, we computed the inter-event interval for different 4AP concentrations for both 4AP only and 4AP + VU0240551 conditions. As shown in figure 3.5A, increasing 4AP concentrations resulted in shorter inter-event intervals for both conditions (i.e. with and without VU0240551). In agreement with our hypothesis, reduction of KCC2 activity increased inter-event intervals (compare figure 3.5A red and black lines). For the condition of 4AP only, we observed higher event frequencies as compared to the condition of reduced KCC2 activity (figure 3.5B). The largest differences in event frequency were observed for lower concentrations (compare figure 3.5B red and black). As the concentration of 4AP increased, the frequency of events observed in the 4AP + VU0240551 condition increased to levels similar to those seen in the 4AP-only condition. A summary of the concentration-dependent differences for both 4AP only and 4AP + VU0240551 conditions are presented in Table 3.1A and B, respectively.

Discussion

K^+-channels regulate the intrinsic excitability of neurons and maintain the repolarization phase of action potentials (Bean, 2007; Birnbaum et al., 2004; Carrasquillo et al., 2012; Cudmore et al., 2010; Hyun et al., 2013; Metz et al., 2007; Mitterdorfer & Bean, 2002; Pathak et al., 2016; Yuan et al., 2005). Specifically, the I_A and I_D seem to account for nearly all of the K^+-current during this repolarization phase in principal neurons (Mitterdorfer & Bean, 2002). Due to the roles of these two currents in the regulation of neuronal excitability, they have been the focus of decades of intense study with the hope of gaining a better understanding of the mechanisms leading to the development of epilepsy (Avoli et al., 2016; D'Adamo et al., 2013; Galvan et al., 1982; Lévesque et al., 2013; Schulte et al., 2006; Singh et al., 2006). In this new study, we tested the hypothesis that the effect of I_A and I_D channel antagonist 4-aminopyridine (4AP) is strongly concentration-dependent. Different 4AP concentrations are characterized by qualitatively different spatiotemporal patterns of epileptiform activity in acute mouse hippocampal brain slices. Our *in vitro* data suggests that the spatiotemporal propagation, underlying frequency components, and inter-event intervals of 4AP-induced epileptiform activity vary with concentration. Furthermore, high concentrations of 4AP lead to the appearance of the high frequency component in epileptiform bursts, which may be dependent on the activation of the KCC2 co-transporter.

We found that for all concentrations used in our study, epileptiform activity originated in the CA3 hippocampal subfield before propagating to CA1 and DG. This result is similar to previously reported findings that the CA3 region is the initiator of

epileptiform activity induced by elevated K^+ (Filatov et al., 2011; Krishnan et al., 2013). The local architecture of the CA3 makes it a prime candidate for seizure generation. Indeed, the pyramidal neurons within the CA3 exhibit a high degree of recurrent connectivity (Le Duigou et al., 2014). The differences in the spatiotemporal patterns of epileptiform activity arise during the application of "transition" 4AP concentrations (75 – 100 µM) and more so at high concentrations (125 – 200 µM). Low 4AP concentrations (25 – 50 µM) generate longer lasting epileptiform bursts as compared to those induced by transitional and high concentrations. This may be due to altered excitability of hippocampal pyramidal neurons in response to reduced I_A and I_D. Previous studies in cultured pyramidal neurons showed that the elimination of I_A, by expression of $K_v4.2$ dominant negative mutant, resulted in increased neuronal excitability to low-amplitude current stimulation (Yuan et al., 2005). Interestingly, large-amplitude current injections generated transient spiking before the neuron ceased spiking activity (Yuan et al., 2005). This reduction of prolonged spiking as a result of I_A reduction may explain the reduced durations of epileptiform bursts seen in at higher 4AP concentrations.

One of the more prominent concentration-dependent features we observed was the change in the frequency components of the induced epileptiform activity. For low concentrations of 4AP (25 – 50 µM), the epileptiform activity was dominated by a low frequency component (~5 Hz). As the concentration was increased towards 200 µM an additional high frequency component (~ 10 Hz) appeared. These changes in frequency were accompanied by overall reduction in the inter-event interval and increases in the frequency of events. This, along with the other observed concentration-dependent

differences may be due to the relative differences in 4AP sensitivity exhibited by I_A and I_D. I_D has been shown to be much more sensitive to 4AP as compared to I_A (Mitterdorfer & Bean, 2002). As such, it is likely that the I_D is selectively blocked at the low concentrations used in this study and is responsible for the low frequency epileptiform activity. As the 4AP concentration was increased, 4AP may also block the I_A, in addition to I_D. This effect may explain the interesting transition observed for 75 – 100 μM 4AP. Additional experiments are needed to determine the relative contributions of these two currents in the development of epileptiform activity.

Recent work has pointed to the role of the KCC2 co-transporter in the development of 4AP-induced seizure (Avoli et al., 2016; González et al., 2018; Hamidi & Avoli, 2015; Lévesque et al., 2016; Viitanen et al., 2010). KCC2-dependent efflux and accumulation of extracellular K^+ may drive transitions to a seizure-state by initiating a positive feedback loop in which elevated K^+ leads to network depolarization, which in turn leads to further accumulation of extracellular K^+ (Bazhenov et al., 2004; Fröhlich & Bazhenov, 2006; González et al., 2015, 2018; Krishnan & Bazhenov, 2011; Somjen, 2002; Wei et al., 2014; Yekhlef et al., 2015). Previous studies have shown that 4AP-induced ictal, seizure-like activity can be abolished in response to reduced KCC2 co-transporter activity (Hamidi & Avoli, 2015). With this in mind, we tested whether reduction of KCC2 co-transporter activity could prevent the changes in epileptiform activity induced at high 4AP concentrations. Our results showed that the high frequency component of the epileptiform activity was abolished in response to KCC2 antagonist VU0240551. Additionally, the inter-event interval was increased at low concentrations,

while the event frequency was reduced for lower 4AP concentrations in the presence of VU0240551 as compared to 4AP only. These data may point to differences in the mechanisms by which I_A and I_D reduction leads to seizure generation, with the former involving KCC2-dependent K^+ efflux and accumulation.

Conclusion

In sum, our study revealed the complex effect of 4AP application, possibly involving several complimentary biophysical mechanisms dependent on both ionic currents and exchangers. It further suggests that the relative contribution of these mechanisms to epileptiform activity and the overall effect of 4AP application may vary with 4AP concentration.

References

Ahn, S., Jun, S. B., Lee, H. W., & Lee, S. (2016). Computational modeling of epileptiform activities in medial temporal lobe epilepsy combined with in vitro experiments. *Journal of Computational Neuroscience*. https://doi.org/10.1007/s10827-016-0614-8

Avoli, M., De Curtis, M., Gnatkovsky, V., Gotman, J., Köhling, R., Lévesque, M., Manseau, F., Shiri, Z., & Williams, S. (2016). Specific imbalance of excitatory/inhibitory signaling establishes seizure onset pattern in temporal lobe epilepsy. *Journal of Neurophysiology*. https://doi.org/10.1152/jn.01128.2015

Barnwell, L. F. S., Lugo, J. N., Lee, W. L., Willis, S. E., Gertz, S. J., Hrachovy, R. A., & Anderson, A. E. (2009). Kv4.2 knockout mice demonstrate increased susceptibility to convulsant stimulation. *Epilepsia*, *50*(7). https://doi.org/10.1111/j.1528-1167.2009.02086.x

Bazhenov, M., Timofeev, I., Steriade, M., & Sejnowski, T. J. (2004). Potassium model for slow (2-3 Hz) in vivo neocortical paroxysmal oscillations. *Journal of Neurophysiology*. https://doi.org/10.1152/jn.00529.2003

Bean, B. P. (2007). The action potential in mammalian central neurons. In *Nature Reviews Neuroscience*. https://doi.org/10.1038/nrn2148

Birnbaum, S. G., Varga, A. W., Yuan, L. L., Anderson, A. E., Sweatt, J. D., & Schrader, L. A. (2004). Structure and function of Kv4-family transient potassium channels. In *Physiological Reviews*. https://doi.org/10.1152/physrev.00039.2003

Carrasquillo, Y., Burkhalter, A., & Nerbonne, J. M. (2012). A-type K+ channels encoded by Kv4.2, Kv4.3 and Kv1.4 differentially regulate intrinsic excitability of cortical pyramidal neurons. *Journal of Physiology*. https://doi.org/10.1113/jphysiol.2012.229013

Cudmore, R. H., Fronzaroli-Molinieres, L., Giraud, P., & Debanne, D. (2010). Spike-time precision and network synchrony are controlled by the homeostatic regulation of the D-type potassium current.

Journal of Neuroscience. https://doi.org/10.1523/JNEUROSCI.0740-10.2010
D'Adamo, M. C., Catacuzzeno, L., di Giovanni, G., Franciolini, F., & Pessia, M. (2013). K+ channelepsy: Progress in the neurobiology of potassium channels and epilepsy. In *Frontiers in Cellular Neuroscience*. https://doi.org/10.3389/fncel.2013.00134
Dazzo, E., Santulli, L., Posar, A., Fattouch, J., Conti, S., Lodén-van Straaten, M., Mijalkovic, J., De Bortoli, M., Rosa, M., Millino, C., Pacchioni, B., Di Bonaventura, C., Giallonardo, A. T., Striano, S., Striano, P., Parmeggiani, A., & Nobile, C. (2015). Autosomal dominant lateral temporal epilepsy (ADLTE): Novel structural and single-nucleotide LGI1 mutations in families with predominant visual auras. *Epilepsy Research*. https://doi.org/10.1016/j.eplepsyres.2014.12.004
De Curtis, M., & Avoli, M. (2016). GABAergic networks jump-start focal seizures. In *Epilepsia*. https://doi.org/10.1111/epi.13370
Filatov, G., Krishnan, G. P., Rulkov, N. F., & Bazhenov, M. (2011). Dynamics of epileptiform activity in mouse hippocampal slices. *Journal of Biological Physics*. https://doi.org/10.1007/s10867-011-9216-x
Fröhlich, F., & Bazhenov, M. (2006). Coexistence of tonic firing and bursting in cortical neurons. *Physical Review E - Statistical, Nonlinear, and Soft Matter Physics*. https://doi.org/10.1103/PhysRevE.74.031922
Galvan, M., Grafe, P., & Bruggencate, G. Ten. (1982). Convulsant actions of 4-aminopyridine on the guinea-pig olfactory cortex slice. *Brain Research*. https://doi.org/10.1016/0006-8993(82)91230-6
González, O. C., Krishnan, G. P., Chauvette, S., Timofeev, I., Sejnowski, T., & Bazhenov, M. (2015). Modeling of age-dependent epileptogenesis by differential homeostatic synaptic scaling. *Journal of Neuroscience*, *35*(39). https://doi.org/10.1523/JNEUROSCI.5038-14.2015
González, O. C., Shiri, Z., Krishnan, G. P., Myers, T. L., Williams, S., Avoli, M., & Bazhenov, M. (2018). Role of KCC2-dependent potassium efflux in 4-Aminopyridine-induced Epileptiform synchronization. *Neurobiology of Disease*. https://doi.org/10.1016/j.nbd.2017.10.011
Guo, Z., Feng, Z., Yu, Y., Zhou, W., Wang, Z., & Wei, X. (2016). Sinusoidal stimulation trains suppress epileptiform spikes induced by 4-AP in the rat hippocampal CA1 region in-vivo. *Proceedings of the Annual International Conference of the IEEE Engineering in Medicine and Biology Society, EMBS*. https://doi.org/10.1109/EMBC.2016.7592050
Hamidi, S., & Avoli, M. (2015). KCC2 function modulates in vitro ictogenesis. *Neurobiology of Disease*. https://doi.org/10.1016/j.nbd.2015.04.006
Hyun, J. H., Eom, K., Lee, K. H., Ho, W. K., & Lee, S. H. (2013). Activity-dependent downregulation of D-type K+ channel subunit Kv1.2 in rat hippocampal CA3 pyramidal neurons. *Journal of Physiology*. https://doi.org/10.1113/jphysiol.2013.259002
Krishnan, G. P., & Bazhenov, M. (2011). Ionic dynamics mediate spontaneous termination of seizures and postictal depression state. *Journal of Neuroscience*. https://doi.org/10.1523/JNEUROSCI.6200-10.2011
Krishnan, G. P., Filatov, G., & Bazhenov, M. (2013). Dynamics of high-frequency synchronization during seizures. *Journal of Neurophysiology*. https://doi.org/10.1152/jn.00761.2012
Lascano, A. M., Korff, C. M., & Picard, F. (2016). Seizures and epilepsies due to channelopathies and neurotransmitter receptor dysfunction: A parallel between genetic and immune aspects. In *Molecular Syndromology*. https://doi.org/10.1159/000447707
Le Duigou, C., Simonnet, J., Teleñczuk, M. T., Fricker, D., & Miles, R. (2014). Recurrent synapses and circuits in the CA3 region of the hippocampus: An associative network. *Frontiers in Cellular Neuroscience*. https://doi.org/10.3389/fncel.2013.00262
Lévesque, M., Herrington, R., Hamidi, S., & Avoli, M. (2016). Interneurons spark seizure-like activity in the entorhinal cortex. *Neurobiology of Disease*. https://doi.org/10.1016/j.nbd.2015.12.011
Lévesque, M., Salami, P., Behr, C., & Avoli, M. (2013). Temporal lobe epileptiform activity following systemic administration of 4-aminopyridine in rats. *Epilepsia*. https://doi.org/10.1111/epi.12041
Metz, A. E., Spruston, N., & Martina, M. (2007). Dendritic D-type potassium currents inhibit the spike afterdepolarization in rat hippocampal CA1 pyramidal neurons. *Journal of Physiology*. https://doi.org/10.1113/jphysiol.2006.127068
Mitterdorfer, J., & Bean, B. P. (2002). Potassium currents during the action potential of hippocampal CA3 neurons. *Journal of Neuroscience*. https://doi.org/10.1523/jneurosci.22-23-10106.2002

Nobile, C., Michelucci, R., Andreazza, S., Pasini, E., Tosatto, S. C. E., & Striano, P. (2009). LGI1 mutations in autosomal dominant and sporadic lateral temporal epilepsy. In *Human Mutation*. https://doi.org/10.1002/humu.20925

Pathak, D., Guan, D., & Foehring, R. C. (2016). Roles of specific Kv channel types in repolarization of the action potential in genetically identified subclasses of pyramidal neurons in mouse neocortex. *Journal of Neurophysiology*. https://doi.org/10.1152/jn.01028.2015

Schulte, U., Thumfart, J. O., Klöcker, N., Sailer, C. A., Bildl, W., Biniossek, M., Dehn, D., Deller, T., Eble, S., Abbass, K., Wangler, T., Knaus, H. G., & Fakler, B. (2006). The epilepsy-linked Lgi1 protein assembles into presynaptic Kv1 channels and inhibits inactivation by Kvβ1. *Neuron*. https://doi.org/10.1016/j.neuron.2006.01.033

Shiri, Z., Manseau, F., Lévesque, M., Williams, S., & Avoli, M. (2016). Activation of specific neuronal networks leads to different seizure onset types. *Annals of Neurology*. https://doi.org/10.1002/ana.24570

Singh, B., Ogiwara, I., Kaneda, M., Tokonami, N., Mazaki, E., Baba, K., Matsuda, K., Inoue, Y., & Yamakawa, K. (2006). A Kv4.2 truncation mutation in a patient with temporal lobe epilepsy. *Neurobiology of Disease*. https://doi.org/10.1016/j.nbd.2006.07.001

Somjen, G. G. (2002). Ion regulation in the brain: Implications for pathophysiology. In *Neuroscientist*. https://doi.org/10.1177/1073858402008003011

Uva, L., Breschi, G. L., Gnatkovsky, V., Taverna, S., & de Curtis, M. (2015). Synchronous inhibitory potentials precede seizure-like events in acute models of focal limbic seizures. *Journal of Neuroscience*. https://doi.org/10.1523/JNEUROSCI.3692-14.2015

Viitanen, T., Ruusuvuori, E., Kaila, K., & Voipio, J. (2010). The K+-Cl- cotransporter KCC2 promotes GABAergic excitation in the mature rat hippocampus. *Journal of Physiology*. https://doi.org/10.1113/jphysiol.2009.181826

Wei, Y., Ullah, G., & Schiff, S. J. (2014). Unification of neuronal spikes, seizures, and spreading depression. *Journal of Neuroscience*. https://doi.org/10.1523/JNEUROSCI.0516-14.2014

Yekhlef, L., Breschi, G. L., Lagostena, L., Russo, G., & Taverna, S. (2015). Selective activation of parvalbumin- or somatostatin-expressing interneurons triggers epileptic seizurelike activity in mouse medial entorhinal cortex. *Journal of Neurophysiology*. https://doi.org/10.1152/jn.00841.2014

Yu, P. N., Hsiao, M. C., Song, D., Liu, C. Y., Heck, C. N., Millett, D., & Berger, T. W. (2014). Unstable periodic orbits in human epileptic hippocampal slices. *2014 36th Annual International Conference of the IEEE Engineering in Medicine and Biology Society, EMBC 2014*. https://doi.org/10.1109/EMBC.2014.6944946

Yuan, W., Burkhalter, A., & Nerbonne, J. M. (2005). Functional role of the fast transient outward K+ current I A in pyramidal neurons in (rat) primary visual cortex. *Journal of Neuroscience*. https://doi.org/10.1523/JNEUROSCI.2858-05.2005

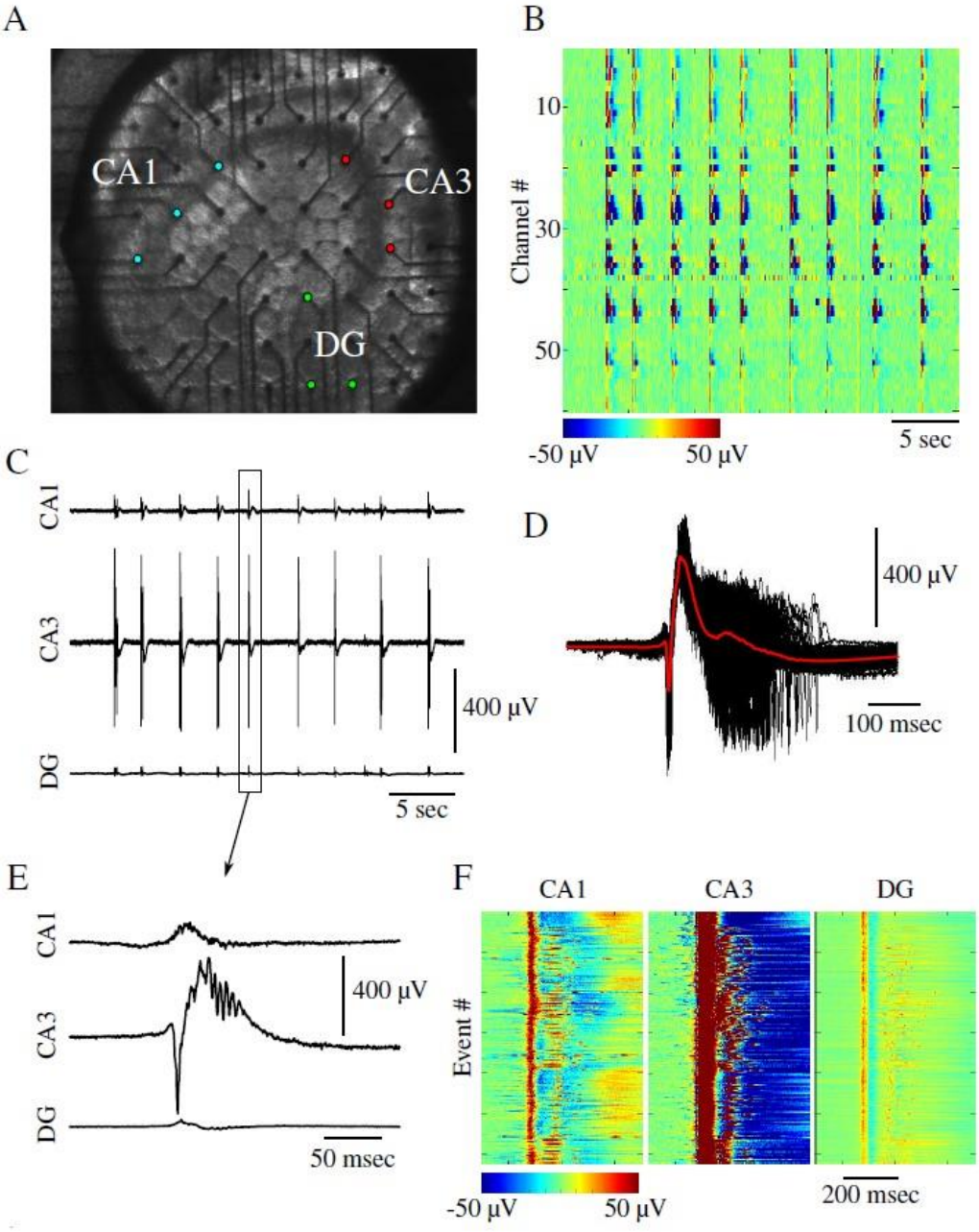

Figure 3.1: 4AP elicits epileptiform activity across the mouse hippocampus. **(A)** Image showing the position of an acute mouse hippocampal brain slice on the multielectrode array (MEA). CA1, CA3 and dentate gyrus (DG) subfields have been labeled, and colored electrodes correspond to electrodes within the structures. **(B)** Epileptiform activity induced with 100 µM 4AP recorded by 60 channel MEA. Color scale represents voltage as indicated by scale bar. **(C)** Epileptiform bursts recorded from single channels within the CA1 (top), CA3 (middle), and DG (bottom). **(D)** Time aligned epileptiform bursts recorded from a single CA3 electrode (black traces). The average signal is superimposed in red. **(E)** Zoom in on a single burst from C. **(F)** All epileptiform bursts recorded from the same channels in C.

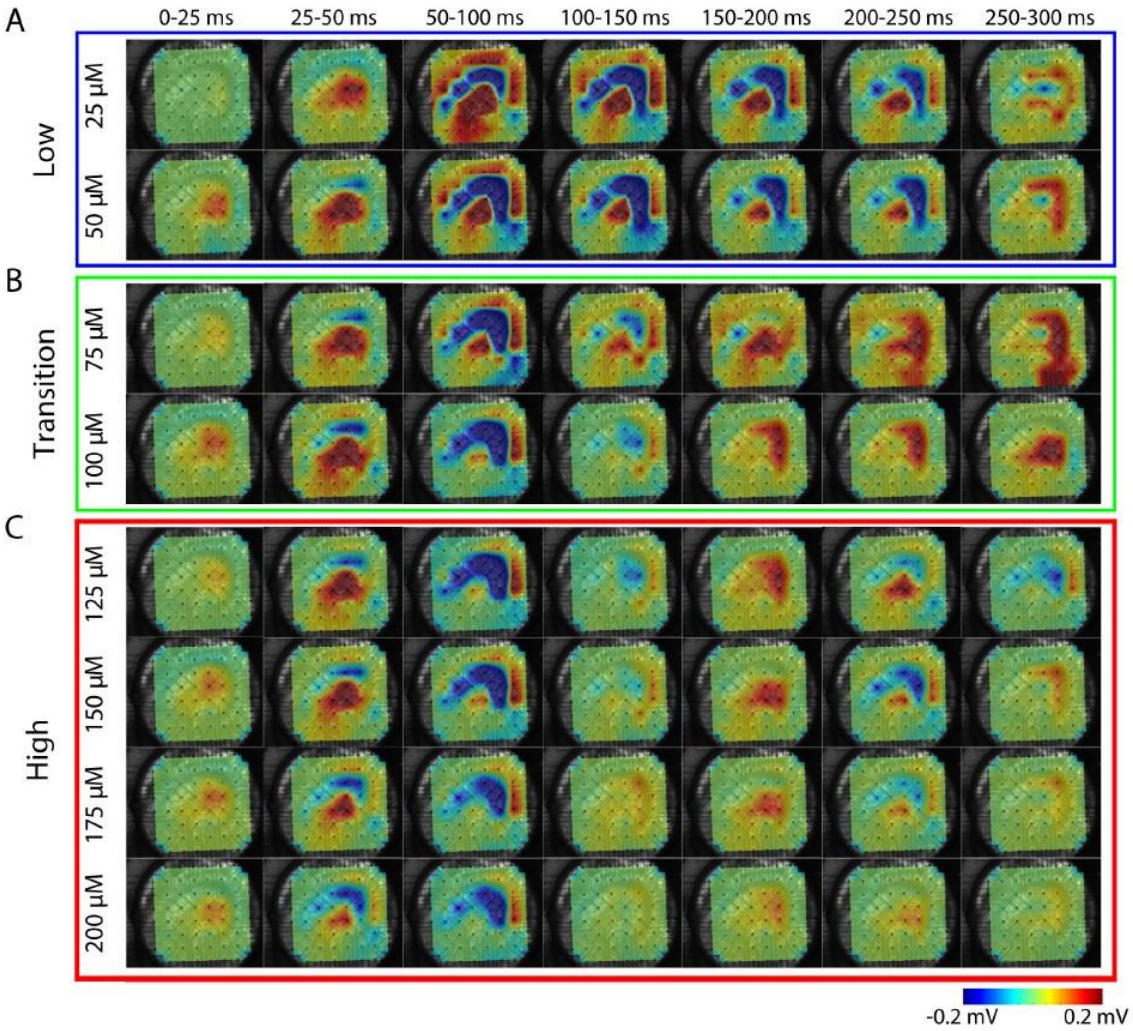

Figure 3.2: Concentration-dependent differences in spatiotemporal propagation of epileptiform activity. Sequence of averaged (25 ms) LFP activity for one epileptiform burst. Each row corresponds to different 4AP concentration. **(A)** low 4AP concentrations **(B)** transition 4AP concentrations **(C)** high 4AP concentrations. Color represents voltage as indicated by the scale bar.

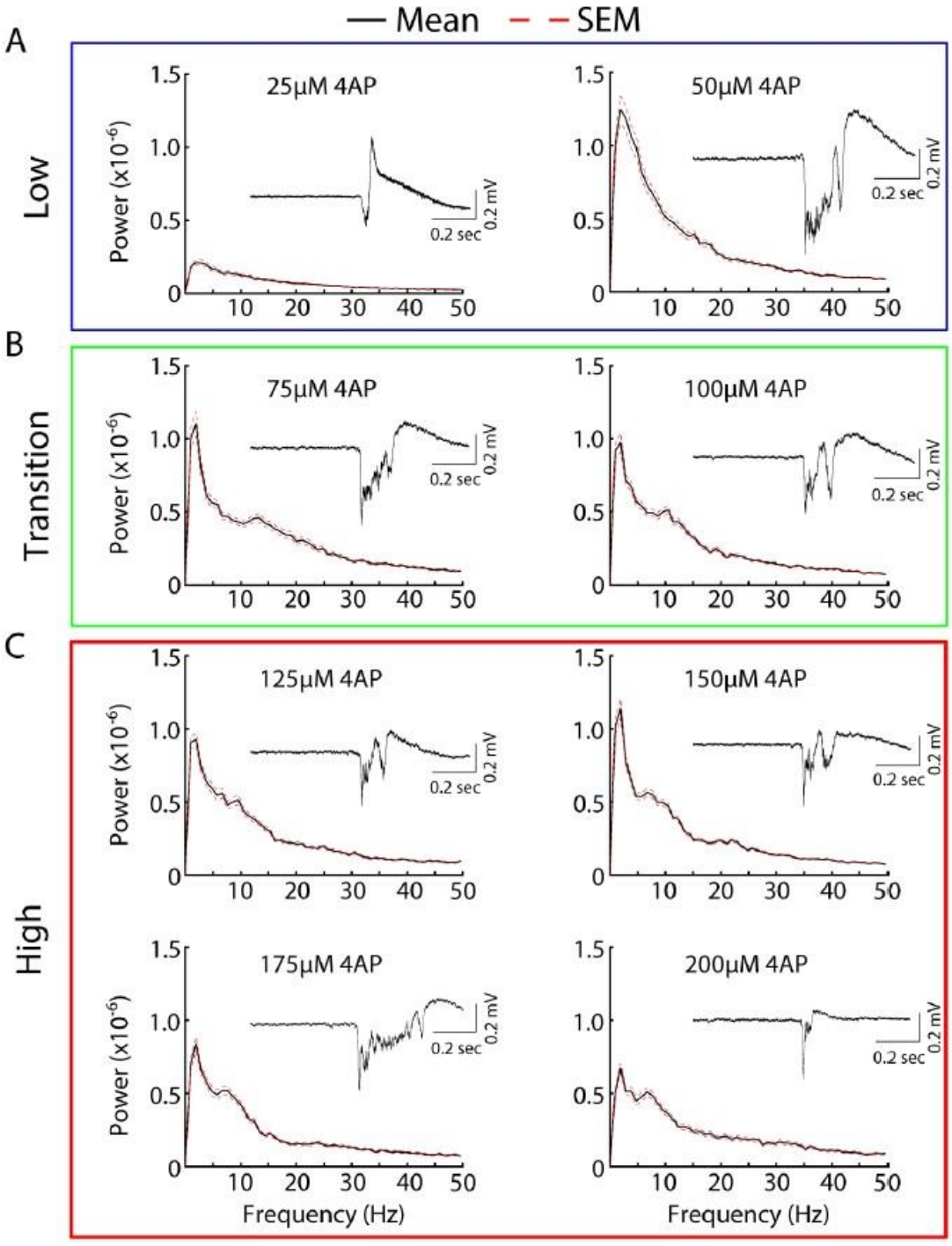

Figure 3.3: Concentration-dependent differences in epileptiform spectrograms. Average spectrograms of activity induced by different concentrations of 4AP. The mean is plotted in black solid line and standard error (SEM) in red broken line. **(A)** low 4AP concentrations **(B)** transition 4AP concentrations **(C)** high 4AP concentrations. Insets are of single representative epileptiform bursts elicited by the corresponding 4AP concentration.

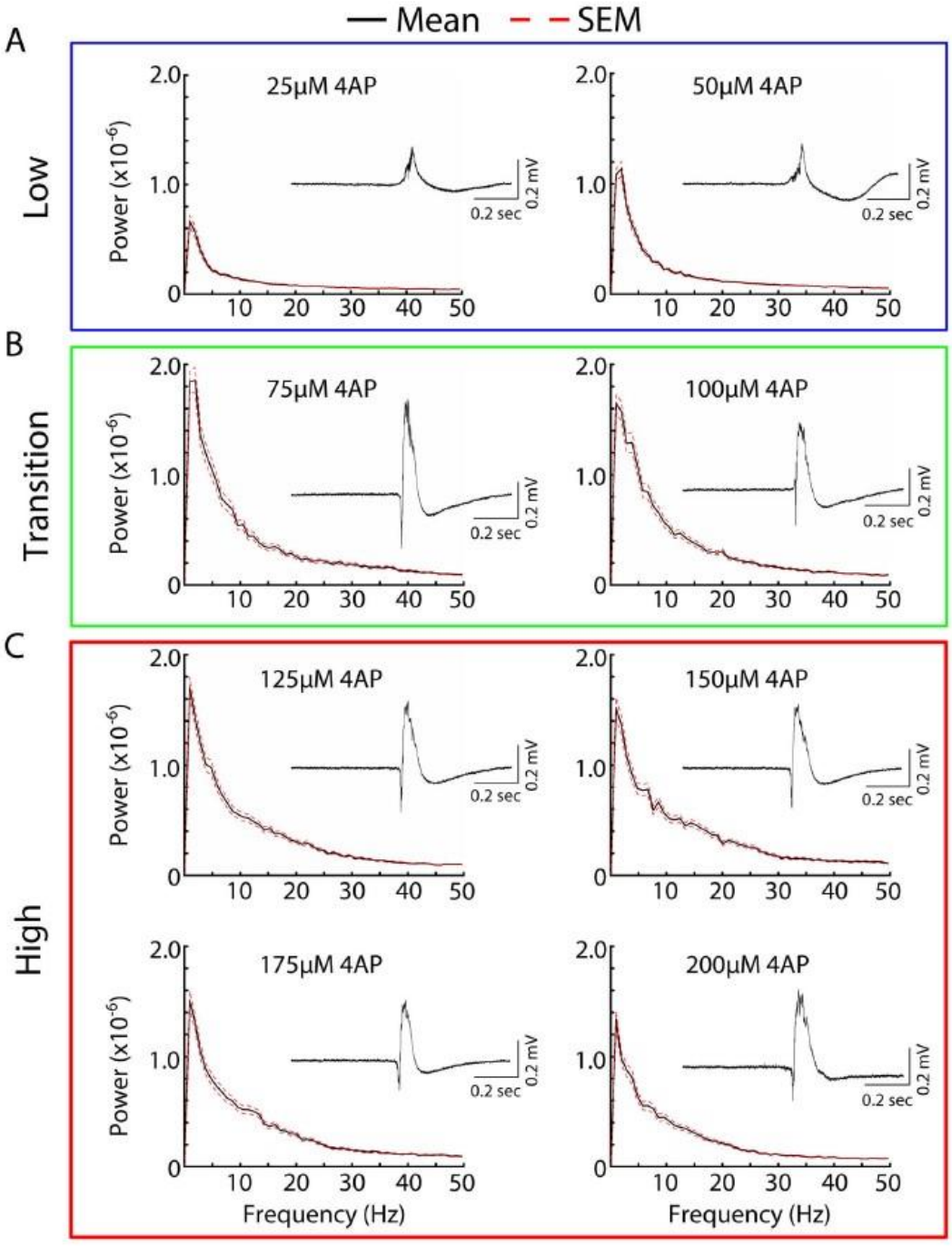

Figure 3.4: Reduction of KCC2 activity prevents concentration-dependent differences in epileptiform spectrograms. Averaged spectrograms of activity induced by different concentrations of 4AP and 10 µM VU0240551. The mean is plotted in black solid line and standard error (SEM) in red broken line. **(A)** low 4AP concentrations **(B)** transition 4AP concentrations **(C)** high 4AP concentrations. Insets are of single representative epileptiform bursts elicited by the corresponding 4AP concentration.

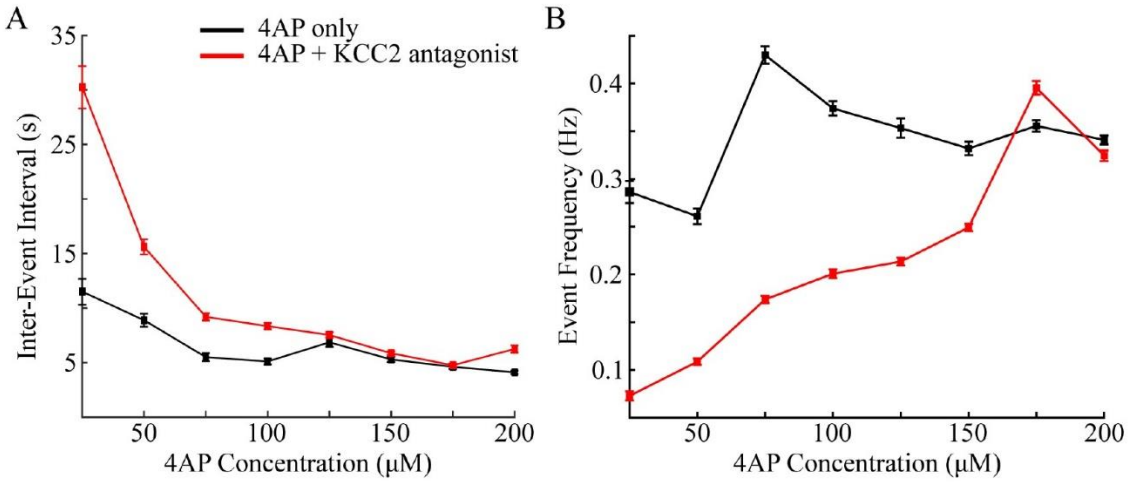

Figure 3.5: Differences in interevent intervals and event frequency of epileptiform bursts. **(A)** Averaged interevent intervals for difference in 4AP concentrations. **(B)** Averaged event frequency of epileptiform bursts per 4AP concentration. Black indicates results for 4AP only, red for 4AP + 10 μM VU0240551.

A. 4AP Only

Condition	Low frequency peak	High frequency peak	Inter-event interval	Event frequency
25 μM 4AP	+	−	11.5 s+/−1.187 s	0.2864 Hz +/−0.01152 Hz
50 μM 4AP	+	−	8.887 s+/−0.5993 s	0.2609 Hz +/− 0.008396 Hz
75 μM 4AP	+	+	5.505 s+/−0.3671 s	0.4298 Hz +/− 0.00909 Hz
100 μM 4AP	+	+	5.105 s+/−0.2711 s	0.3739 Hz +/− 0.00747 Hz
125 μM 4AP	+	+	6.862 s+/−0.4185 s	0.3533 Hz +/− 0.009969 Hz
150 μM 4AP	+	+	5.296 s +/− 0.2263 s	0.3319 Hz +/−0.006969 Hz
175 μM 4AP	+	+	4.615 s+/−0.2102 s	0.3556 Hz +/− 0.005989 Hz
200 μM 4AP	+	+	4.110 s+/−0.1629 s	0.3409 Hz +/− 0.004582 Hz

B. 4AP + VU0240551

Condition	Low frequency peak	High frequency peak	Inter-event interval	Event frequency
25 μM 4AP + VU0240551	+	−	30.25 s +/− 1.939 s	0.07285 Hz +/− 0.004826 Hz
50 μM 4AP + VU0240551	+	−	15.61 s+/−0.6914 s	0.1087 Hz +/−0.003389 Hz
75 μM 4AP + VU0240551	+	−	9.198 s+/−0.3443 s	0.1738 Hz+/−0.003991 Hz
100 μM 4AP + VU0240551	+	−	8.34 s+/−0.2865 s	0.2008 Hz +/−0.004577 Hz
125 μM 4AP + VU0240551	+	−	7.536 s+/−0.2497 s	0.2135 Hz +/−0.004249 Hz
150 μM 4AP + VU0240551	+	−	5.859 s+/−0.1803 s	0.2492 Hz +/− 0.003724 Hz
175 μM 4AP + VU0240551	+	−	4.764 s+/−0.1667 s	0.3954 Hz +/− 0.0071 Hz
200 μM 4AP + VU0240551	+	−	6.25 s +/− 0.3409 s	0.3244 Hz +/− 0.005448 Hz

Table 3.1: Table A, (top) summary of concentration-dependent effects of 4AP only condition. Table B (bottom), summary of concentration-dependent effects of 4AP + VU0240551 condition. Numerical values are presented as the mean +/- standard error.

CHAPTER 4: TRANSLATIONAL STUDY

Non-Contact Detection of Epileptiform Activity in Mouse Hippocampus Using Backscattered Intensity of Optical Coherence Tomography

Abstract

Previous methods for detecting seizures or epileptiform activity in patients and animal models of epilepsy have used various electrophysiological and optical recording techniques such as electroencephalography (EEG), electrocorticography (ECoG), and functional magnetic resonance imaging (fMRI), amongst other techniques. These techniques vary in their invasiveness, and often come with significant trade-offs between spatial and temporal resolution. Intrinsic optical signals recorded with optical imaging techniques such as diffuse optical coherence tomography (OCT) can overcome these limitations and can lead to the detection of neuronal activity during seizure-like activity by measuring changes of the intrinsic optical properties of neural tissue.

OCT is a label free, non-contact-based imaging technique, which can acquire depth-resolved images. In this study, we demonstrate that changes in the intrinsic optical properties of mouse neural tissue during seizure-like activity can be detected using spectral-domain optical coherence tomography (SD-OCT). This was accomplished by inducing seizure-like activity in acute mouse hippocampal brain slices, measuring backscattered light intensity from the tissue over time, quantifying these changes, and validating these results by correlating optical measures with electrophysiology recordings.

During seizure-like activity, we found a 10 to 15% reduction of backscattered light intensity. Additionally, this reduction in backscattered light intensity was significantly correlated with increases in the Hilbert power of the electrophysiological recordings suggesting that the changes in the optical properties of the neural tissue was a

result of increased neural activity observed during seizure-like activity. Our model can detect seizure-like-bursts of activity with high spatial resolution in a label-free manner. Taken together, these findings confirm the validity of the detection of seizure-like activity using spectral-domain optical coherence tomography.

Introduction

Epilepsy remains as one of the most common neurological disorders in the world (World Health Organization, 2019). Epilepsy is used to describe several neurological disorders all characterized by the occurrence of spontaneous recurrent seizures (Huff & Fountain, 2011). Though approximately 70% of epileptic patients have seizures which are well controlled with medications, roughly 30% of patients suffer from pharmacoresistant or intractable epilepsy and require more invasive measures such as resection surgery to find relief (Beghi, 2020). For patients requiring resection surgery, the proper identification of the epileptic focus is of utmost importance. To locate the epileptic focus, clinicians use a combination of both invasive and non-invasive recording techniques including scalp EEG, depth electrodes, ECoG arrays, etc. (Shah & Mittal, 2014). Additionally, these techniques all come with trade-offs between spatial and temporal resolution which can make it challenging to properly identify epileptic activity and its origin (Duez et al., 2019; Rosenow & Lüders, 2001; Shah & Mittal, 2014; Ursino & La Cara, 2006). As such, the development of novel recording techniques which overcome these issues would greatly aid in the identification of epileptic activity and its area of origin in epileptic patients.

Optical coherence tomography (OCT) is a label free, non-contact-based imaging technique, which can acquire depth-resolved images with high temporal resolution (Tanifuji et al., 2009; Yaqoob et al., 2005). OCT has been shown to be a promising method for *in vitro* imaging in highly scattering tissues (De Boer et al., 1999; Graf et al., 2009; Lazebnik et al., 2003). In this new study, we demonstrate that changes in the optical properties of mouse brain tissue during seizure-like epileptiform activity can be detected using spectral-domain optical coherence tomography (SD-OCT). We show that 4-aminopyridine (4AP) induced epileptiform activity in acute mouse hippocampal brain slices result in a decrease in backscattered light intensity. Additionally, these changes in backscattered light intensity were correlated with the onset of epileptiform activity. Together, these data suggest that changes in the optical properties of brain tissue as measured by SD-OCT may provide a novel approach to the detection of epileptiform activity.

Materials & Methods

Animals

All experiments and procedures were performed according to the University of California, Riverside Institutional Animal Care and Use Committee (IACUC) approved protocols. Wild-type (Jackson Laboratory, C57BL/6J, stock number 000664) mouse colonies were bred and maintained in house to generate pups for this study. Both male and female mice were used in this study.

Brain slice preparation

Postnatal day (P) 15-30 mice were anesthetized with isoflurane and quickly decapitated. The brain was rapidly removed and submerged in ice-cold, low $[Ca^{2+}]_o$, high sucrose dissecting solution with carbogen (95%-5% O_2-CO_2) gas continuously applied. 300 μm thick horizontal whole brain slices were made in the dissection solution with a Leica 1200S vibratome. Slices containing hippocampus were recovered in oxygenated normal ACSF for one hour at 32°C and then stored at room temperature until use for imaging. The standard dissection solution contained (in mM): 87 NaCl, 2.5 KCl, 25 $NaHCO_3$, 1.25 NaH_2PO_4, 4 $MgCl_2$, 0.5 $CaCl_2$, 10 D-glucose, 75 sucrose. This solution was maintained at pH 7.4 by continuous oxygenation with carbogen gas mixture. All chemicals were obtained though Fisher Scientific unless otherwise specified.

Electrophysiology data acquisition and processing

Multielectrode array (MEA) recordings were performed on a 60-channel optically clear array (60MEA200/30iR-ITO) with a low-noise amplifier (MEA1060-BC) from MultiChannel Systems. Acute brain slices were prepared, as described above, and positioned on the MEA such that the CA1, CA3, and dentate gyrus (DG) hippocampal subfields were centered over the recording electrodes. Brain slices were continuously perfused during baseline recordings with ACSF (4 ml/min flow rate) containing (in mM): 125 NaCl, 2.5 KCl, 25 $NaHCO_3$, 1.25 NaH_2PO_4, 1 $MgCl_2$, 2 $CaCl_2$, 25 D-glucose, 10 sucrose. Experiments consisted of an initial 20 minutes of ACSF control followed by bath applied 100 μM 4-aminopyridine (4AP) to induce seizure-like epileptiform activity. All MEA recordings were performed at 32°C, which was sufficient to generate stable

epileptiform activity. All MEA recordings were performed simultaneously with OCT recordings.

Local field potentials (LFP) were acquired using MC Rack software (MultiChannel Systems) and exported to MATLAB (MathWorks) for further processing. Data from all 60 MEA channels were collected at 10 kHz. A 2nd order Butterworth bandpass filter (0.1 - 7 Hz) was applied to remove OCT-induced electrical noise. The built-in Hilbert MATLAB function was used to compute the Hilbert power of the bandpass filtered electrophysiology data. The average Hilbert power was then computed within sequential 22 s window bins across all channels. Binned average Hilbert power was used to compute the correlation between the MEA and OCT data.

Due to the lack of perforations in the array, which would allow suction to hold the slice in place, we placed an anchor around the edges of the brain slice to prevent the slice from moving during the recordings. Therefore, there was an unequal distance from the MEA surface and the bottom of the brain slice among experiments. The amplitude of the LFP depends on the distance between MEA and brain slice as well as the intensity of the neural activity. Due to this distance mismatch among experiments, the LFPs exhibited slightly different baselines. Therefore, a correction was required to match the baseline allowing for proper statistical comparisons. The following was used to normalize the LFP data to correct for the differences in distance between MEA surface and bottom surface of the brain slice between experiments:

$$\psi_{i,N} = \left(\frac{\mu_{Ref}}{\mu_i}\right) * \psi_i \qquad (\mathbf{1})$$

where $\psi_{i,N}$ is the normalized signal, μ_{Ref} is the average of the baseline period of a reference dataset (averaged across the first 20 mins), μ_i is the average baseline of the dataset to be normalized, and ψ_i is the signal to be normalized. In order to accurately compare results between slices, all experimental data were normalized with respect to baseline.

OCT imaging system

The SD-OCT system (figure 4.1A) used a broadband, low-coherence light source consisting of two superluminescent diodes (SLD), one centered at 1295 nm with a Full-Width Half-Maximum (FWHM) bandwidth of 97 nm (Thorlabs Inc.) and the other centered at 1350 nm with a FWHM bandwidth of 48 nm (Denselight Semiconductor Pte Ltd), resulting in a combined bandwidth of 120 nm centered at 1298 nm. The system had 8 μm axial and 20 μm lateral resolution. The source was connected to a circulator, which was then connected to a 2x2 fiber-based beam splitter that split 90% of the light to the sample arm and 10% of the light to the reference arm. In the sample arm, a pair of galvanometer (Thorlabs Inc.) mirrors provided transverse scanning of the collimated beam. A lens (AC254-050-C, Thorlabs Inc.) with a 1 inch diameter and focal length of 50 mm was used to direct and collect backscattered light from the sample. The backscattered light from reference and sample arms were collected by a custom-built spectrometer. The spectrometer consisted of a diffraction grating (Wasatch Photonics, 1100 lpmm), focusing lens (JenOptik Optical Systems, f=150 mm), polarization beam splitter cube (Rocky Mountain Instrument Co., 4-inch Cube) and two 1024 pixel line scan cameras (Goodrich SUI SU-LDH linear digital high-speed InGaAs camera).

OCT data acquisition and processing

OCT volumetric data were acquired at an A-line rate of 15 kHz with a single volume consisting of 100 cross-sectional images composed of 1024 A-lines (figure 4.1B). Acquisition time for each volume was 12 s. An imaging depth of 2 mm was obtained with 6.5 mW of incident power on acute brain slices. To have uniform wavenumber spacing, linear interpolation was performed on the nonlinear k-space sampled spectral data. Depth-resolved structural information was retrieved by using the fast Fourier-transform to convert from wavenumber to the spatial domain. In spectrometer-based OCT, the sensitivity of the system decreases as a function of depth. This is due to the finite resolution of the spectrometer. Because of this, a correction was applied by multiplying each A-line by a calculated correction curve to compensate for the decrease of sensitivity as a function of depth as described previously. The correction curve was calculated using the following equation:

$$R(z) = \left(\frac{\sin\zeta}{\zeta}\right)^2 * e^{\left[-\frac{w^2}{2ln2}\zeta^2\right]} \qquad (\mathbf{2})$$

where $\zeta = \left(\frac{\pi}{2}\right) * \left(\frac{z}{z_{RD}}\right)$ is the depth normalized to the maximum depth, $z_{RD} = \frac{\lambda^2}{4\Delta\lambda}$ where $\Delta\lambda$ is the wavelength spacing between pixels, and $w = \frac{\delta\lambda}{\Delta\lambda}$ where $\delta\lambda$ is the spectral resolution (FWHM) of the spectrometer. The spectrometer drop-off from the mirror sample was 11 dB, and equation 2 was used to fit the drop-off and calculated the correction curve. Applying the correction curve ensured that any change in intensity during neural activity was from the tissue under investigation.

Reflection from the MEA caused differences in the noise of each A-line. We corrected for this noise by subtracting noise from each A-line individually. A median filter of size 70 x 70 μm was applied to minimize variation due to coherence speckle. The kernel size was determined by applying a filter to cross-sectional images to achieve a speckle contrast ratio (K_s) below 0.1 over a uniform section of tissue.

$$K_s = \frac{\sigma_s}{\langle I \rangle} \quad (\mathbf{3})$$

where σ_s and $\langle I \rangle$ are the standard deviation and mean of the intensity, respectively. Therefore, the lower the σ_s, the smaller the speckle contrast ratio.

The top and bottom surfaces of the brain slice were detected by SNR thresholding of 80 dB, and an *en face* intensity image was generated by averaging a whole volume in the axial direction. Lateral motion was measured by cross-correlation of an *en face* reference image from a baseline condition with all other *en face* images. The correction was applied to all other volumes with respect to the reference volume. Each volume was segmented into different layers with a height of 50 μm and volume of 2000 x 2000 x 50 μm^3. The average intensity of each layer was calculated for individual datasets. The percent change in intensity from baseline was calculated for each layer. The standard deviation (σ) was calculated for time t for all datasets.

Results

In this study, all experiments were performed at near physiological temperatures (32C) and brain slices were continuously perfused with oxygenated ACSF unless otherwise stated. Experiments consisted of a 20 min ACSF control to gather baseline

OCT and MEA signals. This was then followed by ACSF + 100 μM 4AP which resulted in the development of epileptiform activity throughout the hippocampus. Both OCT and MEA were continuously recorded during both conditions and during solution exchange. OCT cross-sectional images were acquired by sending an optical beam through both control ACSF and ACSF + 4AP solutions. As the addition of 4AP to the ACSF could change the refractive index of the solution and impact the backscattered light, we first tested the effect of 4AP on backscattered light from dead brain slices. Following normal slicing and slice recovery protocols (see Materials and Methods) slices were maintained in un-oxygenated ACSF for 1 hr, which was sufficient time to allow for tissue death. Dead brain slices were then perfused with oxygenated ACSF for 20 mins followed by perfusion of ACSF + 100 μM 4AP. OCT was continuously recorded, and an intensity time trace was generated for the entire duration of the experiment for the top and bottom-most layers (figures 4.2A and B, respectively). The blue vertical line in figures 4.2A and B indicates time when the solution exchange occurred. We calculated the standard deviation (σ) across experiments and plotted ±1.5σ as the shaded areas in figures 4.2A and B. Snapshots of backscattered intensity across the hippocampus at different times within the recording session are presented in figure 4.2C and D showing consistent intensity values across the brain slice throughout the recording (4.2C corresponds to top layer and D to bottom layer). Together, these data show consistent intensity of backscattered light prior to and following the addition of 4AP to ACSF solution suggesting that 4AP does not significantly affect the intensity of backscattered light. Therefore, any changes in OCT intensity in response to 4AP-induced epileptiform

activity would originate from the changes in the scattering of light by the tissue resulting from increased neuronal activity rather than changes in the refractive index of the bath solution.

Having demonstrated that the addition of 4AP to the recording solution did not significantly affect the intensity of backscattered light, we next performed simultaneous OCT and MEA recordings on healthy acute mouse hippocampal brain slices. We began by collecting a baseline intensity profile for healthy slices continuously perfused with ACSF only (figure 4.3). Intensity recordings from the top and bottom most layers of the brain slice are shown in figure 4.3A and B with corresponding *en face* snapshots of backscattered light at different time points (T1-T3) shown in figure 4.3D and E. In both layers, the change in OCT intensity did not significantly deviate from zero. Corresponding Hilbert power averaged across all MEA channels shows no activity within the frequency range used (see Materials & Methods). These data show that at baseline, when there is no large pathological activity in the acute hippocampal slices, both OCT intensity and Hilbert power show no significant change.

To test whether the presence of epileptiform activity can be detected by changes in OCT intensity, we bath applied 100 μM 4AP after a period of baseline ACSF and recorded continuously with both OCT and MEA. OCT images and MEA signals were recorded for 3 different mice. All experimental data were aligned based on the time of solution switching from ACSF to ACSF + 4AP. The time traces of OCT intensity and Hilbert power are shown in figure 4.4A-C. During baseline, prior to the addition of 4AP, both OCT and Hilbert power did not show significant changes (figure 4.4A, B and C,

times 0 – 20 min). After switching bath solution from ACSF only to ACSF + 100 μM 4AP, we observed a 10-18% decrease in OCT intensity in bottom layer (figure 4.4B). The top layer showed a similar trend to that observed in the ACSF only condition (figure 4.3A) as well as the dead slice experiment (figure 4.2A). This is most likely due to the relative difference in the health of the tissue between the top and bottom most region with the bottom region being healthier. These decreases in OCT intensity were accompanied by increases in Hilbert power indicating the presence of epileptiform activity throughout the hippocampal slice (figure 4.4C). *En face* and heat maps of Hilbert power across the MEA show that the CA3 subfield of the hippocampus had the largest decrease in OCT intensity and was the region most activity during epileptiform activity (figure 4.4E and F).

We next computed the correlation between the changes in OCT intensity and Hilbert power. To match the Hilbert power with OCT data, the Hilbert power was segmented into 22 second bins. These 22 second bins of data were converted to a single point in 2 different ways. First, the average of the Hilbert power was taken, second, maximum of the Hilbert power was calculated for the bin.

Figure 4.5A is the time trace of LFP of a single MEA channel in CA3 region of murine brain slice and corresponding Hilbert power (figure 4.5B) which is averaged for a 22 seconds bin to compute the correlation between the MEA and OCT data. The average Hilbert power accounts for amplitude as well as firing rate of neurons.

Before bursts of activities, there were few spikes of activity in the single channel LFP trace resulting in small fluctuations of Hilbert power. The trend of OCT intensity

was similar to both LFP and Hilbert power trace. However, during burst activity, LFPs fluctuated in between -50 μV to 60 μV and the Hilbert power increased as well. OCT intensity decreased during bursts of activity. During the pre-seizure period (blue color in time trace of figure 4.5B), there was a sudden increase of the Hilbert power but the OCT intensity decreased slowly (figure 4.5C), which was due to slow change of the scattering in tissue. During the seizure period, mean Hilbert power was high and the OCT intensity decreased further and then reached a slightly lower steady state.Therefore, we found a negative correlation (figure 4.5D) between the OCT intensity and the Hilbert power of electrophysiology.

The maximum Hilbert power of a bin represents the amplitude of a burst, but can't account for the firing rate. The amplitude of the initial burst was higher than the later time trace. The Hilbert power for the later approach was higher than the former. However, both approaches could separate baseline from pre-seizure and seizure.

Discussion

We developed a label-free, non-contact model that detects seizure-like activity with high spatiotemporal resolution. Here, we demonstrate that SD-OCT can resolve optical changes associated to synchronized postsynaptic potentials in acute hippocampal slices. This novel method shows a 10-15% reduction of backscattered light intensity during seizure-like activity. MEA recordings indicate an inverse relationship between OCT intensity and the Hilbert power of simultaneously obtained electrophysiological data. Together, these experiments suggest that SD-OCT imaging can discriminate

changes in the optical properties of nervous tissue during paroxysmal epileptiform activity.

Advantages of OCT Imaging

Accurate mapping of pharmacoresistant focal epilepsy is critical for resection of the epileptic zone. It is well-documented that OCT imaging can document neural activity (Graf et al., 2009; Lazebnik et al., 2003; Tanifuji et al., 2009). Furthermore, exploring the feasibility of OCT in epilepsy mapping is not a novel consideration (Tsytsarev et al., 2013; Wang & Akkin, 2017; Zhang et al., 2015).

Our model exploits the high spatiotemporal resolution of OCT imaging. With spatial resolving power in the micrometer range, 0.5-10μm (Yaqoob et al., 2005), OCT is well suited to discern epileptiform activity. In fact, OCT has slowly gained biomedical relevance since its discovery in the early 1990s. OCT has demonstrated the ability to distinguish between healthy and oncogenic brain tissue (Bizheva et al., 2005; Böhringer et al., 2006). Further, OCT has been integrated with other intraoperative neurosurgery navigation techniques to aid in tumor resection (Böhringer et al., 2009; Giese et al., 2006). These studies reinforce our data suggesting a role for OCT in precise identification and subsequent intraoperative guidance to epileptic foci.

In addition, OCT imaging is non-contact and label-free requiring no surface electrodes, depth electrodes, or penetrating microelectrodes. Qualitative dual fluorescence spectroscopy is often employed in intraoperative neurosurgery settings, yet a reflectance probe is required to account for changes in the optical properties of the tissue (Valdés et al., 2011). Our data reveal that OCT can reliably detect optical property

changes and discriminate between healthy and epileptic tissue in real-time without additional probes or florescent markers.

Comparison of Techniques

Resective surgery can be an effective treatment for refractory epilepsies (Wiebe et al., 2001), and preoperative localization of the seizure-onset zone is vital to postoperative success rates (Chang et al., 2011). Preplanning intraoperative navigation in resection of the epileptic zone is standard operating procedure (Miller et al., 2007; Sugano et al., 2007). Therefore, innovative strategies for targeting loci of epileptogenesis should be considered, explored, and debated. We propose that SD-OCT imaging be combined with other intraoperative techniques to (1) localize areas of seizure-onset and (2) aid in guidance for lesioning and/or resection.

EEG and ECoG exhibit limited spatial, yet comparable temporal resolutions to OCT imaging. The signal recorded from scalp macroelectrodes in EEG rapidly attenuate due to the low conductivity of osseous connective tissue. However, ECoG overcomes this attenuation in signal fidelity through placement of electrodes beneath the dura. ECoG data is currently the 'gold standard' in the assessment of pathological activity in intractable epilepsy syndromes. Notwithstanding, the subdural electrodes increase infection risk and ECoG imaging exhibits millimeter spatial resolution. These technical limitations of ECoG are addressed by the non-contact and high spatial resolving power characterized by OCT imaging.

MRI and fMRI generate high quality images, but the lackluster spatiotemporal resolution and imaging speeds are insufficient to capture epileptiform activity in real-

time. Additionally, these devices are bulky and cost prohibitive. Ultra-high field MRI imaging characterized by static magnetic fields greater than or equal to 7T can achieve micrometer spatial resolution. However, studies detail multiple issues related to this increase in spatial resolution. Ultra-high magnetic fields are associated with enhanced susceptibility artifacts (Andre et al., 2015), tissue heating (Fiedler et al., 2018), and radio frequency field non-uniformity (Guérin et al., 2017). These issues reduce the reliability of the data and pose questions as to how these high magnetic fields may interact with pathophysiological processes. Moreover, there is an increase in documented side effects from exposure to these fields (Heilmaier et al., 2011). A recent prospective study found a positive correlation between the clinical utility of electromagnetic source imaging compared to electric or magnetic source imaging alone in the accurate localization of the epileptic zone (Duez et al., 2019). These findings must be taken in context as prior work in mice concluded that acute exposure electromagnetic waves may facilitate epileptic seizures (Cinar et al., 2013). Further research into the interactions between the clinical use of ultra-high field MRI and pathological electrical discharges is necessary.

fMRI measures small fluctuations in blood flow associated to localized increases in neural activity, yet reliability of data is key in a preoperative technique to localize the seizure-onset zone. The absence in a hemodynamic signal does not necessarily correlate to quiescence in neural activity. Indeed, anticonvulsant interventions may influence fMRI activation in refractory temporal lobe epilepsy patients (Jokeit et al., 2001).

Together, the presented limitations in spatial resolution, slow imaging speed, and counter indicative research create opportunities for novel imaging techniques, like SD-OCT, in translational medicine.

Application of Microelectrodes with OCT

Depth and surface microelectrodes are often implemented in tandem with imaging technologies to delimit the seizure-onset zone in preparation for surgical resection. While useful, these electrical conductors are sensitive to environmental noise, stimulation artifacts and may be highly invasive. Blind *in vivo* recordings of mouse brain tissue utilized OCT to guide electrode penetration (Watanabe et al., 2011). This study and our method provide sufficient evidence to support the application of OCT in localization of epileptic foci and accurately positioning intraoperative recording electrodes.

Conclusion

We developed a novel technique to detect epileptiform activity using backscattered light. The mechanisms underlying seizure are varied, complex and continue to be rigorously studied and debated (González et al., 2015, 2018; Myers et al., 2018). OCT is limited to a 2-3mm imaging depth and has a restricted field of view. Additionally, OCT output is complex and may precipitate data misinterpretation in clinical practice. However, medical-grade fiber optic OCT probes that transmit source light and record reflectance in the same fiber are commercially available. Recent clinical application of OCT-guided deep-brain stimulation (Tsai & Yi Chiou, 2019) further promotes our argument for clinical consideration of OCT in retractable epilepsy resection surgery.

References

Andre, J. B., Bresnahan, B. W., Mossa-Basha, M., Hoff, M. N., Patrick Smith, C., Anzai, Y., & Cohen, W. A. (2015). Toward quantifying the prevalence, severity, and cost associated with patient motion during clinical MR examinations. *Journal of the American College of Radiology*. https://doi.org/10.1016/j.jacr.2015.03.007

Beghi, E. (2020). The Epidemiology of Epilepsy. In *Neuroepidemiology*. https://doi.org/10.1159/000503831

Bizheva, K., Unterhuber, A., Hermann, B., Považay, B., Sattmann, H., Fercher, A. F., Drexler, W., Preusser, M., Budka, H., Stingl, A., & Le, T. (2005). Imaging ex vivo healthy and pathological human brain tissue with ultra-high-resolution optical coherence tomography. *Journal of Biomedical Optics*. https://doi.org/10.1117/1.1851513

Böhringer, H. J., Boller, D., Leppert, J., Knopp, U., Lankenau, E., Reusche, E., Hüttmann, G., & Giese, A. (2006). Time-domain and spectral-domain optical coherence tomography in the analysis of brain tumor tissue. *Lasers in Surgery and Medicine*. https://doi.org/10.1002/lsm.20353

Böhringer, H. J., Lankenau, E., Stellmacher, F., Reusche, E., Hüttmann, G., & Giese, A. (2009). Imaging of human brain tumor tissue by near-infrared laser coherence tomography. *Acta Neurochirurgica*. https://doi.org/10.1007/s00701-009-0248-y

Chang, E. F., Wang, D. D., Barkovich, A. J., Tihan, T., Auguste, K. I., Sullivan, J. E., Garcia, P. A., & Barbaro, N. M. (2011). Predictors of seizure freedom after surgery for malformations of cortical development. *Annals of Neurology*. https://doi.org/10.1002/ana.22399

Cinar, N., Sahin, S., & Erdinc, O. O. (2013). What is the impact of electromagnetic waves on epileptic seizures? *Medical Science Monitor Basic Research*. https://doi.org/10.12659/MSMBR.883907

De Boer, J. F., Srinivas, S. M., Park, B. H., Pham, T. H., Chen, Z., Milner, T. E., & Nelson, J. S. (1999). Polarization effects in optical coherence tomography of various biological tissues. *IEEE Journal on Selected Topics in Quantum Electronics*. https://doi.org/10.1109/2944.796347

Duez, L., Tankisi, H., Hansen, P. O., Sidenius, P., Sabers, A., Pinborg, L. H., Fabricius, M., Rásonyi, G., Rubboli, G., Pedersen, B., Leffers, A. M., Uldall, P., Jespersen, B., Brennum, J., Henriksen, O. M., Fuglsang-Frederiksen, A., & Beniczky, S. (2019). Electromagnetic source imaging in presurgical workup of patients with epilepsy: A prospective study. *Neurology*. https://doi.org/10.1212/WNL.0000000000006877

Fiedler, T. M., Ladd, M. E., & Bitz, A. K. (2018). SAR Simulations & Safety. *NeuroImage*. https://doi.org/10.1016/j.neuroimage.2017.03.035

Giese, A., Böhringer, H. J., Leppert, J., Kantelhardt, S. R., Lankenau, E., Koch, P., Birngruber, R., & Hüttmann, G. (2006). Non-invasive intraoperative optical coherence tomography of the resection cavity during surgery of intrinsic brain tumors. *Photonic Therapeutics and Diagnostics II*. https://doi.org/10.1117/12.674436

González, O. C., Krishnan, G. P., Chauvette, S., Timofeev, I., Sejnowski, T., & Bazhenov, M. (2015). Modeling of age-dependent epileptogenesis by differential homeostatic synaptic scaling. *Journal of Neuroscience*, *35*(39). https://doi.org/10.1523/JNEUROSCI.5038-14.2015

González, O. C., Shiri, Z., Krishnan, G. P., Myers, T. L., Williams, S., Avoli, M., & Bazhenov, M. (2018). Role of KCC2-dependent potassium efflux in 4-Aminopyridine-induced Epileptiform synchronization. *Neurobiology of Disease*. https://doi.org/10.1016/j.nbd.2017.10.011

Graf, B. W., Ralston, T. S., Ko, H.-J., & Boppart, S. A. (2009). Detecting intrinsic scattering changes correlated to neuron action potentials using optical coherence imaging. *Optics Express*. https://doi.org/10.1364/oe.17.013447

Guérin, B., Villena, J. F., Polimeridis, A. G., Adalsteinsson, E., Daniel, L., White, J. K., & Wald, L. L. (2017). The ultimate signal-to-noise ratio in realistic body models. *Magnetic Resonance in Medicine*. https://doi.org/10.1002/mrm.26564

Heilmaier, C., Theysohn, J. M., Maderwald, S., Kraff, O., Ladd, M. E., & Ladd, S. C. (2011). A large-scale study on subjective perception of discomfort during 7 and 1.5T MRI examinations. *Bioelectromagnetics*. https://doi.org/10.1002/bem.20680

Huff, J. S., & Fountain, N. B. (2011). Pathophysiology and Definitions of Seizures and Status Epilepticus. In *Emergency Medicine Clinics of North America*. https://doi.org/10.1016/j.emc.2010.08.001

Jokeit, H., Okujava, M., & Woermann, F. G. (2001). Carbamazepine reduces memory induced activation of mesial temporal lobe structures: A pharmacological fMRI-study. *BMC Neurology*. https://doi.org/10.1186/1471-2377-1-6

Lazebnik, M., Marks, D. L., Potgieter, K., Gillette, R., & Boppart, S. A. (2003). Functional optical coherence tomography for detecting neural activity through scattering changes. *Optics Letters*. https://doi.org/10.1364/ol.28.001218

Miller, K. J., denNijs, M., Shenoy, P., Miller, J. W., Rao, R. P. N., & Ojemann, J. G. (2007). Real-time functional brain mapping using electrocorticography. *NeuroImage*. https://doi.org/10.1016/j.neuroimage.2007.05.029

Myers, T., C Gonzalez, O., B Stein, J., & Bazhenov, M. (2018). Characterizing Concentration-Dependent Neural Dynamics of 4-Aminopyridine-Induced Epileptiform Activity. *Epilepsy Journal*. https://doi.org/10.4172/2472-0895.1000128

Rosenow, F., & Lüders, H. (2001). Presurgical evaluation of epilepsy. In *Brain* (Vol. 124, Issue 9). https://doi.org/10.1093/brain/124.9.1683

Shah, A. K., & Mittal, S. (2014). Invasive electroencephalography monitoring: Indications and presurgical planning. *Annals of Indian Academy of Neurology*. https://doi.org/10.4103/0972-2327.128668

Sugano, H., Shimizu, H., & Sunaga, S. (2007). Efficacy of intraoperative electrocorticography for assessing seizure outcomes in intractable epilepsy patients with temporal-lobe-mass lesions. *Seizure*. https://doi.org/10.1016/j.seizure.2006.10.010

Tanifuji, M., Suzuki, W., Uma Maheswari, R., & Tsunoda, K. (2009). Depth resolved imaging of neural activity by optical coherence tomography (functional OCT). *Optics InfoBase Conference Papers*. https://doi.org/10.1364/acp.2009.fu3

Tsai, T. Y., & Yi Chiou, D. (2019). An OCT-enable Minimally-invasive Neurosurgical Guide for in-situ Brain Monitoring. *ICIIBMS 2019 - 4th International Conference on Intelligent Informatics and Biomedical Sciences*. https://doi.org/10.1109/ICIIBMS46890.2019.8991485

Tsytsarev, V., Rao, B., Maslov, K. I., Li, L., & Wang, L. V. (2013). Photoacoustic and optical coherence tomography of epilepsy with high temporal and spatial resolution and dual optical contrasts. *Journal of Neuroscience Methods*. https://doi.org/10.1016/j.jneumeth.2013.04.001

Ursino, M., & La Cara, G. E. (2006). Travelling waves and EEG patterns during epileptic seizure: Analysis with an integrate-and-fire neural network. *Journal of Theoretical Biology*, *242*(1). https://doi.org/10.1016/j.jtbi.2006.02.012

Valdés, P. A., Kim, A., Leblond, F., Conde, O. M., Harris, B. T., Paulsen, K. D., Wilson, B. C., & Roberts, D. W. (2011). Combined fluorescence and reflectance spectroscopy for in vivo quantification of cancer biomarkers in low- and high-grade glioma surgery. *Journal of Biomedical Optics*. https://doi.org/10.1117/1.3646916

Wang, H., & Akkin, T. (2017). Brain imaging and mapping with multi-contrast optical coherence tomography. In *Neurophotonics and Brain Mapping*. https://doi.org/10.1201/9781315373058

Watanabe, H., Rajagopalan, U. M., Nakamichi, Y., Igarashi, K. M., Kadono, H., & Tanifuji, M. (2011). Swept source optical coherence tomography as a tool for real time visualization and localization of electrodes used in electrophysiological studies of brain in vivo. *Biomedical Optics Express*. https://doi.org/10.1364/boe.2.003129

Wiebe, S., Blume, W. T., Girvin, J. P., & Eliasziw, M. (2001). A Randomized, Controlled Trial of Surgery for Temporal-Lobe Epilepsy. *New England Journal of Medicine*. https://doi.org/10.1056/nejm200108023450501

World Health Organization. (2019). WHO | Epilepsy: a public health imperative. In *Who*.

Yaqoob, Z., Wu, J., & Yang, C. (2005). Spectral domain optical coherence tomography: a better OCT imaging strategy. In *BioTechniques*. https://doi.org/10.2144/000112090

Zhang, T., Hajihashemi, M. R., Zhou, J., Carney, P. R., & Jiang, H. (2015). Detection of early seizures by diffuse optical tomography. *Biomedical Applications of Light Scattering IX*. https://doi.org/10.1117/12.2075409

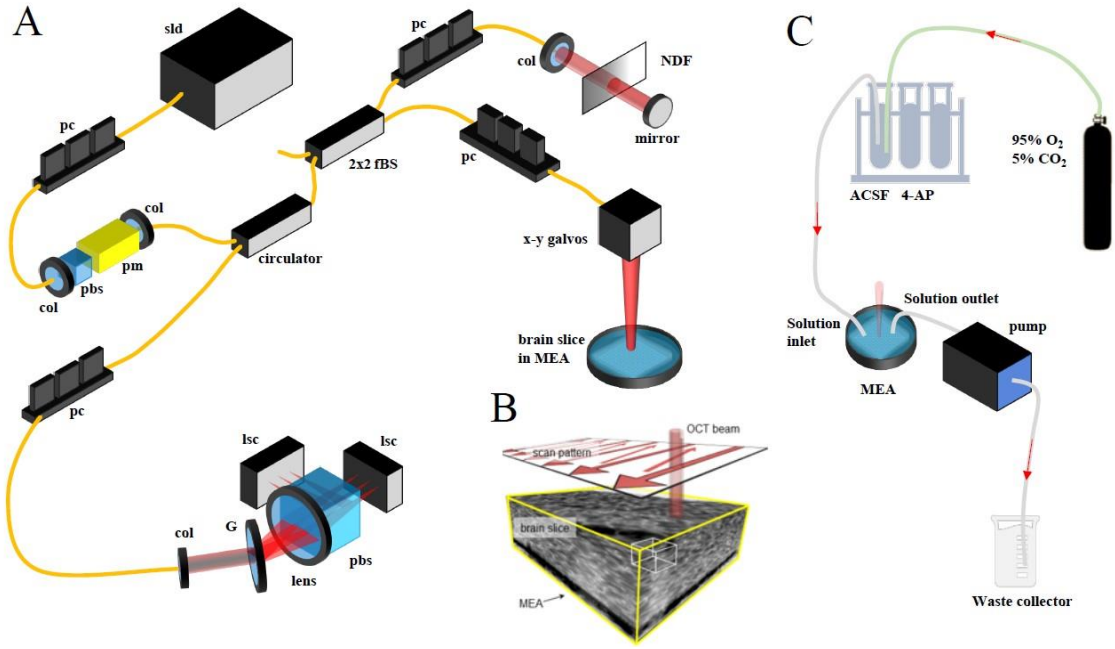

Figure 4.1: OCT system diagram and experimental setup. **(A)** System diagram of 1300nm OCT imaging system. sld: superluminescent diode; MEA: multielectrode array; pc: polarization controller; pm: polarization modulator; G: grating; NDF: neutral density filter; lsc: line scan camera; col: collimator; pbs: polarization beam splitter; 2x2 fbs: 2x2 fiber-based beam splitter. **(B)** 3D construction of brain slice from OCT recordings showing the OCT scan pattern for data collection. **(C)** Basic diagram showing continuous oxygenation of ACSF or 4AP solution with carbogen and perfusion solution over slice on MEA.

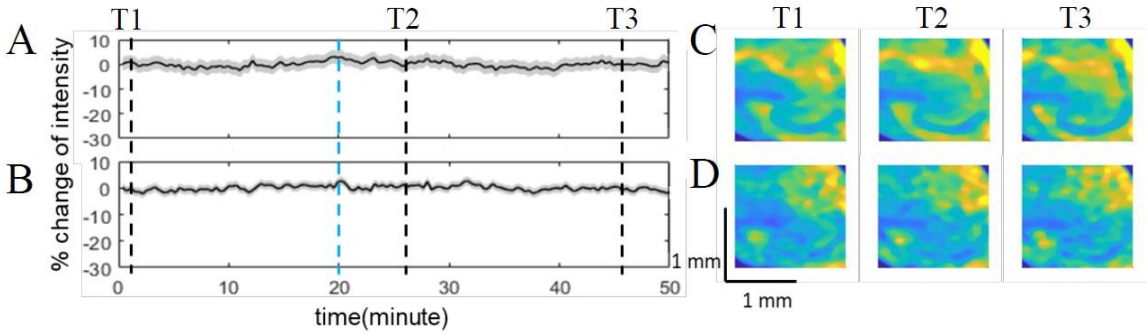

Figure 4.2: Effect of 4AP on backscattered intensity. **(A)** The time trace of intensity on the superficial layer of a dead slice. ACSF solution is perfused over brain slice for 20 minutes then solution exchange from ACSF to ACSF + 100 µM 4AP. After 3-5 minutes, 4AP solution completely perfuses over the slice. The OCT intensity trend is similar to baseline. The dashed blue line indicates solution exchange. **(B)** The time trace of OCT intensity on the deep layer of a dead slice. Intensity does not change over time. **(C & D)** Heatmaps corresponding to OCT intensity in the superficial and deep layers respectively.

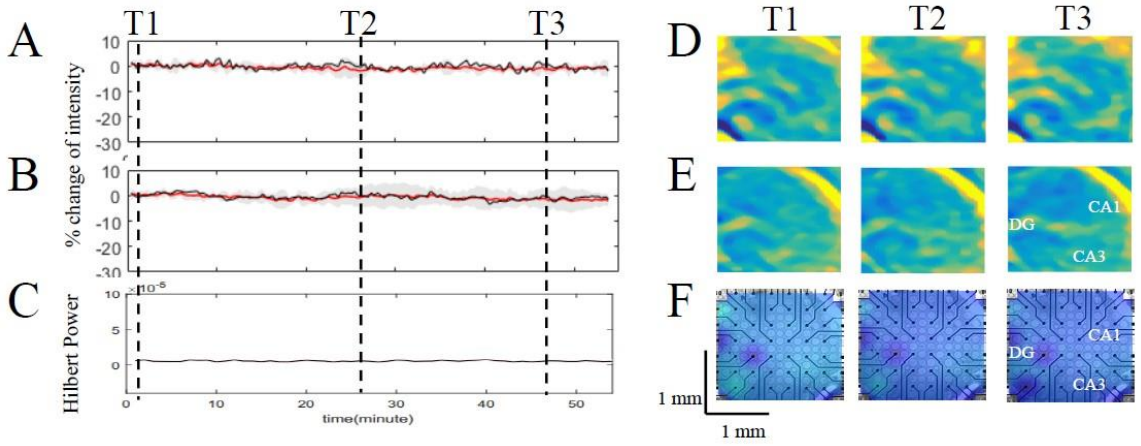

Figure 4.3: OCT and MEA show no activity in absence of pathological discharges. Control experiment with ACSF only in a 'live' brain slice. Lines of intensity, A/B, remain within x4% for OCT intensity and x3% for the averaged Hilbert power of simultaneously acquired electrophysiological data, C. **(B)** Heatmaps of OCT intensity, D/E, and electrophysiology traces, F. CA1, CA3 and DG correspond to hippocampal subfields. T1, T2 and T3 timepoints that refer to the dashed black lines in A-C. **(C)** Averaged Hilbert power of all 60 MEA channels. **(D & E)** Corresponding OCT heatmaps of the superficial and deep layers of the brain slice. **(F)** Heatmap of the averaged Hilbert power. The OCT intensity and MEA Hilbert power do not change over time.

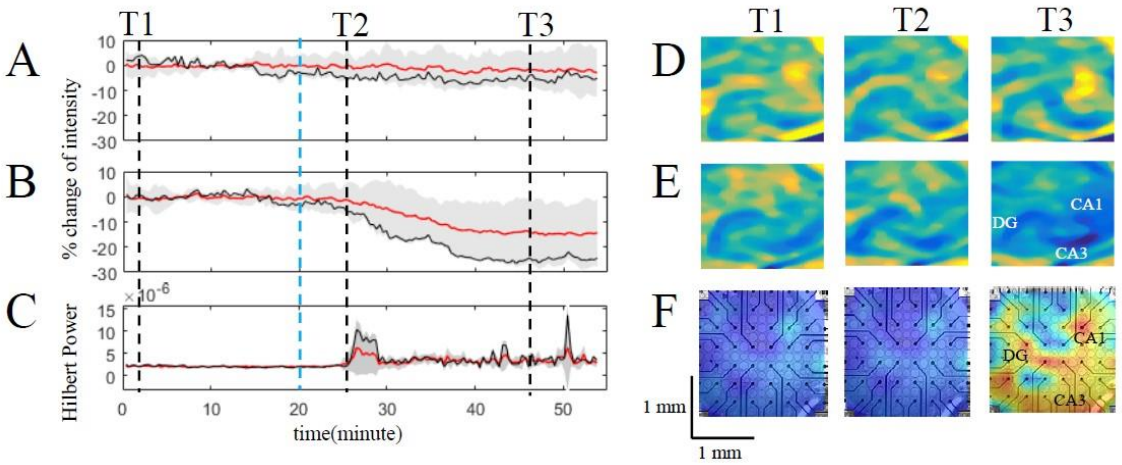

Figure 4.4: OCT intensity decreases during seizure-like bursts. ACSF baseline, 20 min, followed by perfusion of 100 µM 4AP at solution exchange indicated by blue dashed line. **(A & B)** Time traces of OCT intensity in superficial and deep brain slice layers. Observed 10-18% decrease in OCT intensity in deep layer following perfusion of 4AP. **(C)** Averaged Hilbert power of electrophysiological data. Ictogenesis and epileptiform activity following 4AP perfusion correlates to the decrease OCT intensity in B. **(D & E)** Corresponding OCT heatmaps of the superficial and deep layers of the brain slice. CA1, CA3 and DG correspond to hippocampal subfields. T1, T2 and T3 timepoints that refer to the dashed black lines in A-C. **(F)** Heatmap of the averaged Hilbert power. The Hilbert power increases in response to the 4AP-induced epileptiform activity.

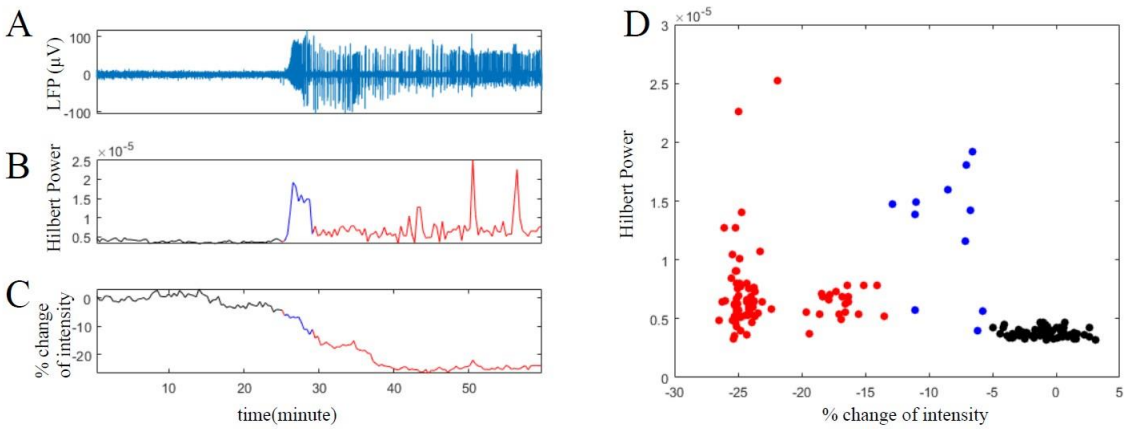

Figure 4.5: Correlation between OCT and MEA data. **(A)** Time trace of single MEA channel. **(B)** Mean Hilbert power of single MEA channel. **(C)** OCT intensity. **(D)** MEA/OCT correlation.

CHAPTER 5: CONCLUSION

I_D and Pathological High Frequency Oscillations in 4AP-Induced Epileptiform Activity & Proconvulsive Role of TNFα in Cortical Deafferentation-Induced Seizure

Synopsis

My research adopted a multimodal approach to explore paroxysmal activity elicited by 4-aminopyridine (4AP) in excitable tissue. In sum, we described and provided experimental support for an inhibitory-induced model of ictogenesis involving the KCC2 cotransporter. We established that varying the concentration of 4AP led to differences in the event complexity and spatiotemporal distribution of epileptiform activity. Furthermore, we demonstrated that pharmacological antagonism of KCC2 reduced the complexity of epileptiform activity resulting in stereotyped seizure-like discharges across multiple 4AP concentrations. Finally, we show that SD-OCT can detect optical changes during 4AP-induced epileptiform activity.

This series of studies provided insight into the pathogenesis of epilepsy with emphasized pertinence to refractory cases involving potassium channelopathies. However, it is feasible that the proposed mechanism extends to a more generalized model of seizure induction. This inhibition-induced ictogenesis model is clinically relevant in that our research indicates that administration of benzodiazepines and/or barbiturates may exacerbate seizure in some epilepsy patients. Our novel mechanism may explain the side effect of increased chance of seizure onset common of many anti-epileptic drugs. Moreover, we provide an initial study supporting a novel application for OCT in the clinical diagnosis of epilepsy syndromes. Importantly, multiple observations from this research propound directions for future experiments.

Future Directions

I_D in 4AP-induced Epileptiform Activity

We found a positively correlated relationship between the average event frequency of epileptiform activity and increased concentrations of 4AP. Additionally, our study revealed that the spatial distribution and durations of epileptiform activity at high concentrations of 4AP evoked more focal and shorter-lived burst activity (Myers et al., 2018). However, the mechanism(s) involved in these observations remain elusive (figure 5.1, 5.2). I_A (A-current) and I_D (D-current) account for nearly all the outward potassium current underlying the repolarization phase of the action potential (Mitterdorfer & Bean, 2002). Moreover, elimination of I_A increases neuronal excitability to low-amplitude current stimulation whereas large-amplitude current injections elicit transient spiking prior to neuron quiescence (Yuan et al., 2005). These studies suggest that the concentration-dependent propagation and bursting activity may reflect differential pharmacokinetics of 4AP on I_A and I_D receptors. Indeed, prior research demonstrated that I_D is more sensitive to 4AP (Mitterdorfer & Bean, 2002). Further research into the divergent spatiotemporal contributions of I_A and I_D in 4AP-induced epileptiform activity is necessary.

Pathological High Frequency Oscillations in 4AP-induced Epileptiform Activity

Post publication signal analysis on 4AP-induced epileptiform events (Myers et al., 2018) revealed pathological high frequency oscillations (pHFOs) at transition and high but not low concentrations of 4AP. These isolated waveforms resemble hippocampal

ripples (data not shown). The characterization and mechanism of these pHFOs in 4AP-induced epileptiform activity is unknown. It is well-documented that inhibitory interneurons are integral to network synchronization (Avoli et al., 1996; Grasse et al., 2013; Lévesque et al., 2016; Uva et al., 2015). If I_D receptors are localized at a higher percentage on inhibitory neurons, low concentrations of 4AP would preferentially excite inhibitory neurons. As the concentration of 4AP is increased, more excitatory pyramidal cells would be recruited by reduction of I_D and I_A. The pyramidal-interneuron gamma (PING) mechanism for ripple generation suggests that network synchronization arises from transient suppression via inhibitory neurons and subsequent rebound spiking from excitatory neurons (Schlingloff et al., 2014; Viriyopase et al., 2016). This oscillating inhibition-excitation behavior may manifest hippocampal ripples; however, this mechanism is hotly debated. Assuming the distribution of D-current receptors is expressed at a higher concentration on inhibitory neurons and that I_D is more sensitive to 4AP (Mitterdorfer & Bean, 2002), it is plausible that these pHFOs reflect a hijack of the ripple generation mechanism and only manifest following recruitment of pyramidal cells at higher concentrations of 4AP. Additional studies are necessary to (1) further characterize this 4AP concentration dependent oscillatory phenomena, (2) determine the distribution of D-current receptors on excitatory and inhibitory neurons, and (3) explore how these 4AP-induced pHFOs modulate epileptiform activity.

TNFα Inhibition Increases Threshold for Seizure Induction in Deafferented Networks

Here, I propose a future project which applies my research experience in homeostatic plasticity (Xie et al., 2014), cortical deafferentation (see Appendix), astrocytic signaling pathways (Devaraju et al., 2013), and astrocyte pathology (Agulhon et al., 2012).

Production of TNFα, a proinflammatory cytokine, has been shown to increase after two days following status epilepticus and is even further enhanced at seven days in a kinate model of epilepsy (De Bock et al., 1996). TNFα is an effector of homeostatic plasticity (HSP) by increasing AMPA expression and endocytocizing $GABA_A$ receptors (Pribiag & Stellwagen, 2013; Stellwagen et al., 2005) through glia-mediated signaling cascades (Stellwagen & Malenka, 2006). Indeed, TNFα triggers glial-mediated synaptic upscaling (Stellwagen & Malenka, 2006). Unpublished computational work in our lab developed a model supporting astrocytic signaling cascades in focal traumatic brain injury (Volman & Bazhenov, 2017) (figure 5.3). The astrocytic release of TNFα in response to a pathophysiological increase in extracellular glutamate may decrease the threshold for epileptogenesis. A traumatized network releases excess glutamate that, in turn, decreases cAMP. This signaling cascade leads to the astrocytic release of TNFα into the extracellular space where it disrupts basal network homeostasis through the trafficking of AMPA and $GABA_A$ receptors (Stellwagen et al., 2005). Cortical deafferentation induces a hyperexcitable network and a decreased threshold for seizure (González et al., 2015). Therefore, I propose that inhibition of TNFα increases seizure threshold in a deafferented network.

I hypothesize that the TNFα inhibitor will prevent/lessen HSP changes in the deafferented areas thus preventing a reduction in seizure threshold. Epilepsy will be induced through a cortical undercut protocol (see Appendix). A TNFα inhibitor will be administered via an implantable infusion device (osmotic pump) to continually dose the mouse for a period of three weeks following undercut surgery. Threshold for epileptiform activity will be assessed using established slice preparation protocols and a 60-channel multielectrode array. Complementary experiments will perfuse forskolin, an adenylyl cyclase agonist, on undercut slices to determine if the frequency and duration of epileptiform discharges are affected compared to control undercut mice. We expect an increase in seizure threshold for the TNFα inhibitor-dosed mice and a decrease in seizure threshold for activator-dosed mice when compared to saline deafferented controls.

References

Agulhon, C., Sun, M. Y., Murphy, T., Myers, T., Lauderdale, K., & Fiacco, T. A. (2012). Calcium signaling and gliotransmission in normal vs. Reactive astrocytes. *Frontiers in Pharmacology*. https://doi.org/10.3389/fphar.2012.00139

Avoli, M., Barbarosle, M., Lücke, A., Nagao, T., Lopantsev, V., & Köhling, R. (1996). Synchronous GABA-mediated potentials and epileptiform discharges in the rat limbic system in vitro. *Journal of Neuroscience*. https://doi.org/10.1523/jneurosci.16-12-03912.1996

De Bock, F., Dornand, J., & Rondouin, G. (1996). Release of TNFα in the rat hippocampus following epileptic seizures and excitotoxic neuronal damage. *NeuroReport*. https://doi.org/10.1097/00001756-199604260-00004

Devaraju, P., Sun, M. Y., Myers, T. L., Lauderdale, K., & Fiacco, T. A. (2013). Astrocytic group I mGluR-dependent potentiation of astrocytic glutamate and potassium uptake. *Journal of Neurophysiology*. https://doi.org/10.1152/jn.00517.2012

González, O. C., Krishnan, G. P., Chauvette, S., Timofeev, I., Sejnowski, T., & Bazhenov, M. (2015). Modeling of age-dependent epileptogenesis by differential homeostatic synaptic scaling. *Journal of Neuroscience*, *35*(39). https://doi.org/10.1523/JNEUROSCI.5038-14.2015

Grasse, D. W., Karunakaran, S., & Moxon, K. A. (2013). Neuronal synchrony and the transition to spontaneous seizures. *Experimental Neurology*. https://doi.org/10.1016/j.expneurol.2013.05.004

Lévesque, M., Herrington, R., Hamidi, S., & Avoli, M. (2016). Interneurons spark seizure-like activity in the entorhinal cortex. *Neurobiology of Disease*. https://doi.org/10.1016/j.nbd.2015.12.011

Mitterdorfer, J., & Bean, B. P. (2002). Potassium currents during the action potential of hippocampal CA3 neurons. *Journal of Neuroscience*. https://doi.org/10.1523/jneurosci.22-23-10106.2002

Myers, T., C Gonzalez, O., B Stein, J., & Bazhenov, M. (2018). Characterizing Concentration-Dependent

Neural Dynamics of 4-Aminopyridine-Induced Epileptiform Activity. *Epilepsy Journal*. https://doi.org/10.4172/2472-0895.1000128

Pribiag, H., & Stellwagen, D. (2013). Tnf-α downregulates inhibitory neurotransmission through protein phosphatase 1-dependent trafficking of GABAA receptors. *Journal of Neuroscience*. https://doi.org/10.1523/JNEUROSCI.0530-13.2013

Schlingloff, D., Káli, S., Freund, T. F., Hájos, N., & Gulyás, A. I. (2014). Mechanisms of sharp wave initiation and ripple generation. *Journal of Neuroscience*. https://doi.org/10.1523/JNEUROSCI.0867-14.2014

Stellwagen, D., Beattie, E. C., Seo, J. Y., & Malenka, R. C. (2005). Differential regulation of AMPA receptor and GABA receptor trafficking by tumor necrosis factor-α. *Journal of Neuroscience*. https://doi.org/10.1523/JNEUROSCI.4486-04.2005

Stellwagen, D., & Malenka, R. C. (2006). Synaptic scaling mediated by glial TNF-α. *Nature*. https://doi.org/10.1038/nature04671

Uva, L., Breschi, G. L., Gnatkovsky, V., Taverna, S., & de Curtis, M. (2015). Synchronous inhibitory potentials precede seizure-like events in acute models of focal limbic seizures. *Journal of Neuroscience*. https://doi.org/10.1523/JNEUROSCI.3692-14.2015

Viriyopase, A., Memmesheimer, R. M., & Gielen, S. (2016). Cooperation and competition of gamma oscillation mechanisms. *Journal of Neurophysiology*. https://doi.org/10.1152/jn.00493.2015

Volman, V., & Bazhenov, M. (2017). Reactive astrocytes - Comprehending when neurons play 4'33". In *bioRxiv*. https://doi.org/10.1101/189134

Xie, A. X., Lauderdale, K., Murphy, T., Myers, T. L., & Fiacco, T. A. (2014). Inducing plasticity of astrocytic receptors by manipulation of neuronal firing rates. *Journal of Visualized Experiments*. https://doi.org/10.3791/51458

Yuan, W., Burkhalter, A., & Nerbonne, J. M. (2005). Functional role of the fast transient outward K+ current I A in pyramidal neurons in (rat) primary visual cortex. *Journal of Neuroscience*. https://doi.org/10.1523/JNEUROSCI.2858-05.2005

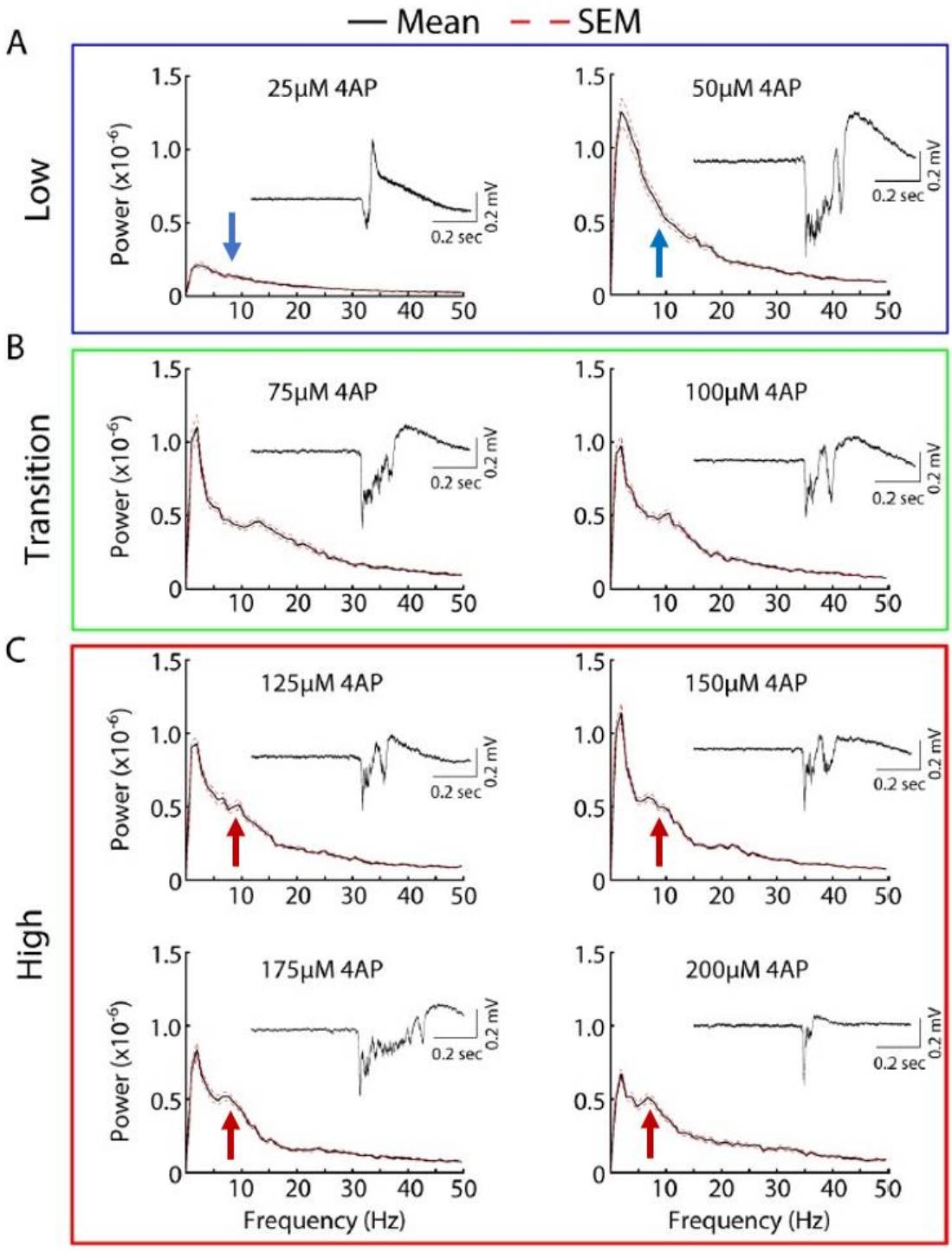

Figure 5.1: Spectrogram images adapted from chapter 3 figure 3.3. **(A)** no high frequency component in low concentrations of 4AP (blue arrows). **(B)** high frequency component in high concentrations of 4AP (red arrows).

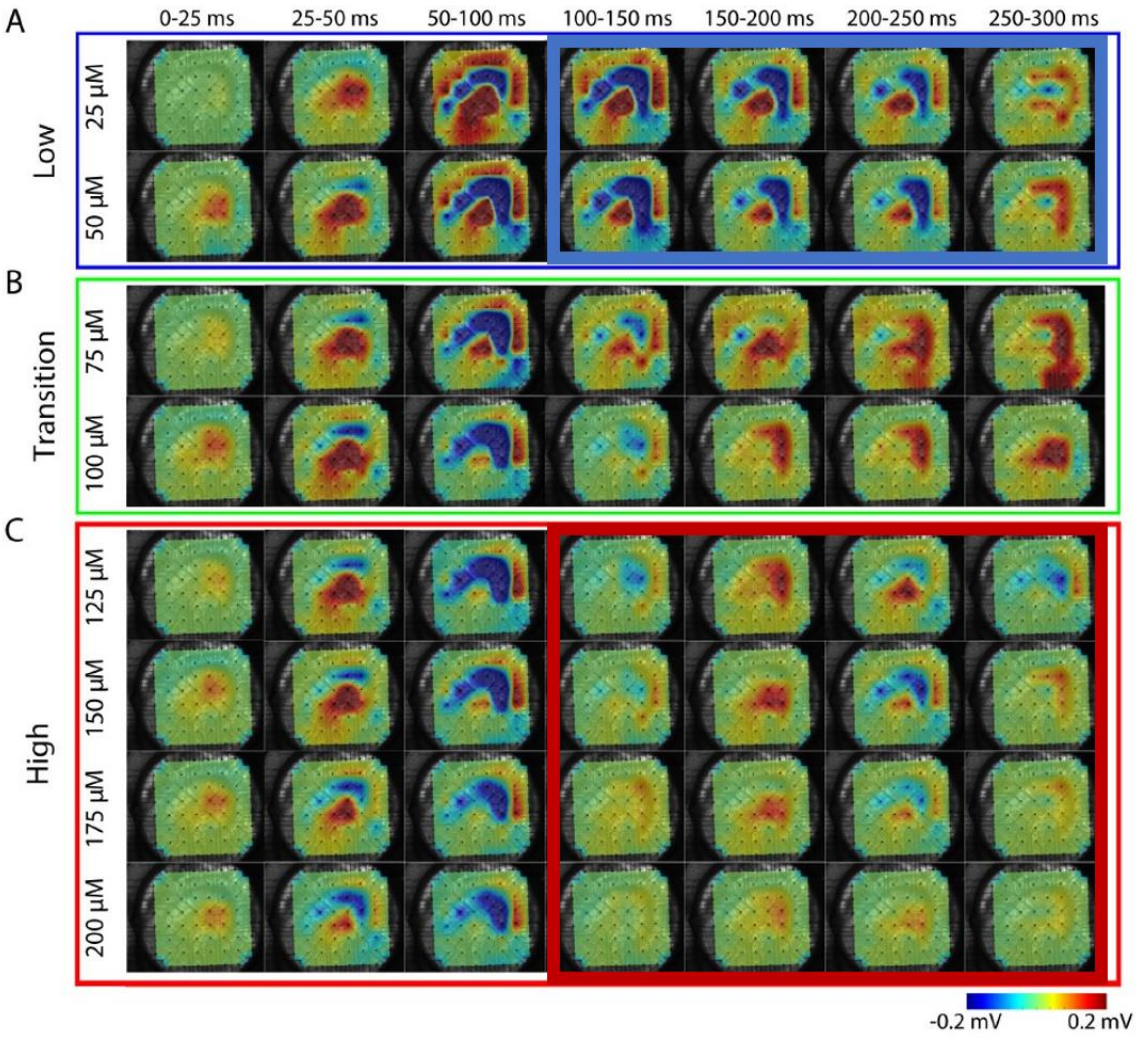

Figure 5.2: Averaged LFP activity of one epileptiform burst image adapted from chapter 3 figure 3.2. **(A)** LFP activity exhibits generalized distribution following ictogenesis in low concentrations of 4AP (thick blue box). **(B)** LFP activity exhibits focal distribution following ictogenesis in high concentrations of 4AP (thick red box).

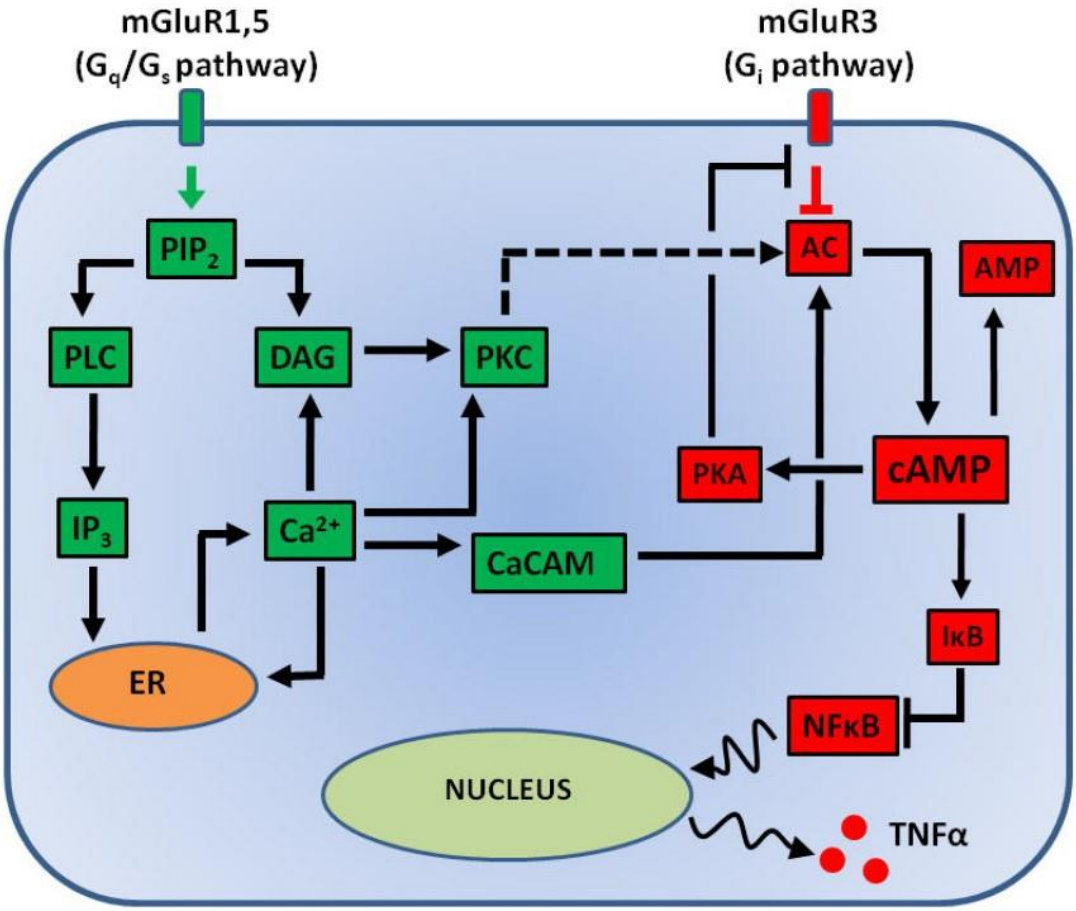

Figure 5.3: Biochemical pathways delineating the role of astrocytic metabotropic glutamate receptors, mGluR5 and mGluR3, in the release of TNFα during pathological activation of astrocytes (reactive astrogliosis). Adapted from (Volman & Bazhenov, 2017). Reprinted with permission.

APPENDIX

Adaptation of an *In Vivo* Cortical Deafferentation Model of Chronic Epilepsy to Investigate Age-Dependent Homeostatic Plasticity Change During Seizure

Unpublished Research

Here, I present unpublished work derived from an *in silico* study examining age-dependent homeostatic plasticity variance in deafferentation-induced epileptogenesis (González et al., 2015). The aims of the project were two-fold: **(1)** optimize a cortical deafferentation (undercut) model in mice and **(2)** acquire preliminary data replicating the computational results *in vitro* using a 60-channel multielectrode array (MEA).

Proof of concept was established (Figures 6.1 & 6.2) adapting a published undercut protocol (Xiong et al., 2011) to create a 180° incision equidistant between the lambda/bregma intersections and lateral to the sagittal suture. The postoperative mortality rate was 17% in deafferented (n = 12) versus 0% in control (n = 4) mice. Furthermore, I demonstrated survivability of an aged undercut mouse (n = 1) and documented status epilepticus and recurrent seizures in 100% of the surviving deafferented mice. The experimental design required animals aged between 18-24 months to approximate 56-69 human years. (Flurkey et al., 2007). The project was tabled, and the mice culled prior to acquisition of *in vitro* electrophysiological data from control and deafferented cortical slices.

References

Flurkey, K., Currer, J. M., & Harrison, D. E. (2007). Mouse Models in Aging Research. In *The Mouse in Biomedical Research* (Vol. 3). https://doi.org/10.1016/B978-012369454-6/50074-1

González, O. C., Krishnan, G. P., Chauvette, S., Timofeev, I., Sejnowski, T., & Bazhenov, M. (2015). Modeling of age-dependent epileptogenesis by differential homeostatic synaptic scaling. *Journal of Neuroscience*, *35*(39). https://doi.org/10.1523/JNEUROSCI.5038-14.2015

Xiong, W., Ping, X., Gao, J., & Jin, X. (2011). Preparing undercut model of posttraumatic epileptogenesis in rodents. *Journal of Visualized Experiments*. https://doi.org/10.3791/2840

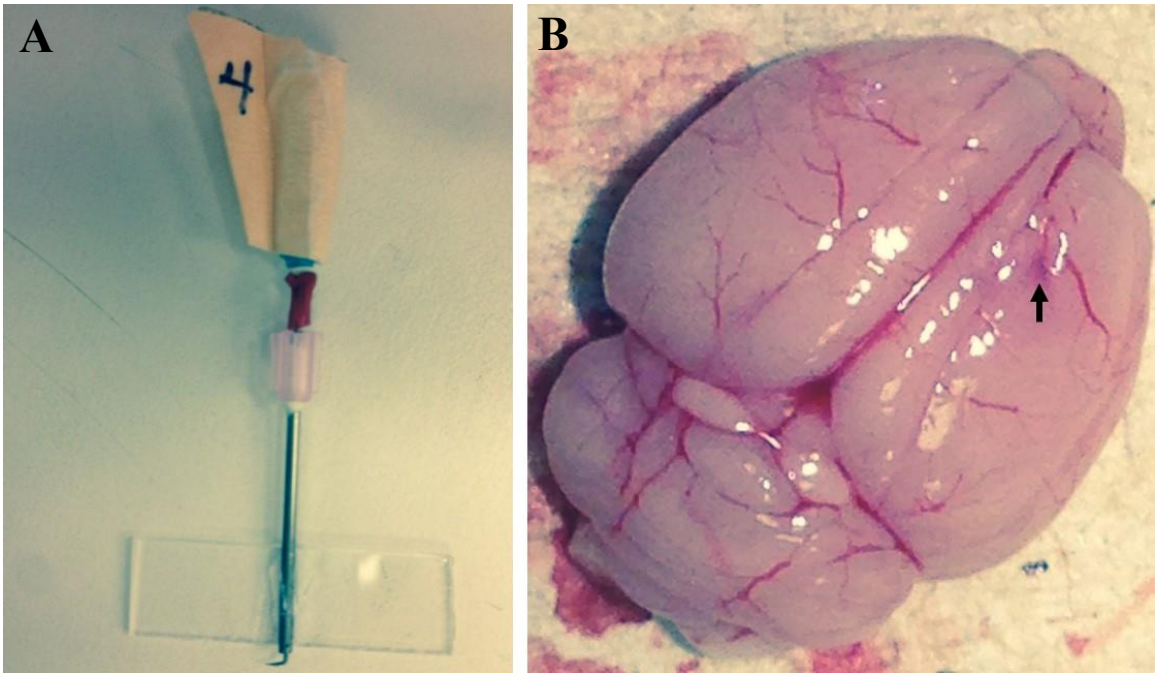

Figure 6.1: Proof of principle for modified cortical deafferentation model of epilepsy. **(A)** The undercut device. **(B)** Mouse brain excised three weeks following undercut surgery. The location of undercut device insertion indicated by the black arrow.

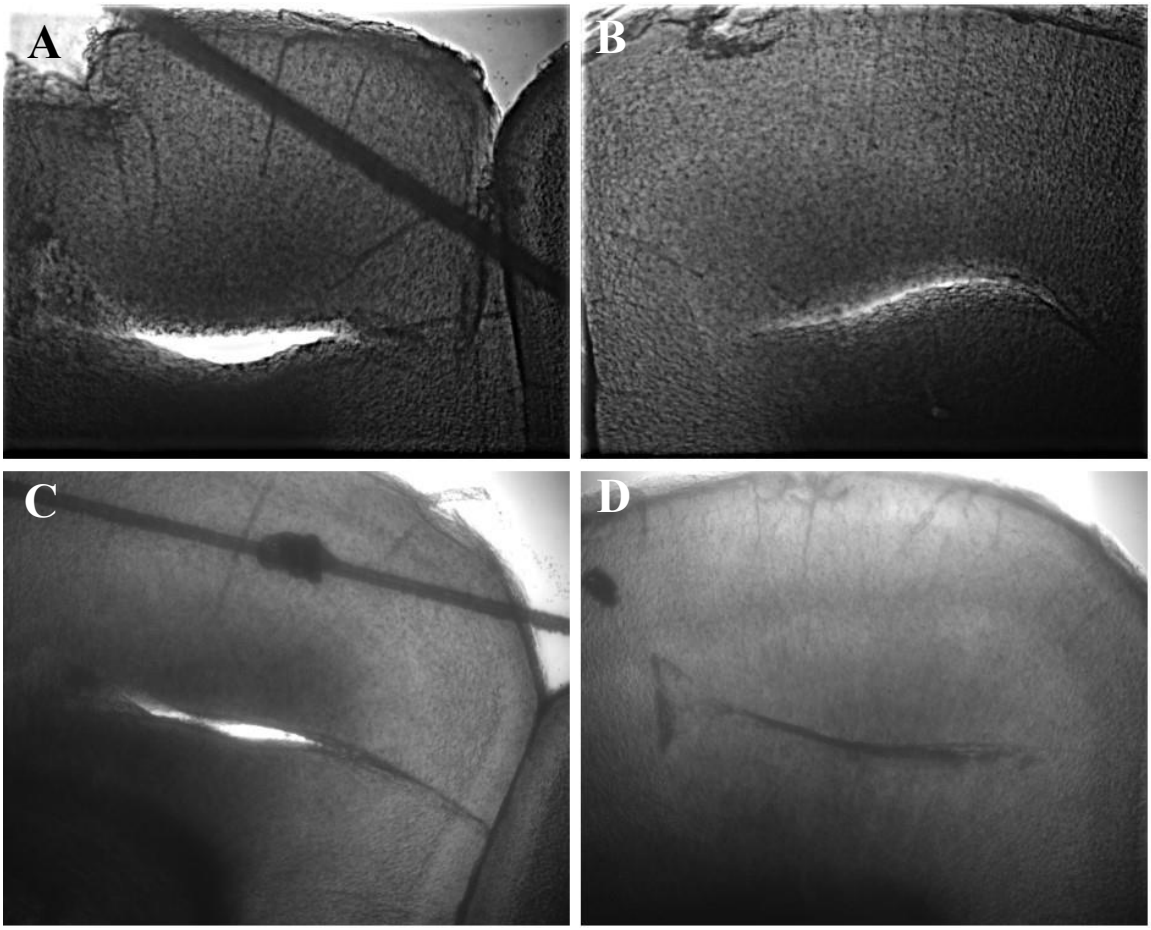

Figure 6.2: (A-D) 200 µm cortical slices showing undercut from different mice. The dark line in panels A and D indicate a thread from the platinum anchor securing the slice to the microelectrode array during perfusion.